(3)

FINAL REPORT: RESULTS OF NEAR FIELD PROBE SCANNING TESTS FOR ULTRALOW SIDELOBE ARRAYS

May 30, 1986

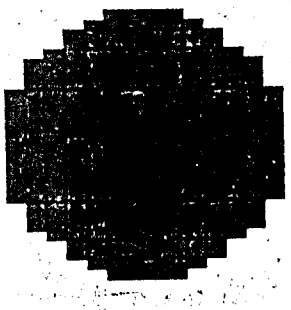

Technology Service Corporation

Technology Service Corporation

Washington Division: 962 Wayne Avenue, Silver Spring, Maryland 20910 Phone: (301) 565-2970

FINAL REPORT: RESULTS OF NEAR FIELD PROBE SCANNING TESTS FOR ULTRALOW SIDELOBE ARRAYS

May 30, 1986

Prepared by:

Kenneth R. Grimm (TSC)
John B. Hoffman (TSC)
Allen C. Newell (NBS)
Michael H. Francis (NBS)

Approved by:

Dr. Joe Frank
Manager, Washington Group

Prepared for:

Office of Naval Research
Code 260
800 North Quincy Street
Arlington, VA 22217

Attention: LCmdr R. Wyatt
Contract N00014-83-C-0671

UNCLASSIFIED

SECURITY CLASSIFICATION OF THIS PAGE (When Data Entered)

REPORT DOCUMENTATION PAGE		READ INSTRUCTIONS BEFORE COMPLETING FORM
1. REPORT NUMBER TSC-W41-405/kks	2. GOVT ACCESSION NO. AD-A178 141	3. RECIPIENT'S CATALOG NUMBER
4. TITLE (and Subtitle) Final Report: Results of Near Field Probe Scanning Tests for Ultralow Sidelobe Arrays		5. TYPE OF REPORT & PERIOD COVERED Final Report June 6, 1983 - March 1986 6. PERFORMING ORG. REPORT NUMBER
7. AUTHOR(s) K. R. Grimm, J. B. Hoffman, A. C. Newell, M. H. Francis		8. CONTRACT OR GRANT NUMBER(s) N00014-83-C-0671 N00014-83-F-0180
9. PERFORMING ORGANIZATION NAME AND ADDRESS Technology Service Corporation 962 Wayne Ave Silver Spring, MD 20910		10. PROGRAM ELEMENT, PROJECT, TASK AREA & WORK UNIT NUMBERS A3035K
11. CONTROLLING OFFICE NAME AND ADDRESS Office of Naval Research 800 North Quincy Street Arlington, VA 22217 (Code 260)		12. REPORT DATE May 1986 13. NUMBER OF PAGES
14. MONITORING AGENCY NAME & ADDRESS(if different from Controlling Office)		15. SECURITY CLASS. (of this report) Unclassified 15a. DECLASSIFICATION/DOWNGRADING SCHEDULE

16. DISTRIBUTION STATEMENT (of this Report)

Approved for Public Release; Unlimited Distribution

17. DISTRIBUTION STATEMENT (of the abstract entered in Block 20, if different from Report)

18. SUPPLEMENTARY NOTES

Prepared as part of the Defense Small Business Advanced Technology Program (DESAT)--Phase II

19. KEY WORDS (Continue on reverse side if necessary and identify by block number)

Near Field Testing
Low Sidelobe Arrays
Measurement Errors
Mainbeam Nulling Probe

20. ABSTRACT (Continue on reverse side if necessary and identify by block number)

This report documents a unique Navy research program regarding fundamental measurement accuracy issues of near field antenna scanning. This work has accomplished both analytic studies and demonstration testing with very low sidelobe antennas. The program results have affirmed known relations between near field scanning errors and the resulting inaccuracies of the transformed far field sidelobe patterns. An existing planar near field scanner at the National Bureau of Standards in Boulder, Colorado has been modified to accept the large test antennas, and subsequently used for scanning tests with the

DD FORM 1 JAN 73 1473 EDITION OF 1 NOV 65 IS OBSOLETE

UNCLASSIFIED

SECURITY CLASSIFICATION OF THIS PAGE (When Data Entered)

AWACS phased array as well as a second experimental ultralow sidelobe slotted waveguide array. Results show that far field sidelobe accuracy is ultimately limited by uncontrollable random near field measurement error, multipath, and probe pattern directivity. A novel "mainbeam nulling" probe has been shown to increase measurement accuracy of wide angle sidelobes by greatly minimizing the error gain in the coupling product during scanning. Classical probe correction post-processing is then necessary to recover the improved sidelobe pattern, but with degraded accuracy in mainbeam directions. The new probe radiates a fixed-direction null aligned with test antennas steered mainbeam. Catalogs of available data and results from unclassified antenna scanning tests are given in appendices.

PREFACE

This report documents a unique Navy research program regarding fundamental measurement accuracy issues of near field antenna scanning. This work has accomplished both analytic studies and demonstration testing with very low sidelobe antennas. The program results have affirmed known relations between near field scanning errors and the resulting inaccuracies of the transformed far field sidelobe patterns. An existing planar near field scanner at the National Bureau of Standards in Boulder, Colorado has been modified to accept the large test antennas, and subsequently used for scanning tests with the AWACS phased array as well as a second experimental ultralow sidelobe slotted waveguide array. Results show that far field sidelobe accuracy is ultimately limited by uncontrollable random near field measurement error, multipath, and probe pattern directivity. A novel "mainbeam nulling" probe has been shown to increase measurement accuracy of wide angle sidelobes by greatly minimizing the error gain in the coupling product during scanning. Classical probe correction post-processing is then necessary to recover the improved sidelobe pattern, but with degraded accuracy in mainbeam directions. The new probe radiates a fixed-direction null aligned with test antennas steered mainbeam. Catalogs of available data and results from unclassified antenna scanning tests are given in appendices.

Table of Contents

		Page
1.0	INTRODUCTION AND BACKGROUND	1
2.0	DESCRIPTION OF EXPERIMENT	4
	2.1 Facility Description	4
	2.2 Test Issues	8
	2.3 DESAT Arrays	12
	2.4 Test Organization	17
	2.5 Probe Design	17
3.0	MEASUREMENT ACCURACY EXPECTATIONS	25
	3.1 Room Scattering Errors--SCAT	25
	3.2 Probe-Parameter Errors	34
	3.3 Data-Point Spacing--Aliasing	39
	3.4 Scan Area Truncation	40
	3.5 Systematic Scanning Errors	43
	3.6 Multiple Reflection Error	51
	3.7 Random Measurement Error	55
4.0	ULSA RESULTS FROM TWO-DIMENSIONAL NF SCANNING	57
	4.1 Aliasing Test Results	67
	4.2 Scan Area Truncation	72
	4.3 Probe Z-Position Error Results	81
	4.4 Receiver Amplitude Error Results	84
	4.5 Random Error Results	89
	4.6 Multipath Results	95
5.0	CONCLUSIONS	104
REFERENCES		106
APPENDICES		
A.1	Catalog of Test Data Files	107
A.2	Description of Data Processing Software	118
A.3	Bibliography of Reports and Publications	179

List of Figures

Figure No.		Page
1	Schematic of Low Sidelobe Array Antenna in Three Positions Relative to the Fixed Location DESAT Probe Scanner	5
2	Location of Optical Auto-Collimator, Precision Levels, and Transits Used to Manually Correct for Rotational Misalignment of DESAT Arrays Following Translation During Sectioned-Scanning	7
3	ULSA Array Azimuth Pattern at 3.025 Ghz Measured on the Westinghouse Far Field Antenna Range (1978)	13
4	ULSA Array Azimuth Pattern at 3.0 Ghz as Measured Following DESAT Refurbishment on the Westinghouse Far Field Range (1983)	14
5	Photograph of ULSA Array Mounted for DESAT Scanning Tests at NBS, Boulder, CO	15
6	Photograph of AWACS Face Array Mounted for DESAT Scanning Tests at NBS, Boulder, CO	18
7	Testing Organization for DESAT II Test Demonstration	19
8	Two-Element Waveguide Probe Response Overlayed on the Ideal Wavenumber Filter Response for Low Sidelobe Testing	22
9	Photograph of the New Two-Element Waveguide Probe	22
10	ULSA Azimuth Plane Pattern as Measured by Both the Σ Probe (Mainbeam) and Δ-Probe (Sidelobes) During DESAT Testing at NBS (3.1 Ghz)	24
11	Schematic of Moving Array SCAT Test Used to Quantify Room Scattering Errors During DESAT Testing at NBS	26
12	Sketch of DESAT Room/Array/Scanner Geometry as Used in SCAT Analysis	28
13	Measured NF Amplitude for a Y-Scan with the ULSA Array Located at X_{R1} During SCAT Testing Using the Open-Ended Waveguide Probe	31
14	Comparison of Measured NF Amplitude for Y-Scans with the ULSA Array Located at X_{R1} (solid) and then translated to X_{RN} for SCAT Testing Using the Open-Ended Waveguide Probe	32

List of Figures (cont'd)

Figure No.		Page
15	Sample Perspective Plot of $\delta(x_R, x_o, y_a)$ Residuals from 95 Relocations of the ULSA Array and Probe Tower During SCAT Testing at NBS. The peak NF SCAT Error is 39 dB Below Peak NF Signal	35
16	Perspective Plot of the SCAT Error Spectrum Due to Random Room Scathering as a Function of Wavenumber Coordinate (k_x, k_y). The Peak Spectral Error is 70 dB Below ULSA Mainbeam Gain at f_1 as Measured with the Open-Ended Waveguide Probe	36
17	Schematic Relationship Between Scan Length and Maximum Angle to Which the Far Field Pattern Can be Accurately Measured During Planar NF Scanning	41
18	Schematic of Scan Area Truncation for Evaluating the Yaghjian Error Bound for a Sidelobe at Angle (θ, ϕ). The Perimeter Fields are $E_t(\rho', \phi_\rho)$ and γ_{max} is Shown in Figure 17	42
19	Form of the Bounding Far Field Sidelobe Error Due to Groups 1-3 Near Field Measurement Errors (Table 1)	44
20	Basic Coupling Product Relation for Planar Near Field Scanning	45
21	Measured Scanner Rail Straightness of NBS Planar Scanner	48
22	First-Order Multiple Reflection Error Between Probe and Test Array Produces Interference Ratio as a Function of Z at Fixed Locations in the Scan Plane	53
23	Higher-Order Multiple Reflections Between Probe and Array are Revealed by a Scan Plane Survey to Collect Multiple Centerline Scans at Offset Z-Separations	54
24	Measured NF Amplitude Perspective for the ULSA Array and Open-Ended Waveguide Probe Scanning at 3.1 Ghz	58
25	Measured NF Amplitude Perspective for the ULSA Array and Δ-Probe Scanning at 3.1 Ghz	59
26	Perspective Plot of Probe-Corrected ULSA Array Far Field Pattern as Measured by NF Scanning with the Open-Ended W/G Probe at 3.1 Ghz	61

List of Figures (cont'd)

Figure No.		Page
27	Far Field Probe Patterns Overlayed on the ULSA Array Pattern Computed from Transformed Probe Scan Data at 3.1 Ghz	62
28	Centerline ULSA NF Scans Measured with the Three DESAT Probes at 3.1 Ghz	62
29	ULSA Coupling Product Spectrum Azimuth Plane Patterns for the NF Scans of Figure 28 (Open-Ended W/G Probe and Δ-Probe) at 3.1 Ghz	63
30	Equal-Amplitude Contours of the Azimuthal Far Field Pattern of the Open-Ended W/G Probe at 3.1 Ghz	64
31	Equal-Amplitude Contours of the Azimuthal Far Field Pattern of the Δ-Probe at 3.1 Ghz	65
32	Equal-Amplitude Contours of the Azimuthal Far Field Pattern of the Σ-Probe at 3.1 Ghz	66
33	Equal-Amplitude Contours of the Elevation (cross-polarized) Far Field Pattern of the Open-Ended W/G Probe at 3.1 Ghz	68
34	Equal-Amplitude Contours of the Elevation (Cross-Polarized) Far Field Pattern of the Δ-Probe at 3.1 Ghz	69
35	Equal-Amplitude Contours of the Elevation (Cross-Polarized) Far Field Pattern of the Σ-Probe of 3.1 Ghz	70
36	Coupling Product Spectrum from Centerline Scanning with the Σ-Probe and ULSA Array at 3.1 Ghz for Spacings of 1.0λ and 0.1λ	71
37	Summary of Peak Sidelobe Error Due to NF Aliasing for the Σ-Probe at 3.1 Ghz	73
38	Summary of rms Sidelobe Error Due to NF Aliasing for the Σ-Probe at 3.1 Ghz	74
39	Coupling Product Spectrum from Centerline Scanning with the Δ-Probe and ULSA Array at 3.1 Ghz for spacings of 1.0λ and 0.1λ	75
40	Summary of Peak Sidelobe Error Due to NF Aliasing for the Δ-Probe at 3.1 Ghz	76
41	Summary of rms Sidelobe Error Due to NF Aliasing for the Δ-Probe at 3.1 Ghz	77

List of Figures (cont'd)

Figure No.		Page
42	Sidelobes Selected (#1,2,3) for Measuring Gain Error Due to Scan Area Truncation With the Three DESAT Probes	79
43	Measured Gain Error for Sidelobe #1 as a Function of Normalized Scan Length for the Three DESAT Probes	79
44	Measured Gain Error for Sidelobe #2 as a Function of Normalized Scan Length for the Three DESAT Probes	80
45	Measured Gain Error for Sidelcbe #3 as a Function of Normalized Scan Length for the Three DESAT Probes	80
46	Comparison of the Yaghjian Upperbound for Sidelobe Error Due to Scan Area Truncation, with the Measured Error, for Sidelobe #1 and Σ-Probe Scanning	82
47	Comparison of the Yaghjian Upperbound for Sidelobe Error Due to Scan Area Truncation, with the Measured Error, for Sidelobe #1 and Δ-Probe Scanning	83
48	ULSA Azimuth Plane Pattern Computed from Σ-and Δ-Probe Scanning With and Without Induced Z-Position Error	85
49	ULSA Centerline NF Amplitude Error Ratio Due to Induced Receiver Error as a Function of Scan for the Open-Ended W/G Probe	88
50	ULSA Centerline NF Amplitude Error Ratio Due to Induced Receiver Error as a Function of Scan for the Δ-Probe	88
51	ULSA Azimuth Plane Pattern Computed from Open-Ended W/G Probe Data With and Without Induced Receiver Error (Table 10)	90
52	ULSA Azimuth Plane Pattern Computed from Δ-Probe Data With and Without Induced Receiver Error (Table 10)	90
53	Evanescent Spectrum Contours Due to All Sources of Random and Systematic Measurement Error, Computed from AWACS Scanning With the Open-Ended W/G Probe at 3.3 Ghz	91
54	Evanescent Spectrum Contours Due to All Sources of Systematic and Random Measurement Error, Computed from AWACS Scanning with the Δ-Probe at 3.3 Ghz	92
55	NF Amplitude Comparison of Measured NF to Room Scattering as Derived by SCAT Testing Using the Open-Ended W/G Probe and the AWACS Array	96

List of Figures (cont'd)

Figure No.		Page
56	NF Amplitude Comparison of Measured NF to Room Scattering as Derived by SCAT Testing Using the Δ-Probe and the AWACS Array	96
57	ULSA Mainbeam Gain Error Due to First-Order Near Field Multipath for the Σ-Probe	98
58	ULSA Azimuth Plane Peak Sidelobe Gain Change Due to Higher-Order Near Field Multipath	99
59	ULSA Azimuth Plane RMS Sidelobe Gain Change Due to Higher-Order Near Field Multipath	100
60	Five-Spectra Average Coupling-Product Pattern Overlays Measured During Tests to Quantify Higher-Order Near Field Multipath Due to Σ-Probe Scanning at 3.1 Ghz	102
61	Five-Spectra Average Coupling Product Pattern Overlays Measured During Tests to Quantify Higher-Order Near Field Multipath Due to Δ-Probe Scanning at 3.1 Ghz	103

List of Tables

Table		Page
1	Error Sources in Planar Near Field Measurements	29
2	Typical Far Field Probe Calibration Errors at NBS	39
3	Measured Scanner Position Errors on the NBS NF Range	47
4	Predicted Far Field Sidelobe Errors Due to Residual Mechanical Positioning Errors at NBS for Open-Ended Waveguide Probe	49
5	Predicted Far Field Sidelobe Errors Due to Residual Mechanical Positioning Errors at NBS (Δ-Probe)	49
6	Predicted Far Field Sidelobe Errors Due to NBS Instrumentation Inaccuracy and Open-Ended Waveguide Probe Scanning	51
7	Predicted AWACS Spectral Signal-to-Noise Ratios Due to Random Error of Digitizer Quantization Only	56
8	Induced Sinusoidal Z-Position Scanner Error Parameters	86
9	Predicted and Measured Sidelobe Error Ratios Due to Induced Scanner Z-Position Offsets When Scanning with Σ and Δ-Probes	86
10	Induced NF Receiver Amplitude Error Parameters	87
11	Predicted and Measured Random Noise Ratios for ULSA and AWACS Scanning with Three DESAT Probes	93
12	SCAT Spectral Error Due to Facility Room Scattering	94

Acknowledgements

This technology program has been initiated by the Office of Naval Research in order to advance the art of measuring low sidelobe antenna patterns. Probably the foremost facility in the United States for performing such research is operated by the Electromagnetic Division of the National Bureau of Standards in Boulder, Colorado. Mr. A. C. Newell of NBS has served as principal engineer at NBS during this study. He also led the team at NBS which first conducted near field scanning tests with a phased array antenna in 1972. This present undertaking has established the state-of-the measurement art for ultralow sidelobe antennas. The work of M. H. Francis and D. P. Kremer also at NBS has been instrumental to the success of this project. Mr. John Hoffman at TSC has performed nearly all of the test data processing and reduction as well as contributing innovative test design suggestions.

Kenneth R. Grimm

Kenneth R. Grimm

1.0 INTRODUCTION AND BACKGROUND

This report documents a unique Navy research project which has addressed fundamental measurement accuracy issues associated with antenna pattern testing for very low sidelobe antennas. In cooperation with scientists of the US National Bureau of Standards in Boulder, Colorado, TSC has successfully performed near field probe scanning experiments with ultralow sidelobe array antennas, as a phase II demonstration for the Defense Small Business Advanced Technology program (DESAT)*. The success of these tests is believed to have established the state of the antenna measurement art by near field scanning in the United States.

Purpose of Project

The intent of this project has been to certify by test the general relationships between sources of near field measurement errors and their resulting far field sidelobe pattern effects. This approach allows a prioritization of key measurement errors, extension of the known analytic tools for predicting far field error, and demonstration of useful (and possibly novel) error compensation techniques. Overall, the goal of the project has been to demonstrate the limits of measurement accuracy for testing low sidelobe antennas by planar near field scanning. The demonstration being reported herein was directed by the Office of Naval Research as a DESAT Phase II project, following a successful Phase I feasibility study conducted by TSC during 1982 [1].

A newly developed "nulling" probe has been shown to offer advantages for minimizing the far field effects of many sources of near field measurement errors. The new probe acts as a main beam wavenumber filter and reduces the far field error gain compared with scanning with a standard broad pattern probe. A description of probe design is given in Section 2.5.

---

*Exploratory development contract support provided by the Office of Naval Research under contract N00014-83-C-0671 to TSC and N00014-83-F-0180 to NBS.

Facility Description

All near field scanning tests were performed at NBS, Boulder Colorado between November 1984 and September 1985. The existing NBS planar probe scanner was modified to allow mounting of large aperture antennas. A set of floor rails was installed in the NBS range parallel to the fixed probe scanner, and the mounted array was then translated in sections in front of the scanner. This technique allows the merging of near field scan sections prior to transform processing, and is based on an earlier similar scanner design at Wright Patterson AFB [2]. The modification and operational use of the NBS scanner was provided as a government-furnished service for this DESAT project. It's enhanced capability to test antennas with dimensions up to 11m x 4m is an auxiliary benefit of this DESAT investigation.

Both a standard open-ended waveguide probe and the new "mainbeam nulling" probe were scanned on receive. The two test arrays (as well as the nulling probe) were provided under subcontract by Westinghouse Electric/Defense Electronics Systems Center. Both arrays are slotted waveguide travelling wave designs. The smaller array (Ultralow Sidelobe Array--ULSA) is approximately 1.2 ft x 16 ft, and is designed for 60 dB peak sidelobes in the azimuth plane. All results in this report are from probe scanning tests with this array. A second larger array tested extensively during this program is the brassboard model of the production AWACS array. The results of these tests are classified and are being reported separately, although several random error test results are reported in Section 4.5.

Probe Scanning Tests

Both one-and-two dimensional scans were measured for each array when the probe was receiving. Three probes were used at selected CW test frequencies in the S-band. Some test included repeated scans for both probe polarization orientations. The primary test objectives are described in [3], and included measurement of far field error magnitudes introduced by controlled near field scanning tolerances. Lastly, an original scanning experiment to measure small radar target bistatic scattering was conducted

to show feasibility of improved near field antenna measurement techniques for the more difficult problem of target-scattered near field measurement. This so-called "transition experiment" was an expansion to the original DESAT demonstration, and successfully measured the forward scattering of a small cylinder target placed between the AWACS array and the probe scanner. Test results for this RCS demonstration are presented in a separate classified memo [4]. Section 3.0 gives an analytic prediction of measurement accuracy expectations for these DESAT tests, and Section 4.0 summarizes test results with the ULSA array.

2.0 DESCRIPTION OF EXPERIMENT

Section 2.0 contains details of the near field scanning facility, the test array antennas, and the DESAT probes used during the scanning tests at NBS. Also included is description of the principal test issues, scanning procedures, and data processing procedures.

2.1 Facility Description

The pre-DESAT NBS Planar near field antenna range includes a fully automated probe scanner having an active region of 3.85m x 4.4m. Peak positioning errors anywhere in the scan plane have been measured to be less than $\pm$.005 inch, but are even less over smaller subregions. Typical NBS pattern measurement accuracies are 1.0 dB at the -40 dB far field level from all error sources, with measurement capability to the -60 dB level. Certification of these accuracies is by documented analysis. A minicomputer data acquisition system is used to perform probe motion control and data acquisition. The scanning is accomplished with continuous chain and DC motor. Probe transverse position is continuously LASER monitored. RF instrumentation includes standard microwave two channel receiver and a synchronized power-level RF source. This facility was used to perform the first near field phased array tests in the United States in 1973. Many additional test programs have since established the preeminence of this facility for pattern testing of directive microwave antennas.

The original planar NF scanner at NBS was modified in 1983 to allow the two dimensional scanning of antennas with maximum dimensions of 11m x 4m. Figure 1 shows a sketch of the modified scanner. It incorporates a fixed scan plane and a new test antenna mount which can translate to selected offsets in front of the fixed scanner. This technique allows "sectioned" scanning of antennas having a large horizontal aperture; however, it also introduces additional sources of measurement error which include at least mount repositioning tolerances and changing room scattering effects.

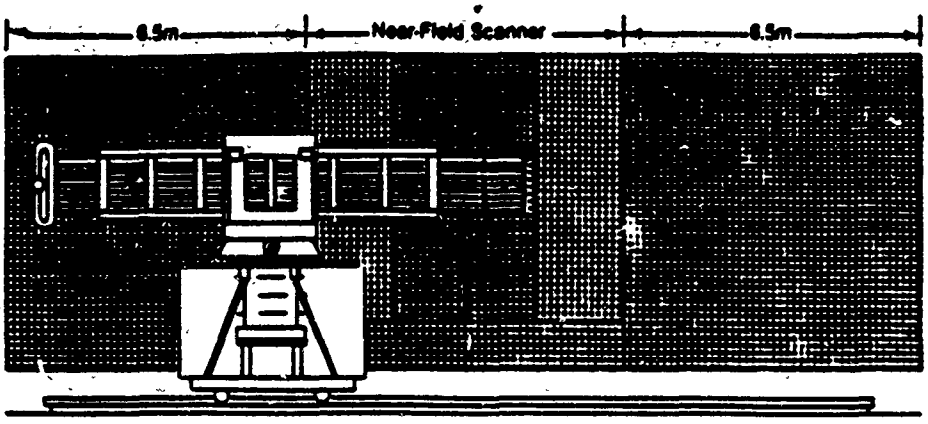

ANTENNA ON NEAR-FIELD SCANNER, POSITION 1

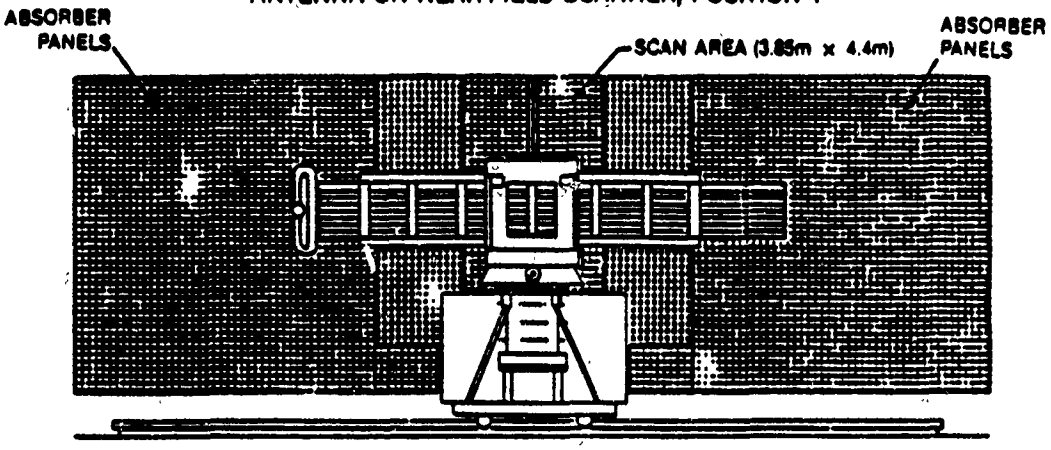

ANTENNA ON NEAR-FIELD SCANNER, POSITION 2

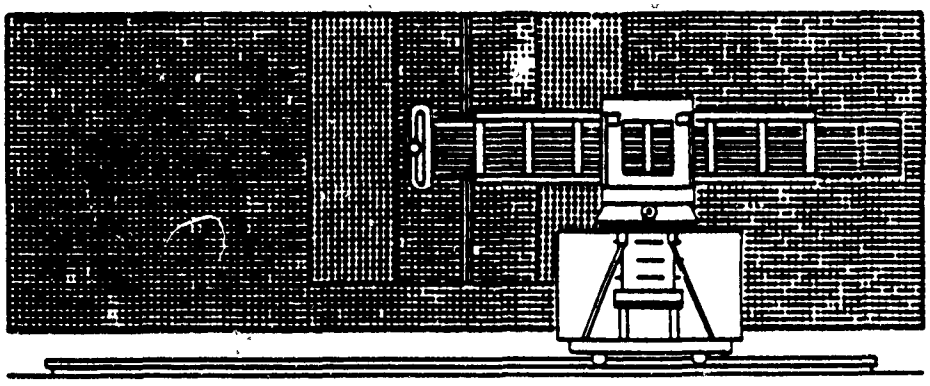

ANTENNA ON NEAR-FIELD SCANNER, POSITION 3

Figure 1. Schematic of ULSA Array Antenna in Three Positions Relative to the Fixed-Location DESAT Probe Scanner at NBS, Boulder, CO

Figure 2 is a simplified schematic of the optical monitoring equipments which are used to sense test antenna rotational offsets about the X, Y and Z axes · incurred during array translation. The precision levels detect rotational offsets of .002° or less about any axis. These angular errors are then manually corrected (levels rezeroed) by precisely adjusting the mount following each of its three translations. In this way, the inertial alignment of the large AWACS array to the probe scan plane can be guaranteed to within 0.004 inches in any linear axis. This represents positioning error no longer than that expected from the probe's own translation.

To minimize room scattering effects when the mount is translated, additional large anechoic fences and wall coverings were added to the existing facility. Nevertheless, room effects may introduce detectable NF measurement error in the modified facility. Therefore a unique test called SCAT was conducted as part of the overall testing program. During SCAT testing, the probe and the mount are translated in the X-direction synchronously. Then, repeated Y-scanning will measure the same NF, but for changing locations of the array throughout the quiet zone, i.e., along the X-axis. By averaging all such scans and comparing the average to each of the actual scans, a measure of NF repeatability error is determined. Although repeatability error may be due to any (or all) of the known NF random error sources, a significant contributor is due to room scattering. Results in Section 4.5 show that NF repeatability error averages about ±2 dB at the -40 dB level when testing the AWACS array with an open-ended waveguide probe. These NF errors, however, are insignificantly small for pattern sidelobes in the range -50/-60 dB following far field transform processing. Similarly, the delta probe has rather large repeatability error of about ±4 dB at the -40 dB NF signal level, but this error is again insignificant in the AWACS far field, following transform processing. Extensive details of the mechanical design modification of the scanner is available in [5].

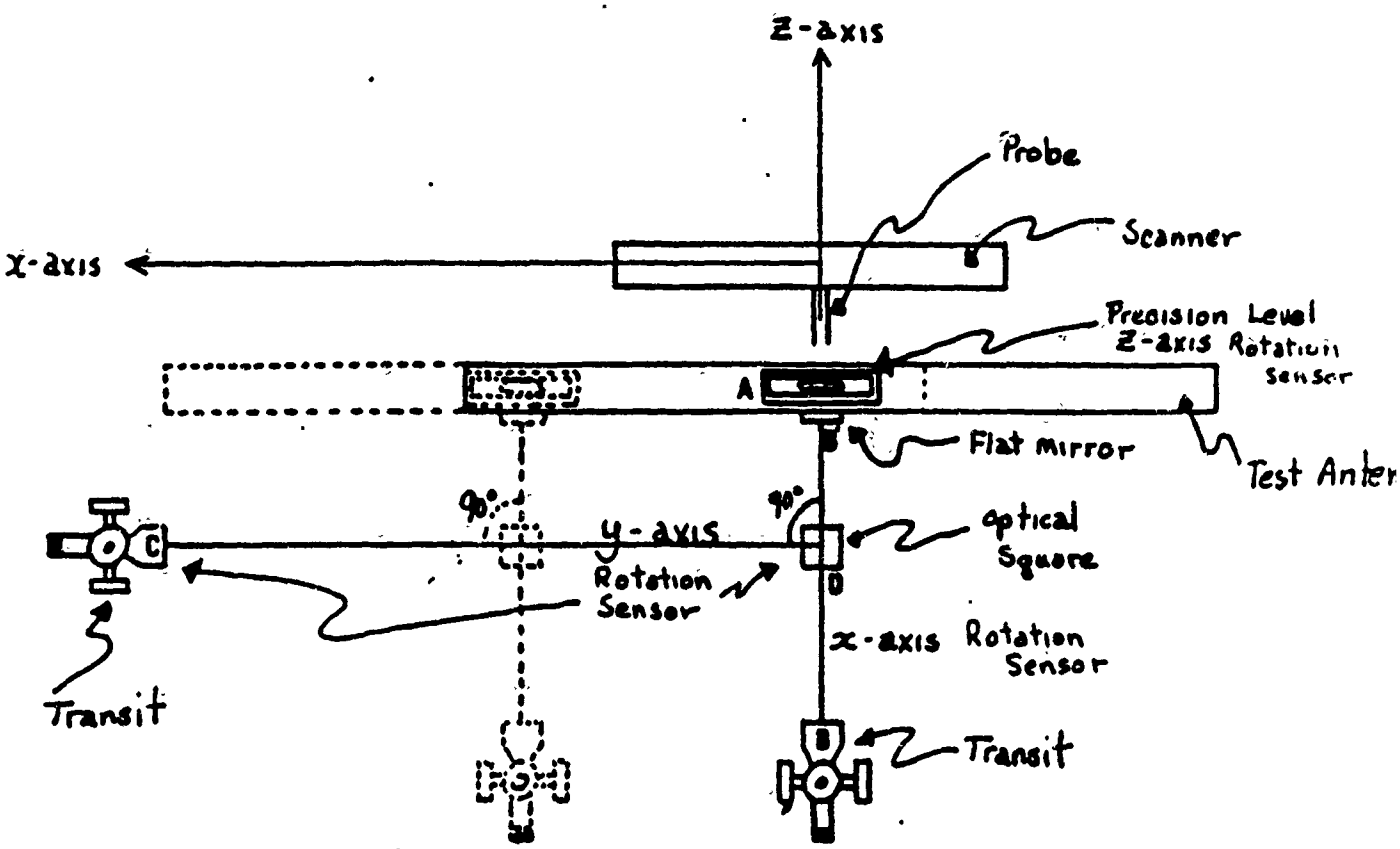

Figure 2. Location of Optical Auto-Collimator, Precision Levels, and Transits Used to Manually Correct for Rotational Misalignment of AWACS Array Following Translation During Sectioned Scanning

2.2 Test Issues

This section describes the antenna pattern measurement issues which were identified during the DESAT Phase I feasibility study, and which set the limit on achievable accuracy by near field scanning for an arbitrary antenna. In large part, these issues, summarized below, are the same issues studied experimentally during the original near field scanning tests with phased arrays in 1973 [6]. Interestingly, the 1973 tests were undertaken by the same NBS/TSC team now conducting the DESAT phase II demonstration, but for antennas which were then of only moderate sidelobe design. The present DESAT test arrays are believed to have sidelobes at levels as low as has ever been achieved at microwave frequencies.

2.2.1 Key Test Issues

During the course of DESAT phase I feasibility study, the known sources of NF measurement error were investigated in order to predict the probable and bounding far field sidelobe error. The Phase I investigation recommended that the following key test issues be addressed during Phase II::

- Scan area limitations
- Instrumentation accuracy
- Probe/array multiple scattering effects
- Probe-position error effects and sampling density
- Probe pattern effects.

The relationship between these forms of near field measurement error and their resulting far field effects are described in Section 3.0. The following testing blocks constituted the DESAT Phase II demonstration.

2.2.2 Block 1 Tests

Block 1 tests included preliminary tests necessary to insure that the DESAT array is adequately operating, mounted, and aligned with respect to the NF scanner, and that probe calibrations have been completed.

Test 1A - Mounting Certification

The DESAT test arrays were mounted on the modified array positioner and laterally translated right and left from a reference location. Centerline NF amplitude and phase data demonstrated the accuracy and repeatability of the proposed "scan-length-merging" sampling strategy. Both electrical and optical references defined the array and the probe coordinate system under translation. The ability to costeer the Δ-pattern probe null in the main beam pointing direction for both arrays at all frequencies was confirmed. Initial scan plane-to-array and scan plane-to-room multipath effects were measured.

Test 1B - Probe Pattern Calibrations

A series of far field probe pattern scans were measured in both polarizations at all frequencies and modes for which probe correction files were required. These data are pattern cuts in amplitude and phase formatted for use in the preprocessing computer program LPRINT. An index of these probe pattern files is included in Appendix A.1.

Test 1C - Pre-Test Preparation

All normal instrumentation calibration, initial multipath estimates, probe position reference tests, etc., was performed prior to the conduct of performance tests below.

2.2.3 Block 2 Tests

Block 2 events include tests needed to verify the predictions of sidelobe measurement accuracy made during DESAT Phase I feasibility study, and to resolve the key testing issues of this section.

Test 2 - Scan Length Certification

Technical Objective: This test certifies the predicted minimum probe scan length criterion by measuring the DESAT array FF sidelobe sensitivity to decreasing NF probe scan length, and by comparing these results to know scan length requirements and to previous results for moderate sidelobe arrays. Scan length restrictions that will produce sidelobe error of specified magnitude will be established by this test. The data reduction program SUMSQAV was used to analyze these data.

Test 3 - Sample Spacing Certification

Technical Objective: This test certifies the predicted FF sidelobe sensitivity due to various NF sample spacings (aliasing) in the scan direction. The data reduction program TESTSPAC or its equivalent was used to analyze these data.

Test 4 - Receiver Accuracy Certification

Technical Objective: This test certifies the predicted sidelobe error due to known receiver amplitude and phase conversion errors. Sidelobe pattern transform processing with and without induced receiver calibration errors have confirmed the expected FF sidelobe measurement sensitivity to NF voltage errors and has additionally shown the utility of the Δ-probe to discriminate against receiver error.

Test 5 - Multiplane Scanning

Technical Objective: This test measures the facility-unique reflectivity necessary to predict the worst-case and probable far field sidelobe error due to NF multipath. These degradations will be compared to bounding estimates confirmed during the Phase I study.

Test 6 - Probe Position Error Effects

Technical Objective: This test purposely corrupts measured NF data (assumed error free) by systematically offsetting the antenna mount in Z during probe scanning in X and Y. Such systematic Z-position errors will produce measureable low level echo error lobes at predicted angles and magnitudes.

Test 7 - Probe Pattern Accuracy

Technical Objective: This test is designed to show the sensitivity of sidelobe measurement accuracy due to the special features of the "Δ-probe" pattern. Intentional errors are introduced into the probe pattern, and their effect on transformed sidelobes were measured. These intentional errors included pattern null pointing offsets, null depth changes, and Δ-pattern shape differences, and controlled probe scattering. Results from test 7 scanning are not available at this writing.

2.2.4 Block 3 Tests

Block 3 DESAT tests were conducted during the expansion period, and attempted to apply low sidelobe antenna scanning techniques to the problem of small radar target bistatic RCS measurement using the AWACS array as the plane wave source illuminator. Previous demonstrations of bistatic RCS testing via NF probing have been conducted [7], but this DESAT block 3 test is the first to measure small target scattering in forward scatter geometries.

Test 8 - RCS Transition Experiment

Technical Objective: This test demonstrates the utility of the DESAT innovations (extended scanner size and Δ-pattern probe) to make very low radar target scatter measurements for amenable target geometries. RCS below -30 dBm^2 were measured in the near forward scatter directions for a simple body of revolution (cylinder).

2.3 DESAT Arrays

Two low sidelobe planar slotted waveguide test arrays were provided for this demonstration by Westinghouse Electric Defense Electronics Systems Center. Both the experimental Ultralow Sidelobe Array (ULSA) and the engineering face AWACS array were refurbished and beam pattern tested on the Westinghouse far field antenna range prior to their shipment to NBS, Boulder Colorado, in July 1984. Further description of these two antenna arrays is included below.

2.3.1 Ultra-Low Sidelobe Array (ULSA)

The S-band Ultra-Low Sidelobe Array is a rectangular planar array of eight equal-length slotted waveguides, fed at one end by a resonant waveguide manifold and terminated at the other end by high quality matched loads. The waveguide feed manifold has eight identical slotted T-junctions, fed in groups of four from each end of the vertical manifold waveguide which has a short circuit as its center. The ULSA has a rectangular aperture (16 ft by 1.2 ft), and is designed for a -60 dB Chebyschev azimuth plane sidelobe level with uniform illumination in elevation.

An ULSA azimuth pattern measured in 1978 at 3.025 Ghz is shown in Figure 3. In this pattern, three things are to be noted: (1) the main lobe is squinted off normal (toward the feed end) to an angle of -13°; (2) there is an anomalous lobe at $+44^{\circ}$ about 31 dB down; and (3) the wide angle sidelobe peaks are well below -50 dB.

After this array was refurbished, azimuth patterns were again measured at 2.9, 3.0, and 3.1 Ghz on the same Westinghouse outdoor far field range. The 3.0 Ghz pattern is plotted in Figure 4 which shows reasonable agreement with the 1978 pattern, particularly in terms of the wide-angle sidelobe levels. Note that the recent patterns were recorded in the opposite direction from that shown in Figure 3, i.e., the anomalous lobe is shown to the left of the main lobe instead of the right. A photograph of the ULSA array is shown in Figure 5 mounted for test at the NBS NF facility.

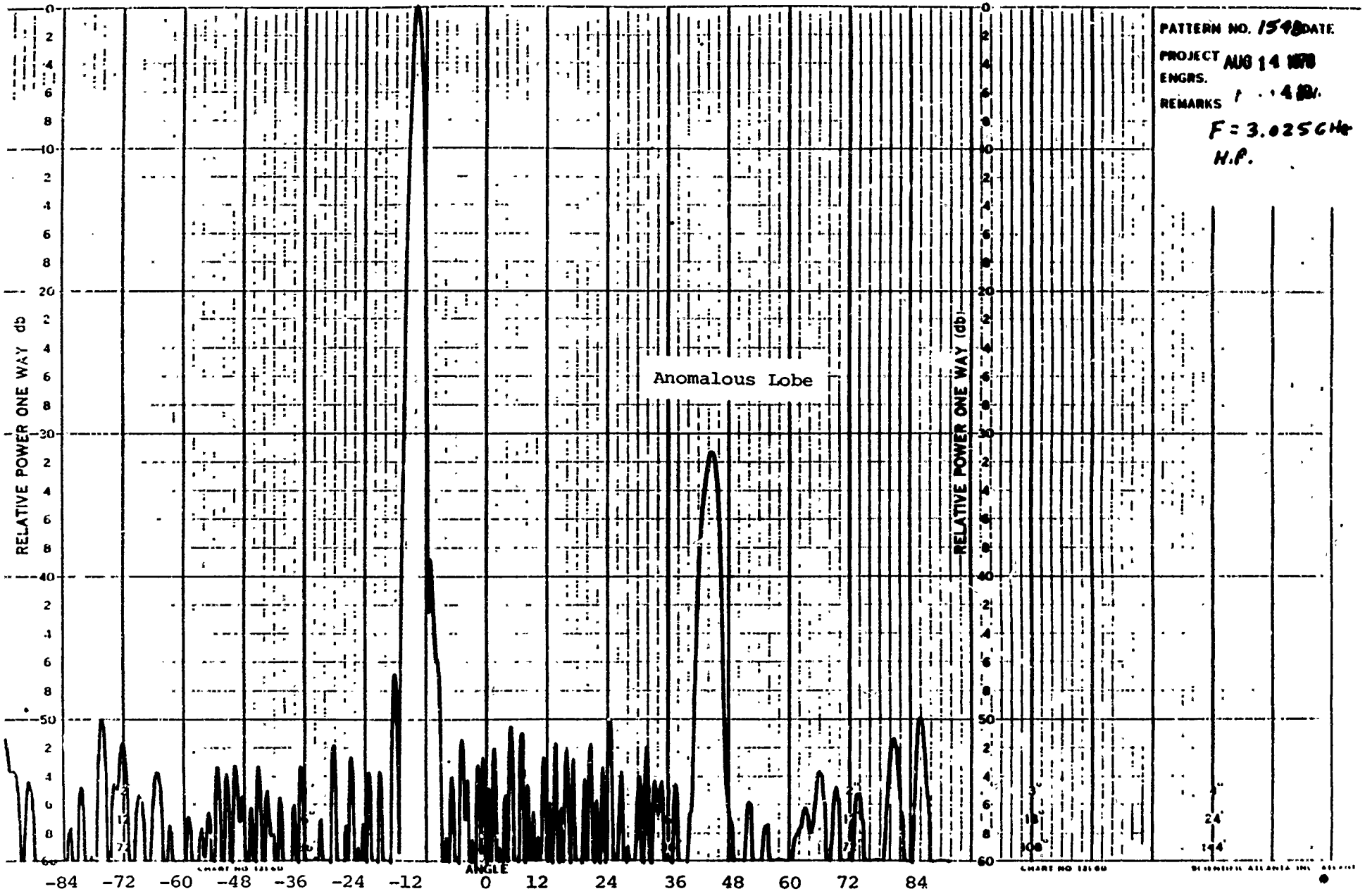

Figure 3. ULSA Array Azimuth Pattern at 3.025 Ghz Measured on the Westinghouse Far Field Antenna Range (1978)

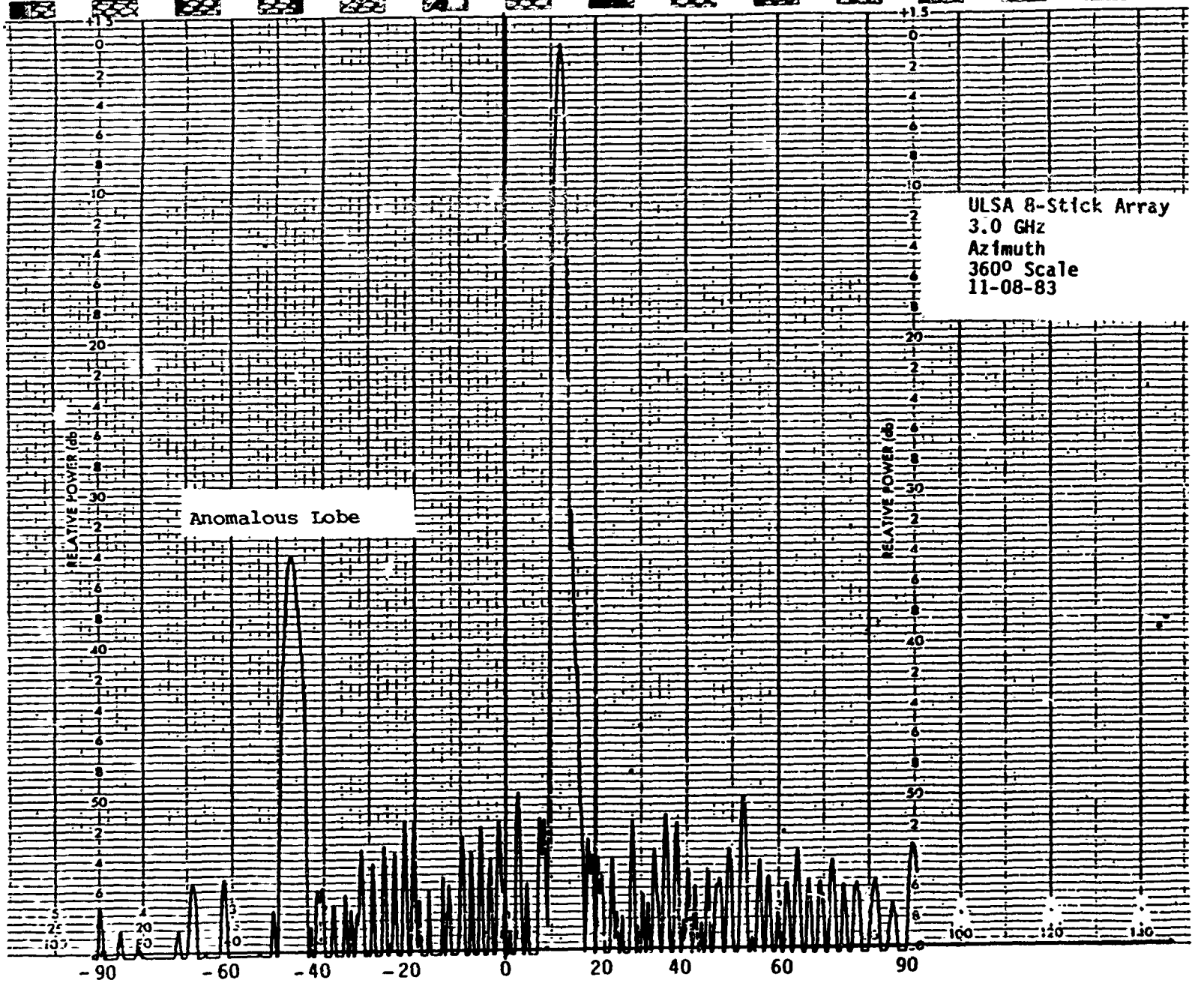

Figure 4. ULSA Array Azimuth Pattern at 3.0 Ghz as Measured Following Refurbishment, on the Westinghouse Far Field Range (1983)

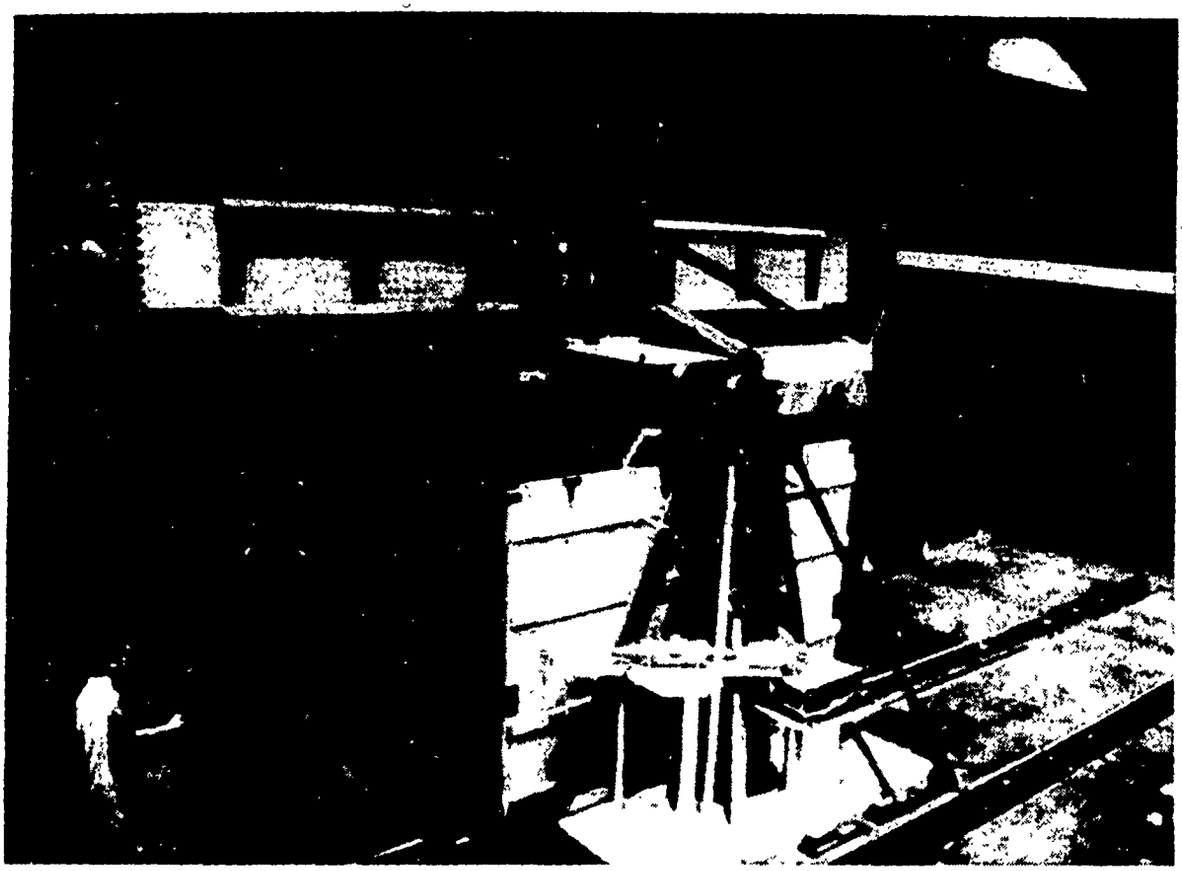

Figure 5. Photograph of ULSA Array Mounted for DESAT Scanning Tests at NBS, Boulder, CO

2.3.2 AWACS Engineering Face Array

The E-3A "test face" was built as an engineering prototype model of the production E-3A antenna. It has the same aperture dimensions (approximately 25 ft by 5 ft) and number of edge-slotted waveguides (28) as does the production antenna, but uses manually-driven "trombone" phase shifters instead of the electrically controlled fox phasers for elevation beam pointing. The azimuth pattern sidelobes of this array are actually slightly lower than those finally designed for the production array. This engineering model is ideally suited for the NF tests at NBS because it avoids the need for transporting and operating the bulky phase shifter drive circuits and liquid cooling system apparatus normally used with production AWACS antenna. The manual phase shifters can be adjusted for a single elevation beam pattern and locked for the NBS measurements.

2.3.3 Azimuth Squint Angles

The beam radiated by a traveling-wave fed slotted waveguide array (with alternating slot angles) is not normal to the array face, but is squinted to an angle off normal toward the feed end, given by:

$$\sin\theta = \lambda/2S - \lambda/\lambda g \qquad (1)$$

where λ is the free space wavelength, S is the slot spacing, and λg is the guide wavelength. This expression can be rewritten as:

$$\theta = \sin^{-1} [\lambda/2S - \sin (\cos^{-1} \lambda/2a)] \qquad (2)$$

where a is the inside wide dimension of the waveguide. Using this expression, the squint angles can be predicted for each frequency using a = 2.290 inches (WR-229) and S = 0.5λ. At 3.1 Ghz and 3.3 Ghz the squint angles are 30.58° and 22.05°, respectively. For the ULSA array, a different design was used, with a = 2.840 inches and S = 0.5315λ, yielding squint angles of 12.68° and 9.69° at 3.0 Ghz and 3.1 Ghz, respectively. DESAT test frequencies are f_1 = 3.0 Ghz, f_2 = 3.1 Ghz, f_3 = 3.3 Ghz. Figure 6 is a

photograph of the AWACS face array mounted for NF scanning tests at the NBS facility in Boulder.

2.4 Test Organization

The DESAT II test organization is shown in Figure 7. TSC had principal responsibility for the overall accomplishment of the Phase II demonstration. Engineering services performed by TSC include:

- Test Planning
- Sidelobe Error Estimation
- Probe Design
- Test Results Reduction and Analysis
- Reporting
- Applications Analysis

NBS Laboratories, Boulder, Colorado, performed all actual NF scanning, probe calibration, and testing services under the direction of the TSC engineering manager. In this way, the existing high quality NF test range at NBS was used as a Government Furnished Facility (GFF) during the DESAT II demonstration. Funding for NBS support was independently arranged by the Navy sponsor.

Westinghouse Defense and Electronic Systems Center in Baltimore operated as a TSC subcontractor. They provided array rework and certification services for both of the Westinghouse-owned AWACS and ULSA arrays. Westinghouse also built the TSC-designed Δ-probes.

2.5 Probe Design

A fundamental measurement task during this program was to evaluate the ability of a new class of near field measurement probes designed specifically for testing ultralow sidelobe antennas. The new probe has the property of reducing the effect of many NF scanning error sources by artifically minimizing the gain of the peak coupling product during test. Such a probe may be thought of as a spatial filter, improving the accuracy of

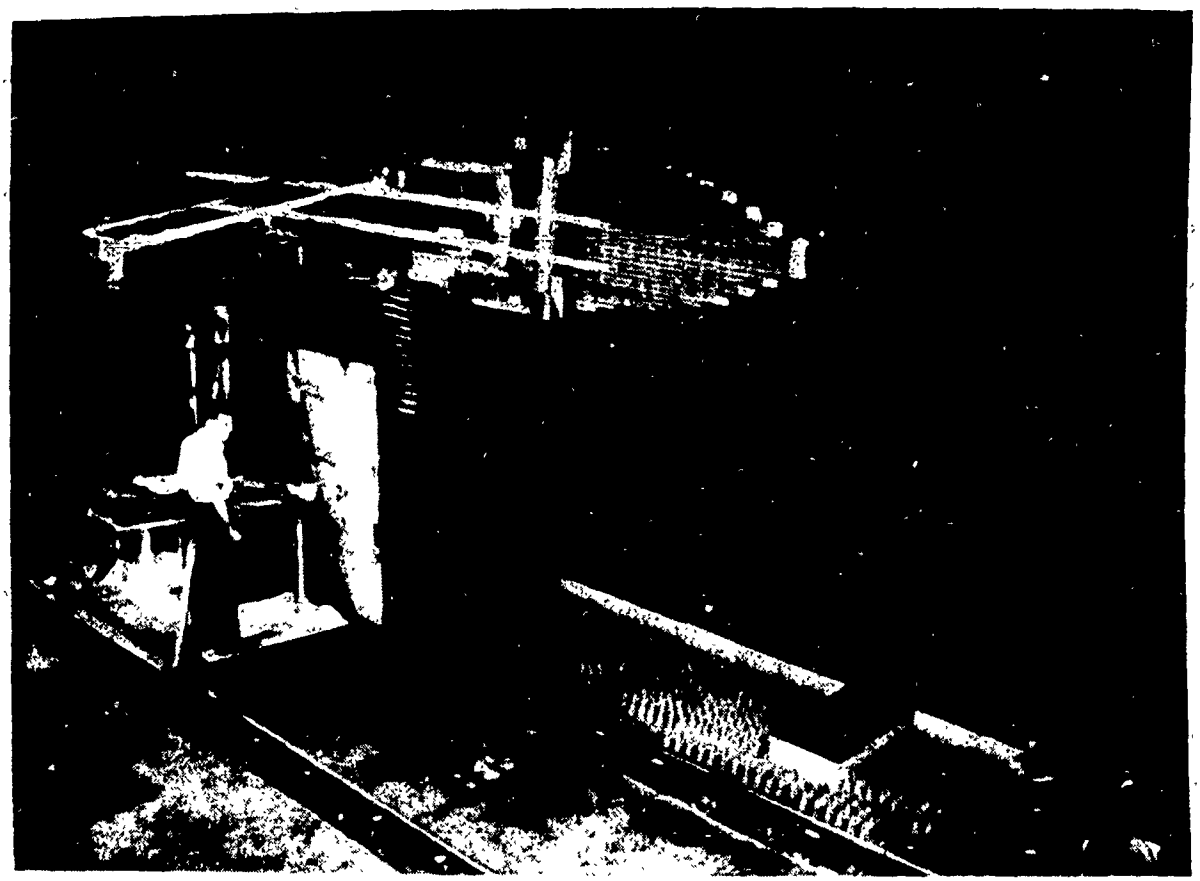

Figure 6. Photograph of AWACS Face Array Mounted for DESAT Scanning Tests at NBS, Boulder, CO

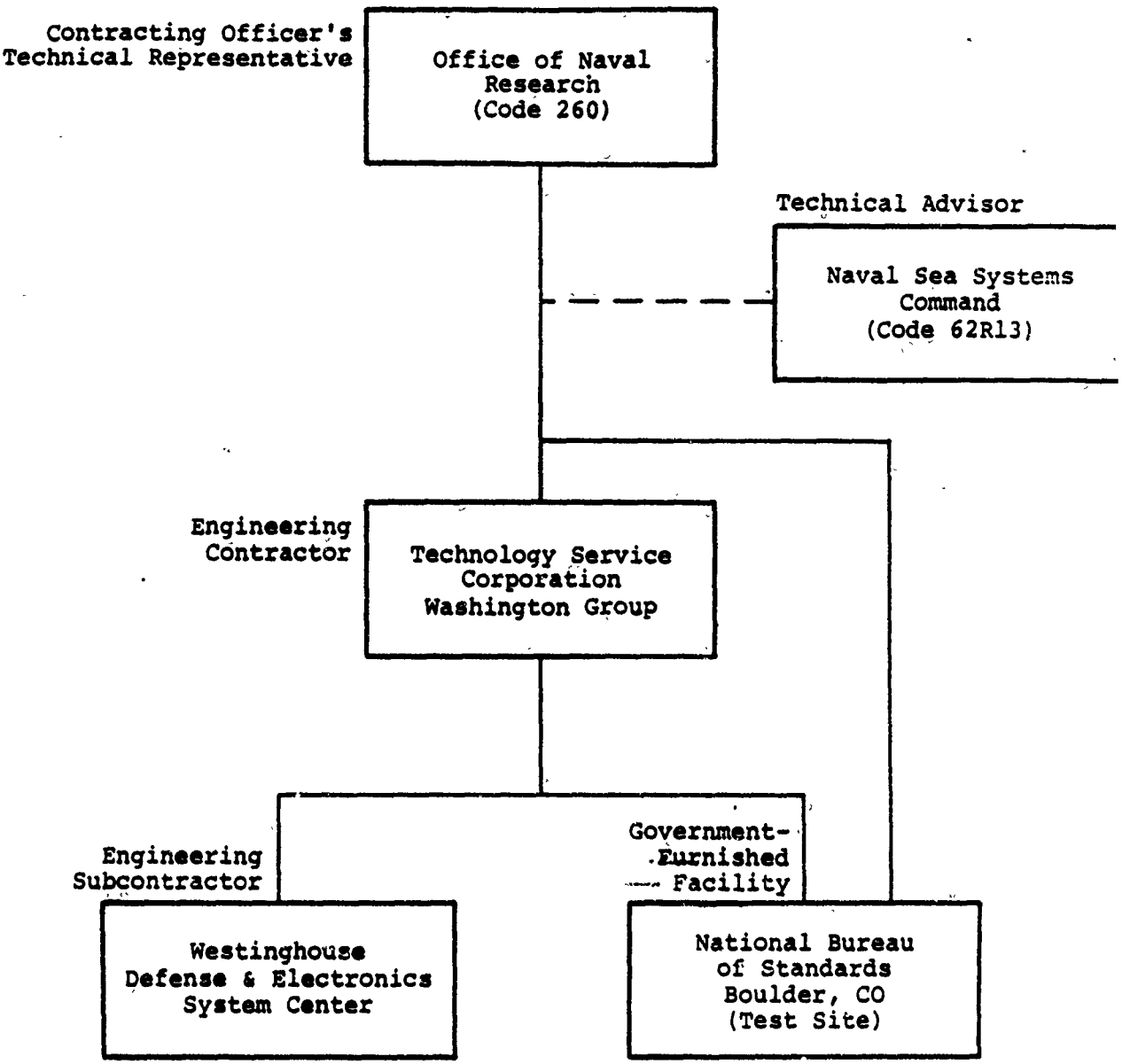

Figure 7. DESAT Phase II Testing Organization

measuring the test antenna's spectrum in the band pass (sidelobes), at the expense of measurement inaccuracy in the mainbeam region (stopband). The following section reviews the design of this new probe.

Wavenumber-Filtering Probes

All planar near field measurements are based on the transmission equation written by Newell [8] as:

$$b_0(\underline{P}) = C \int \underline{s}_{02}(\underline{K}) \cdot \underline{t}_{10}(\underline{K}) e^{i\gamma d} e^{i\underline{K}\cdot\underline{P}} d\underline{K} \qquad (3)$$

where:

$\underline{s}_{02}(\underline{K})$ is the probe pattern receiving characteristics,

$\underline{t}_{10}(\underline{K})$ is the sought test antenna transmitting characteristics,

γ z-component of the propagation vector,

$\underline{P}$ is the probe position vector,

$\underline{K}$ is the transverse wavenumber vector, $k_x\underline{e}_x + k_x\underline{e}_y$,

d is the separation distance between NF plane and test antenna, and

C is a complex constant.

What is measured is $b_0(\underline{P})$, which by an FFT inversion of equation (3), yields the band limited coupling product, $D'(\underline{K})$ written as

$$D'(\underline{K}) = \underline{s}_{02}(\underline{K}) \cdot \underline{t}_{10}(\underline{K}) e^{i\gamma d}$$

$$\text{where} \quad \gamma = \left[(k)^2 - (k_x^2 + k_y^2)\right]^{1/2} \qquad (4)$$

$D'(\underline{K})$ is band limited most usually by the selection of sample spacing δ_x and δ_y, such that $k_1 \leq \pi/\delta_x$ and $k_2 \leq \pi/\delta_y$. The exponential $e^{i\gamma d}$ in equation (4) weights (or filters) the product $\underline{s}_{02}(\underline{K})\ \underline{t}_{10}(\underline{K})$ when γ is imaginary and d is non-zero. Thus D'(K) becomes negligibly small whenever $k_{x'y} \geq k_{1,2}$ except

when multipath or other periodic measurement errors produce systematic lobes in the evanescent spectrum.

The factor $e^{i\gamma d}$, however, is not the only band limit operating in equation (4). If either the probe spectrum, $\underline{s}_{02}(\underline{K})$, or the test antenna spectrum itself, $\underline{t}_{10}(\underline{K})$, or their dot product, is negligingly small in a given band region, then the coupling product, $D'(\underline{K})$, is practically cut off for those values of $\underline{K}$ regardless of the sample spacings selected. By designing a probe which imposes a stop band centered on the test antenna's main beam, the remaining field of view, i.e., the sidelobe region, can be measured with minimum mean square error. Thus, we seek a probe whose pattern $\underline{s}(\underline{K})$ minimizes the sidelobe region measurement error, only, i.e.,

$$\epsilon = \text{Min} \int \underline{t}(\underline{K}) - \underline{t}(\underline{K})\ \underline{s}(\underline{K}) * \underline{p}(\underline{K})\ d\underline{K} \qquad (5)$$

where $\underline{t}(\underline{K})$ is the true spectrum of the test antenna,

$$\underline{s}(\underline{K}) = \begin{cases} \text{probe pattern} \\ 1 \quad K_c \leq \underline{K} \leq K_{max} \quad \text{(sidelobes)} \\ 0 \quad 0 \leq K \leq K_c \quad \text{(mainlobe)} \end{cases}$$

$\underline{p}(\underline{K})$ is the spectral transform of the sampling window, and

$*$ indicates convolution

The ideal wavenumber filter for low sidelobe testing is sketched in Figure 8. Its bandstop is exactly matched to the main beam null-to-null width, but it is of course non-realizable. A simple approximation to the ideal wavenumber filter is also sketched in Figure 8 as an overlay pattern radiated by a simple 2-element waveguide probe having anti-phased elements. The new probe imposes a spectral wavenumber filter during NF scanning which approximates the ideal wavenumber filter as long as its null direction is coincident with the test antenna's main beam steering angle. K_{max} is the evanescent band region limit, and K_c corresponds to the test antenna's first

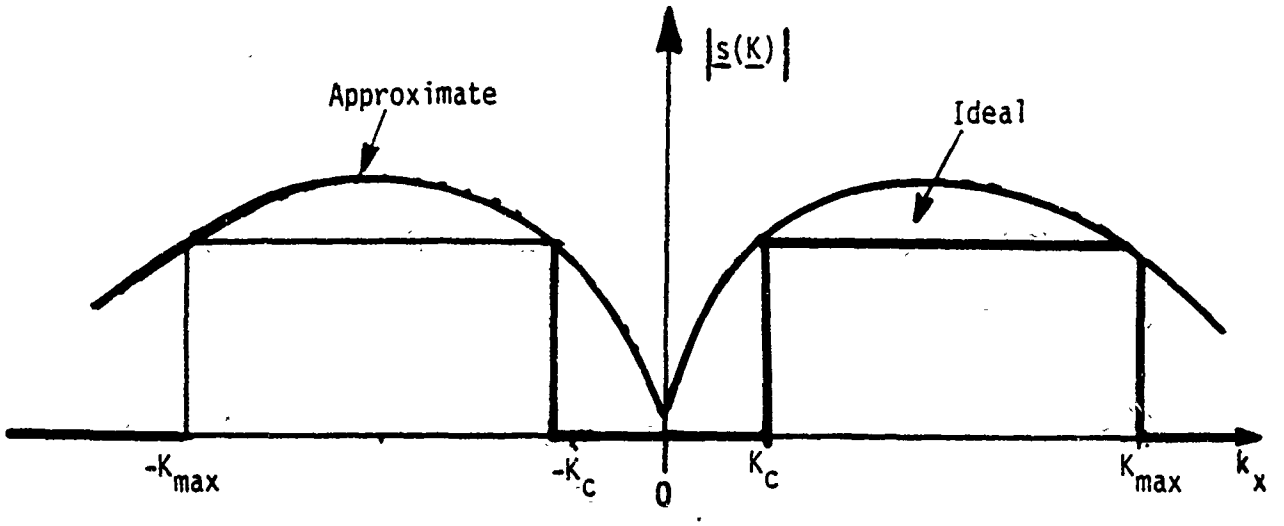

Figure 8. 2-Element Waveguide Probe Response Overlayed on the Ideal Wavenumber Filter Response for Low Sidelobe Testing

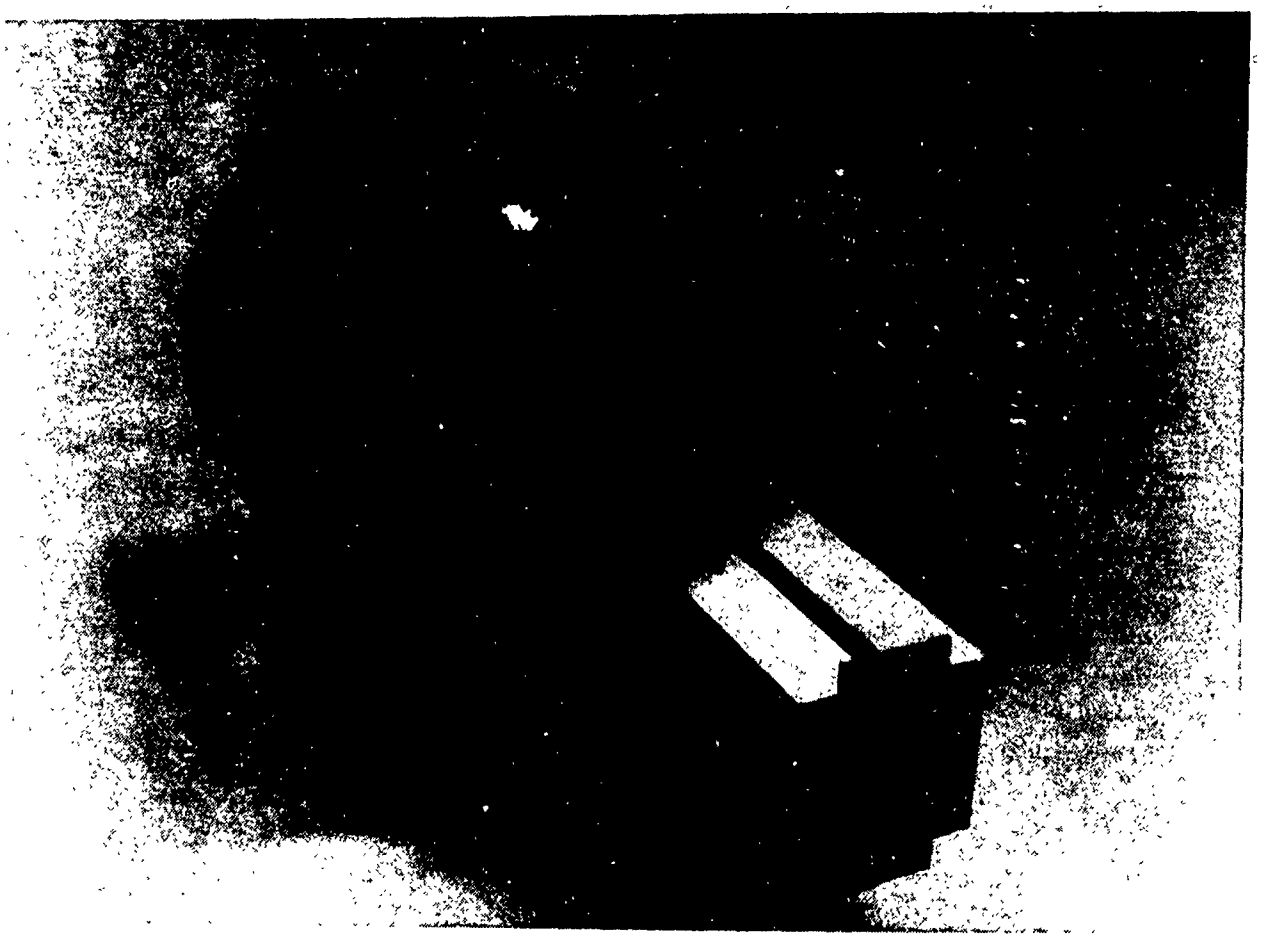

Figure 9. Photograph of the New 2-Element Waveguide Probe Which Approximates the Ideal Mainbeam Filter Response

null locations. A photograph of one of three such Δ-probes built for this DESAT project is shown in Figure 9.

A second probe design criterion requires that its directivity within the passband, i.e., in the sidelobe spectrum, also be "matched" to the available scan length. Huddleston has shown that the "matched" probe directivity most concentrates its near field response over the available scan area, and thereby maximizes the measure of the radiated power intercepted by the finite scanner [9]. This criterion is written as:

$$\int \left|v(x,y)\right|^2 \, dxdy = P\,(1-\epsilon^2_{xy}) \qquad (6)$$

where $v(x,y)$ is the NF probe voltage measured in the scan area,

P is the total power radiated by the test antenna in the forward hemisphere, and

ϵ^2_{xy} is the fraction of power not intercepting the finite scan plane.

The new 2-element delta-probe in Figure 9 simultaneously satisfies probe design criterion for both optimum directivity (approximately) in equation (6), and the new criterion for wavenumber filtering in equation (5). Results of tests at NBS with the ULSA and AWACS arrays demonstrate the improved measurement accuracy for the sidelobes (but not the main beam) afforded by the new delta probe. Additional tests were also conducted with the new probe when its elements were combined in-phase. This probe has been called the Σ probe. Overlays of both the Σ and Δ-probe patterns as used to measure the ULSA array azimuth plane pattern are shown in Figure 10.

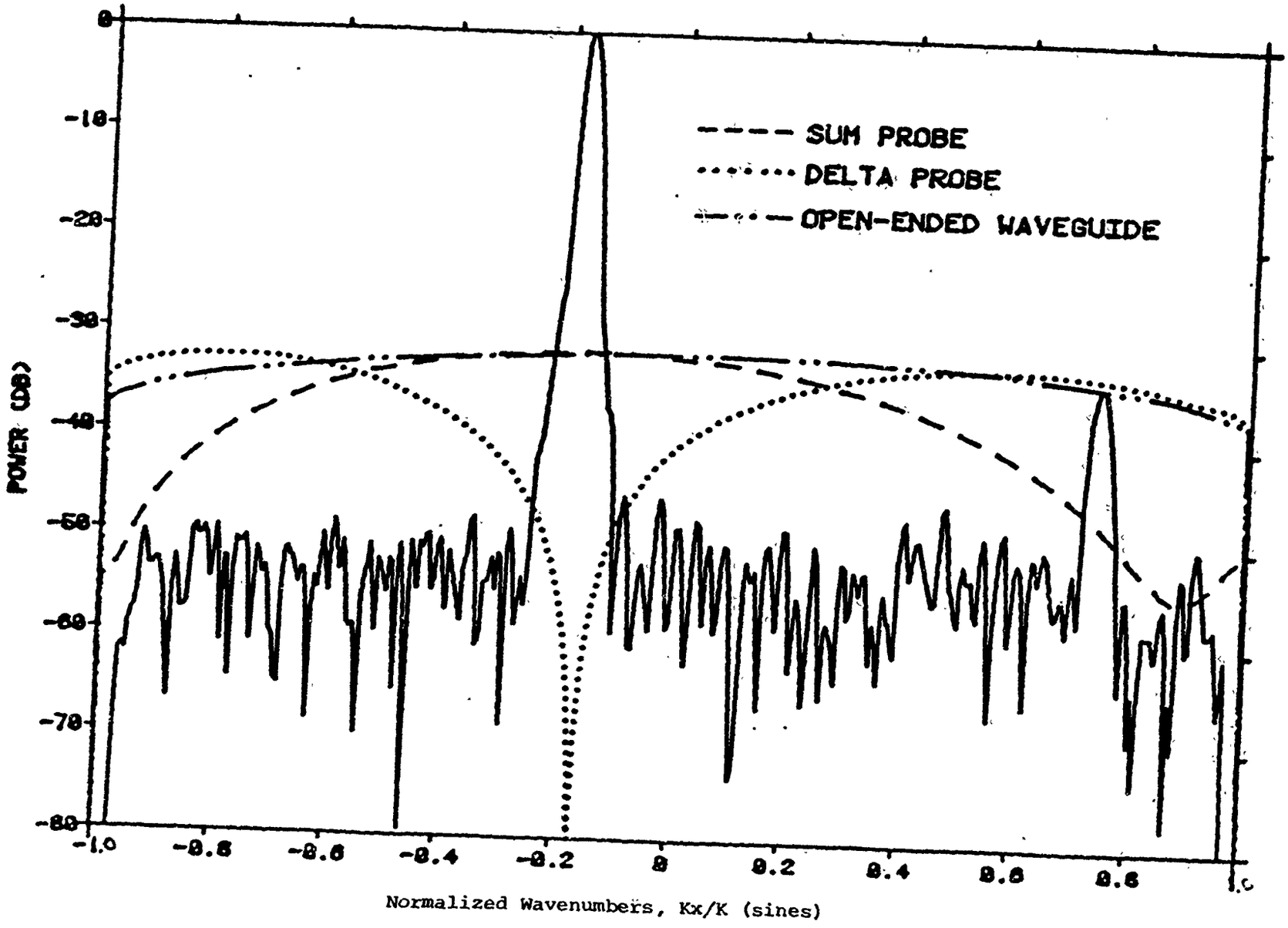

Figure 16. DESA Azimuth Plane Pattern as Measured by both the $\sum$-Probe (mainbeam) and the Δ-Probe (Sidelobes) During DESAT Testing at NBS (3.1 Ghz)

3.0 MEASUREMENT ACCURACY EXPECTATIONS

This section applies known NF measurement accuracy models to the estimation of far field sidelobe errors for the DESAT arrays as measured on the NBS scanner. Section 3.1 discusses a unique test called SCAT which quantifies the effect of random room scattering as a fundamental and noncompensatable source of low sidelobe measurement error. Section 3.2 gives analytic estimates for all other sources of NF measurement error.

3.1 Room Scattering Errors - SCAT

A new NF scanning test, called SCAT, measures the errors on low sidelobe patterns introduced by uncontrollable random room scattering. The test is based on repeating the same NF scan as both the array mount and the probe tower are stepped synchronously through the quiet zone. A full description of its procedure and results are given in this section.

3.1.1 Purpose

The purpose of the SCAT tests is to determine the level and character of the signals scattered by the room and subsequently received by the probe, since the DESAT arrays must be scanned in sections.

If we want to test for the effects of multiple reflections we must fix the probe and antenna in X and Y, and move the antenna (or the probe) in Z. The SCAT test is like the multiple reflections test in that a change is made to the measurement system in order to expose the effect of a single error source (here room scattering).

Conceptually we want to fix the X-Y-Z position for both the probe and antenna and move the room. Changes in signal are then due to room scattering. This can be accomplished by moving both the probe and antenna together relative to the room (see Figure 11).

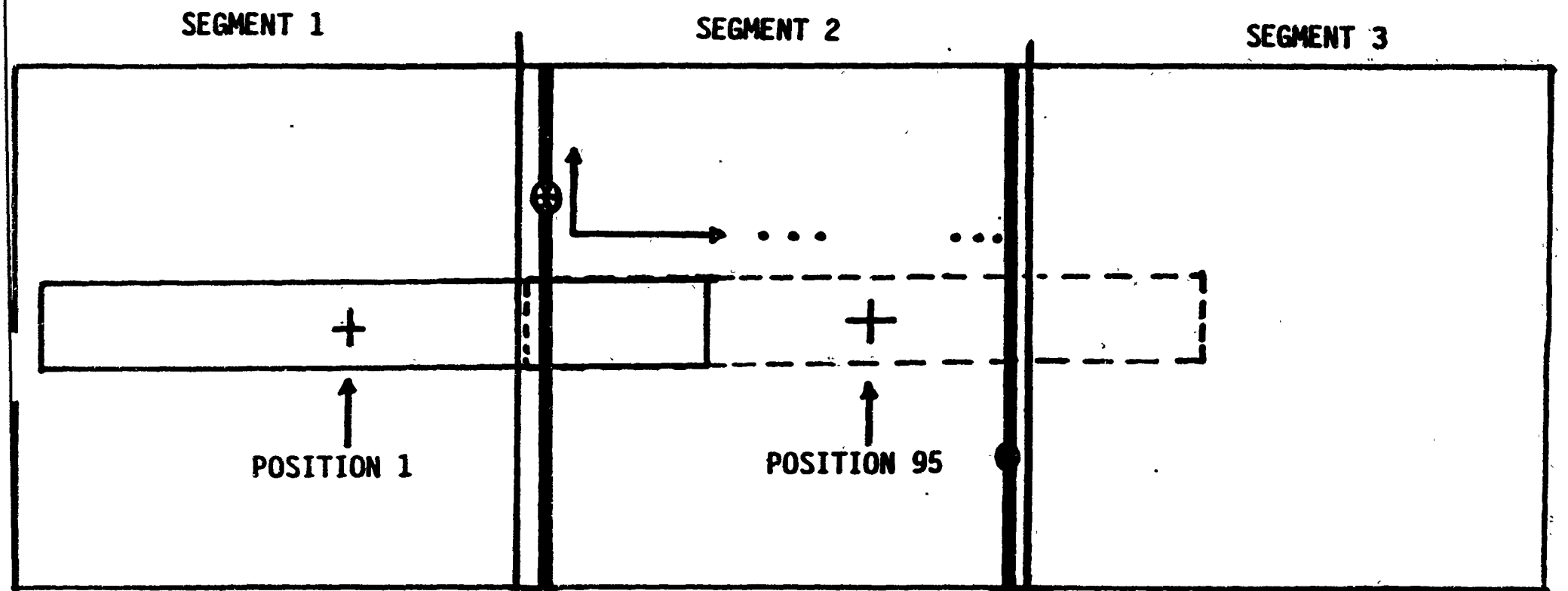

Figure 11. Schematic of Moving Array SCAT Test Used to Quantify Room Scattering Errors Prior to DESAT Array Testing at NBS

3.1.2 Analysis

Figure 12 gives a geometry sketch for SCAT testing analysis. The x-coordinate of the antenna origin relative to the room is represented by X_R and the x and y coordinates of the probe relative to the antenna origin are represented by x_a and y_a. Then writing the measured data as a sum of the error free data plus the error terms, the following equation is obtained:

$$B_m (X_R, x_a, y_a) = B (x_a, y_a) + \sum_{n=1}^{17} \epsilon_n (X_R, x_a, y_a) \qquad (7)$$

where B_m is the measured near-field data, B the error free near-field data and ϵ_n the error term due to error source number n in Table 1.

The errors fall into four natural groups:

(1) errors which are constant and independent of X_R, x_a, y_a are represented by ϵ_c; error sources 1, 3, 4, 15, and part of 2 fall into this category;

(2) errors which are the same for every scan, that is they are independent of X_R and for a fixed x_a depend only on y_a, will be symbolized by $\epsilon_y (x_a = x_o, y_a)$; errors 5, 7, 8, 9, 13, 14a, 14b, 17 and the part of 11 and 12 due to the position error of the y-rails are in this category;

(3) errors which are a function of X_R only are represented by $\epsilon(X_R)$; errors in this category are 6, 14c, the part of 11 and 12 due to the probe x-rails and the antenna tower rails;

(4) errors which are be different at every data point; these will be symbolized by $\epsilon_R (X_R, x_a, y_a)$ for random errors (error 16) and $\epsilon_S (X_R, x_a, y_a)$ for room scattering errors (error 10).

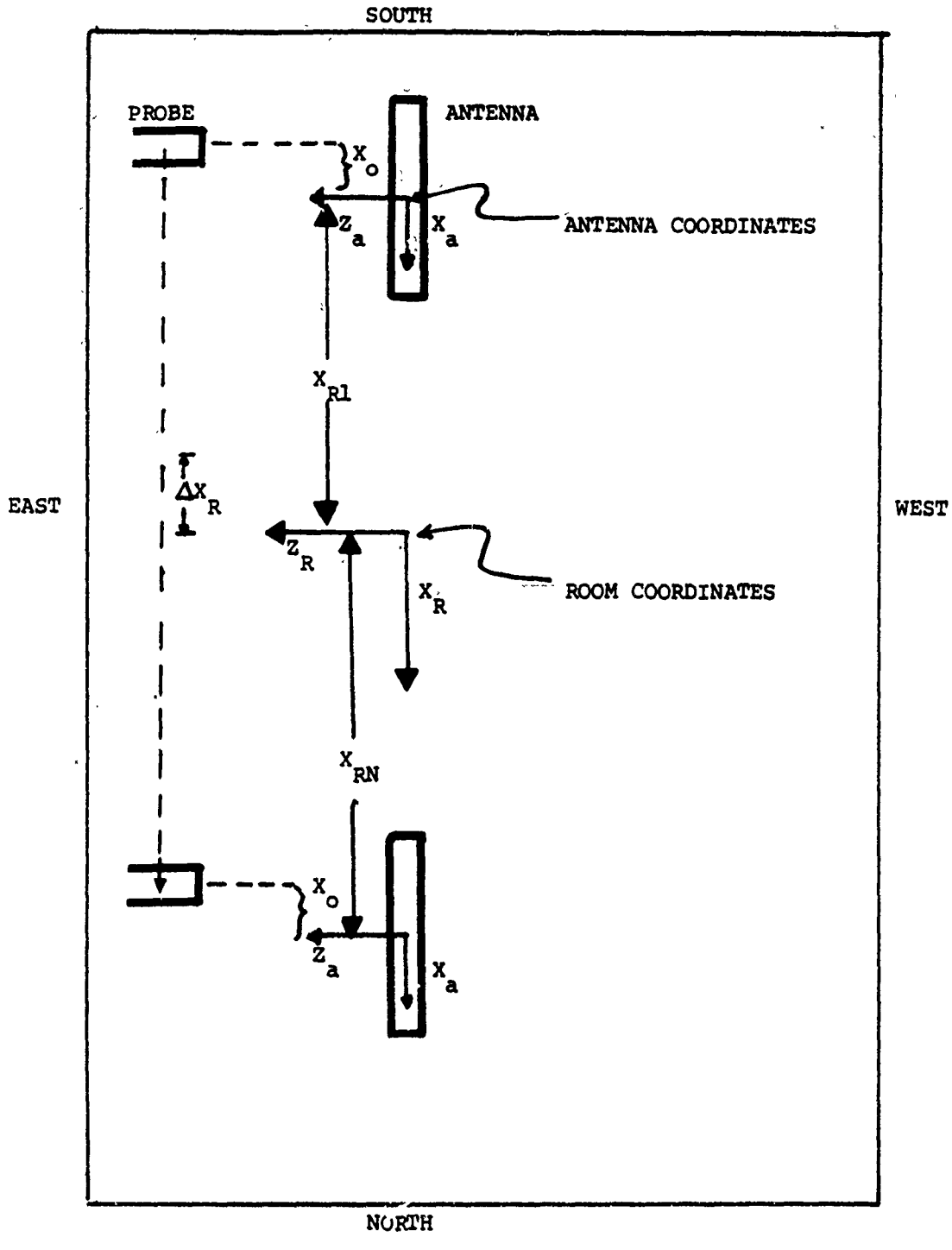

Figure 12. Illustration Showing How the Probe and Antenna are Moved Simultaneously Relative to the Room During SCAT Testing

Table 1. Error Sources in Planar Near-Field Measurements

Source of Error	Group	Group Error Type
1. Probe Gain Measurement	1	Constant with Step or Scan
2. Probe Relative Pattern	1	
3. Probe Polarization Ratio	1	
4. Normalization Constant	1	
5. Probe Alignment Error	2	Constant with Step
6. Antenna Alignment Error	3	Constant with Scan
7. Measurement Area Truncation	2	
8. Data Point Spacing (Aliasing)	2	
9. Multiple Reflections	2	
10. Room Scattering	4	Random in Scan or Step
11. Probe x-y Position Errors	2,3	
12. Probe z-Position Errors	2,3	
13. Receiver Amplitude Non-Linearity	2	
14. System Phase Error Due to:		
(a) Receiver Phase Errors	2	
(b) Flexing Cables/Rotary Joints	2	
(c) Temperature Effects	3	
15. Impedance Mismatch Factor	1	
16. Random Errors in Amplitude/Phase	4	
17. Leakage and Crosstalk	2	

Thus, equation (7) can be written in the form

$$B_m (X_R, x_o, y_a) = B (x_o, y_a) + \epsilon_c + \epsilon_y (x_o, y_a) + \epsilon(X_R) + \epsilon(X_R, x_o, y_a) + \epsilon_S(X_R, x_a = x_o, y_a) \quad (8)$$

3.1.3 Measurement Process

First, a fixed x-position is chosen for the probe in the antenna coordinate system, that is $x_a = x_o$ = constant. Second, the probe is moved in the y-direction for a y-scan (in the direction perpendicular to the paper in Figure 12) and $B_m (X_{R1}, x_a = x_o, y_a)$ is measured. Figure 13 shows a sample result (on a dB scale) for such a scan. The antenna and probe are then both moved by an amount ΔX_R. A second y-scan is performed to measure $B_m (X_{R2}, x_a = x_o, y_a)$. This second scan would be the same as the first if there were no sources of error. Two such scans are overplotted on a linear scale in Figure 14. The antennna and probe are moved across the room together and y-scans taken at intervals of $\Delta X_R \leq \lambda/2$ until the desired portion of the room is covered.

3.1.4 SCAT Data Processing

The goal of the data processing is to obtain an estimate of the effect of the room scattering on the far field. Averages with respect to X_R and y_a are obtained and manipulated with equation (8) so as to subtract out the effects of all terms except those due to the random errors, ϵ_R, and those due to the room scattering ϵ_S.

In order to correct for the errors due to $\epsilon(X_R)$, a weighted difference between the first scan and each subsequent scan is computed. The weight used is the amplitude squared of the appropriate point in the first scan. Thus,

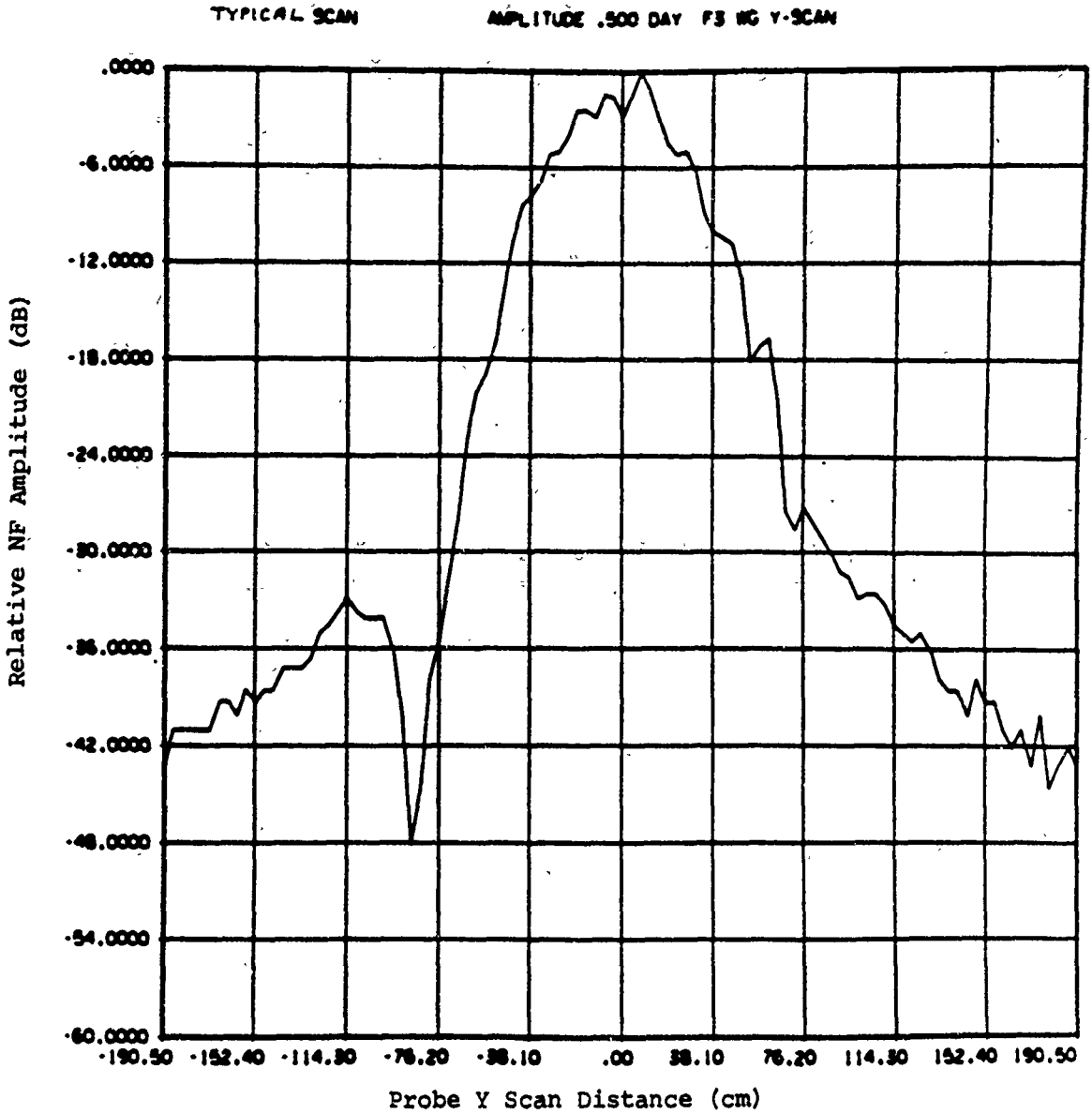

Figure 13. Measured NF Amplitude for a Y-Scan with ULSA Array at Coordinate X_{R1} for SCAT Testing Using the Open-Ended Waveguide Probe

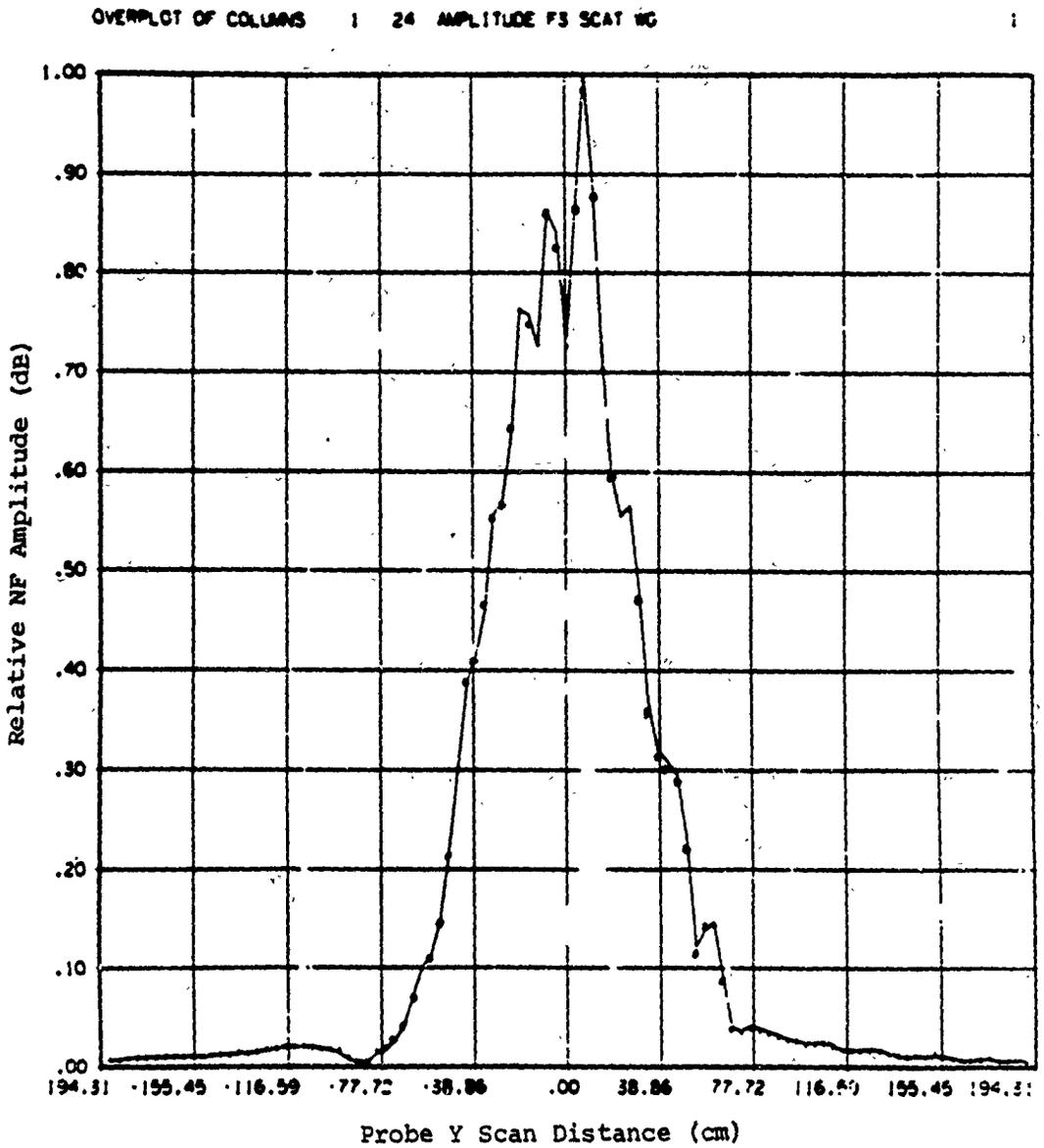

Figure 14. Comparison of Measured NF Amplitude for Y-Scans With the ULSA Array Located at X_{R1} (Solid) and then Translated to X_{RN} for SCAT Testing Using the Open-Ended Waveguide Probe

$$\frac{\sum_{n_y} (B_m(X_{R1}, x_o, y_a) - B_m(X_{R2}, x_o, y_a)) |B_m(X_{R1}, x_o, y_a)|^2}{\sum_{n_y} |B_m(X_{R1}, x_o, y_a)|^2} = \epsilon(X_{R1}) - \epsilon(X_{R2})$$

$$+ \bar{\epsilon}_S(X_{R1}, x_o) - \bar{\epsilon}_S(X_{R2}, x_o) + \bar{\epsilon}_R(X_{R1}, x_o) - \bar{\epsilon}_R(X_{R2}, x_o) \tag{9}$$

$$\text{where } \bar{\epsilon}_1(X_{R1}, x_o) = \frac{\sum_{n_y} \epsilon_1(x_o, y_a) |B_m(X_{R1}, x_o, y_a)|^2}{\sum_{n_y} |B_m(X_{R1}, x_o, y_a)|^2}$$

By adding the results of equation (9) to each y-scan, the errors due to $\epsilon(X_R)$ are eliminated.

This result is represented by $B'_m(X_{R2}, x_o, y_a)$. The next step is to average over X_R to obtain an average scan:

$$\langle B'_m \rangle (x_o, y_a) = \frac{\sum_{n_x=1}^{N_x} B'_m(X_R, x_o, y_a)}{N_x} \tag{10}$$

At this point, to correct for ϵ_c and $\epsilon_y(x_o, y_a)$ and to eliminate $B(x_o, y_a)$, the average scan $\langle B'_m \rangle$ is subtracted from each of the individual scans in order to obtain the scan residuals containing only the random errors and the scattering. The residuals, $\delta(X_R, x_o, y_a)$, can be written as:

$$\delta(X_R, x_o, y_a) = B'_m(X_R, x_o, y_a) - \langle B'_m \rangle (x_o, y_a) \tag{11}$$

$$= \epsilon_R(X_R, x_o, y_a) - \bar{\epsilon}_R(X_R, x_o) - \langle \epsilon_R \rangle (x_o, y_a) + \langle \bar{\epsilon}_R \rangle (x_o)$$

$$+ \epsilon_S(X_R, x_o, y_a) - \bar{\epsilon}_S(X_R, x_o) - \langle \epsilon_S \rangle (x_o, y_a) + \langle \bar{\epsilon}_S \rangle (x_o)$$

where < > represents an average over X_R in the same manner as that used to obtain $\langle B'_m \rangle$. A sample residual for $\delta(X_R, x_a = x_o, y_a)$ is shown in Figure 15. The highest peak in this pattern is about 39 dB below the peak of the near-field data.

By doing a Fourier transform of δ one obtains an estimate of the effect of the SCAT residuals on the far field. An example of this is shown in Figure 16 where the peaks are at about -70 dB relative to the peak of the far field. This SCAT spectrum is random, and there are no well-formed lobes which could be generated by correlated room scattering sources. Based on this original analysis and test results, it is demonstrated that no detectable systematic scanning errors will be introduced when scanning the DESAT arrays in sections. It is also shown that uncorrectable (random) errors due to room scattering are at least 70 dB below the peak test antenna gain, and although acceptably small, do represent a fundamental measurement accuracy limit at NBS.

3.2 Probe-Parameter Errors (Group 1)

This section summarizes known error models for estimating the far field errors in the test antenna's pattern due to tolerances in the probe far field pattern calibration. These errors are classified as Group 1 in Table 1, and their effect is constant with scan motion.

3.2.1 Theory of Probe Pattern Error

Newell has shown that the test antenna's transmitting coefficients, t_m (main component), and t_c (cross component) are given by [8]:

$$t_m(\underline{K}) = \frac{\dfrac{D'(\underline{K})}{S'_m(\underline{K})} - \dfrac{D''(\underline{K})\rho'_s(\underline{K})}{S''_c(\underline{K})}}{1 - \rho'_s(\underline{K})/\rho''_s(\underline{K})} \qquad (12a)$$

and

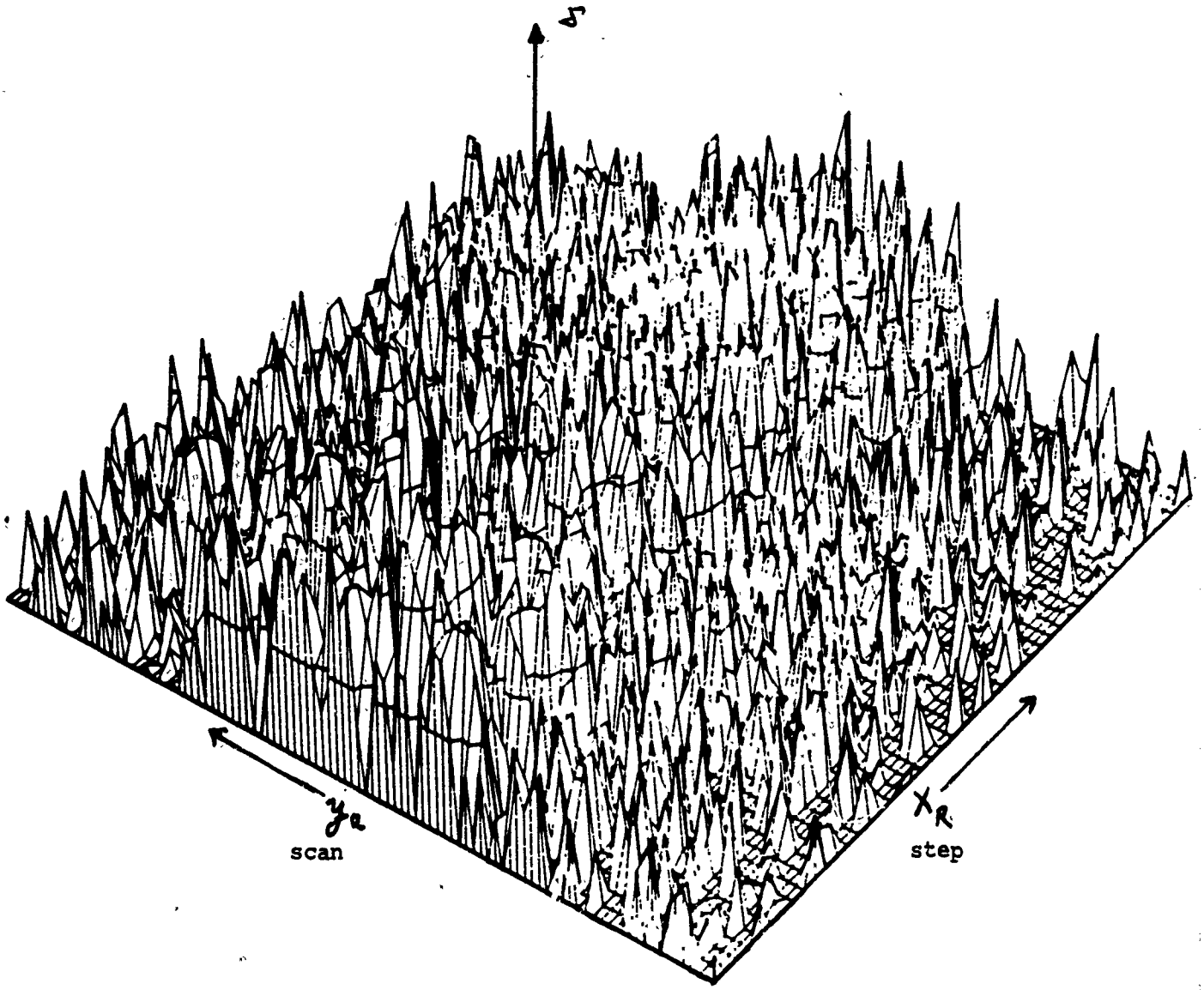

Figure 15. Sample Perspective Plot of $\delta(X_R, X_o, Y_a)$ Residuals From 95 Relocations of the ULSA Array and Probe Tower During SCAT Testing at NBS. The Peak NF SCAT Error is 39 dB Below the Peak NF.

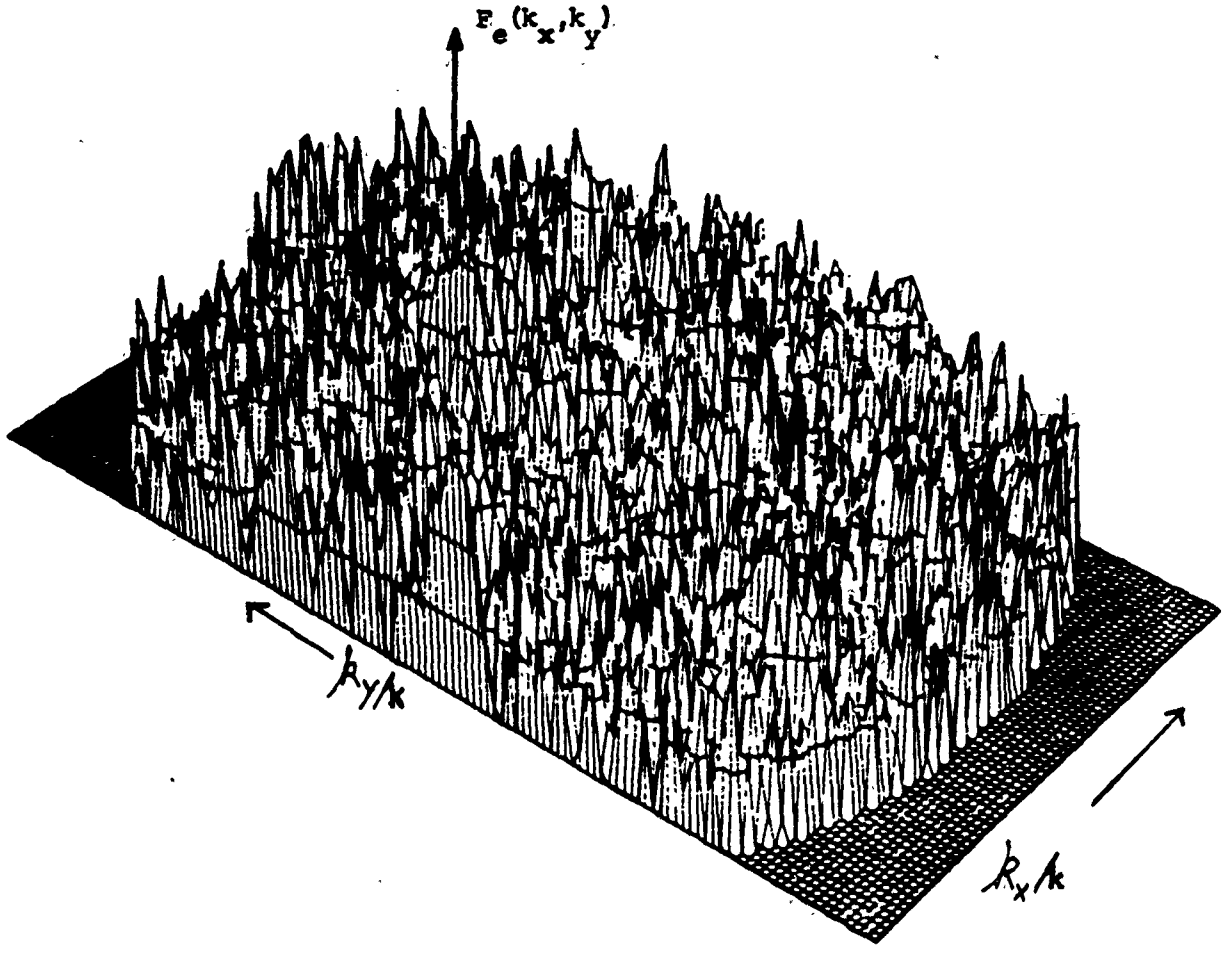

Figure 16. Perspective Plot of the SCAT Error Spectrum Due to Random Room Scattering as a Function of Wavenumber Coordinate (k_x,k_y). The Peak Spectral Error is 70 dB Below ULSA Mainbeam Gain at f_1 as Measured with the Open-Ended Waveguide Probe

$$t_c(K) = \frac{\frac{D''(K)}{S''_c(K)} - \frac{D'(K)}{S'_m(K)\rho_s''(K)}}{1 - \rho''_s(K)/\rho_s''(K)} \tag{12b}$$

where D' is the coupling product spectrum obtained using probe 1 whose main component is the same sense as the antenna under test (hereafter abbreviated AUT), D" is the coupling product spectrum obtained using probe 2 whose main component is the same sense as the cross component of the AUT, S'_m is the receiving coefficient of the main component of probe 1, S''_c represents the receiving coefficient of probe 2 corresponding to the cross component of the AUT, and ρ'_s and ρ''_s are the polarization ratios for probe 1 and probe 2 respectively. For those values of K where:

$$\left(\frac{S_c'(K)}{S_m'(K)}\right)\left(\frac{S_m''(K)}{S_c''(K)}\right) = \rho'_s(K)/\rho''_s(K) \ll 1 \tag{13a}$$

and $$\left|\rho'_s(K)\ P_t(K)\right| \ll 1 \text{ where } P_t(K) = t_c(K)/t_m(K), \tag{13b}$$

then the probe correction equations become

$$t_m(K) = \frac{D'(K)}{S'_m(K)} \tag{14a}$$

$$t_c(K) = \frac{D''(K)}{S''_c(K)} - \frac{D'(K)}{S'_m(K)\rho''_s(K)} \tag{14b}$$

Then the fractional error equations for the main and cross component can be shown to be:

$$\frac{dt_m}{t_m} = \frac{dD'}{D'} - \frac{dS'_m}{S'_m} \tag{15a}$$

$$\frac{dt_c}{t_c} = \left(1 + \frac{1}{P_t(K)\rho''_s(K)}\right)\left(\frac{dD''}{D''} - \frac{dS''_c}{S''_c}\right) + \left(\frac{1}{P_t(K)\rho''_s(K)}\right)\left(\frac{d\rho''_s}{\rho''_s} - \frac{dD'}{D'} + \frac{dS'_m}{S'_m}\right) \tag{15b}$$

The terms involving the uncertainties in S'_m, S''_c, and ρ''_s are the cause of errors in the far field. First we will note that given the conditions of equations (13), the polarization ratio of Probe 1, ρ'_s, has no significant effect on either component. Second, we note the probe's effect on the AUT cross component depends on the relative polarization ratios of the AUT and Probe 2. Finally, we note that since the main component errors are proportional to the errors in S'_m, the errors in the probe gain and pattern have a one-to-one correspondence to the errors in the AUT's main component.

3.2.2 Typical Probe Pattern Errors

Table 2 below gives typical tolerances for expected probe pattern calibrations at NBS.

Table 2. Typical FF Probe Calibration Errors at NBS

Relative Probe Pattern Level (dB)	Error (dB)
0	0.10
-5	0.15
-15	0.35
-30	1.60

Using the DESAT sum probe or open ended waveguide probe, we would expect an error of 0.1 dB in the test antenna gain and an error of about 0.5 dB at wide angles where the probe pattern is down by about 20 dB. This implies a 0.5 dB error in the test antenna's low sidelobes due only to the probe pattern uncertainty. On the other hand the difference probe has a 30 dB null in the direction of the AUT's main beam. Thus, the difference probe would be unable to determine the test antenna gain to better than about 1.6 dB due only to probe pattern uncertainty. However, the difference probe at wide angles is similar to the open-ended waveguide probe, so that uncertanties due to the difference probe in the far-out sidelobe levels will be about the same as that due to the open-ended waveguide, that is about 0.5 dB.

3.3 Data-Point Spacing--Aliasing

NF sample density is a group 2 error source because it depends on the frequency of sampling in the scan coordinate. Under sampling produces aliased spectra, and oversampling burdens the data acquisition and processing plan. In principle, data point spacing can be chosen so that aliasing errors are arbitrarily small. However, noise and/or rapidly varying systematic errors, for example multiple reflections, set the practical lower limit. If the data spacing in x and y is δ_x and δ_y respectively, then the aliased Fourier transform of the data $F_e(\underline{K})$, in terms of the true Fourier transform, is given by:

$$F_e(\underline{K}) = \sum_{m,n=-\infty}^{\infty} F(k_x + 2m\pi/\delta_x,\ k_y + 2n\pi/\delta_y) \qquad (16)$$

The aliasing error is contributed by terms for which $m \neq o$, $n \neq o$. The terms for $m = \pm 1$, $n = \pm 1$ are usually the only terms contributing a significant error. The aliasing error can be estimated using a centerline test called TESTSPAC. In this test, a centerline near-field scan is measured using very small sample spacing (usually less than about .1λ). The FFT is then done using the complete set of data, then every other point, then every third point, etc. Using the 1-D centerline tests, we expect to be able to make the aliasing error small compared to other errors for both the sum probe and the difference probe. The aliasing error should be about the same for both probes depending on the relative noise level and rapidly varying systematic error levels in the facility.

3.4 Scan Area Truncation

This Group 2 error source has two effects. First the far-field pattern results are only valid within the angular region defined by the geometry of the antenna and the scan area, as shown in Figure 17. The second effect of area truncation produces pattern errors within the region of validity. Yaghjian [10] showed that this error can be estimated from a knowledge of the measured data on the boundary of the scan area. Denoting the plane polar coordinates of the boundary by (p', ϕ_p), the normalized data on the boundary by $E_t(p', \phi_p)$, the spherical coordinates in the far field by (θ,ϕ), the magnitude of the far electric field by $|E(r)|_{r\to\infty}$ and the maximum acute angle between the plane of the scan area and a line connecting the edges of the antenna aperture and the scan area by γ_{max}; then the fractional error in the far field is given by the so-called Yaghjian perimeter bound, shown in Figure 18. Also shown is a sketch of the truncation geometry as implemented by the computer program SUMSQAV. By evaluating the perimeter fields around each successive truncation boundary, the numerator in the Yaghjian bound represents a fractional error in the full set sidelobe at a selected angle (θ,ϕ). Results from truncation tests are given in Section 4.2.

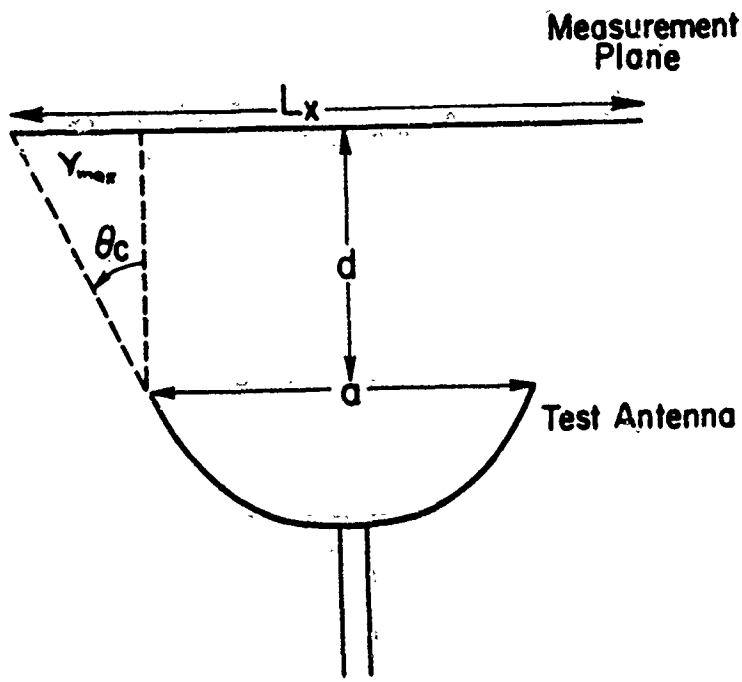

Maximum Angle for Accurate Far Field = θ_c

$$\theta_c \simeq \text{Tan}^{-1}\left(\frac{L_x - a}{2d}\right)$$

$$\gamma_{max} = 90 - \theta_c$$

Figure 17. Schematic Relationship Between Scan Length and Maximum Angle to Which the Far Field Pattern Can Be Accurately Measured During Planar NF Scanning

SCHEMATIC OF AREA TRUNCATION PROGRAM

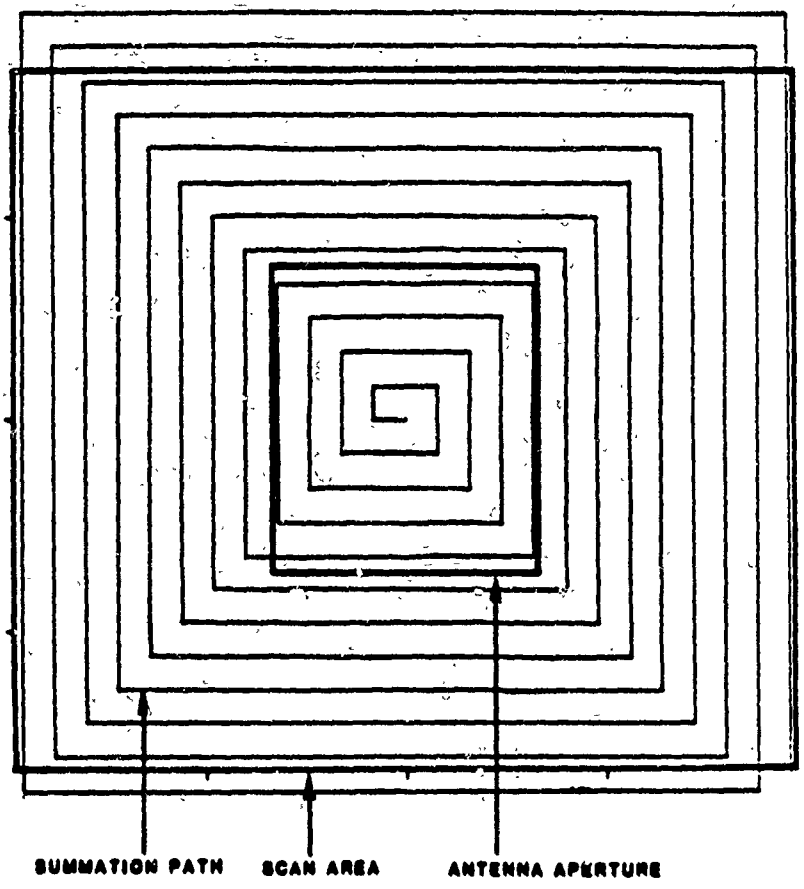

YAGHJIAN ERROR BOUND

$$\eta(\bar{r}) \leq \frac{\left| \int_0^{2\pi} \bar{E}_t(\rho', \phi_p) e^{-ik\rho' \sin\theta \cos(\phi - \phi_p)} \rho' \, d\phi_p \right|}{2\pi r \, |\bar{E}(\bar{r})|_{r\to\infty} \cos\gamma_{max}}$$

Figure 18. Schematic of Scan Area Truncation for Evaluating the Yaghjian Error Bound for a Sidelobe at Angle (θ,ϕ). The Perimeter fields are E_t (ρ', ϕ_p) and γ_{max} is shown in Figure 17

3.5 Systematic Scanning Errors

All sources of NF measurement errors in Groups 1-3 (Table 1) produce FF sidelobe errors which are inversely proportional to the relative error-free sidelobe level under test. Figure 19 summarizes the form of the far field bounding error for these groups of NF scanning errors.

Consequently, improved sidelobe measurement accuracy depends upon efforts to reduce mechanical and RF sources of amplitude and phase error in the scan data. And all high quality facilities attempt to do this by good facility design or systematic error compensation of the scan data. However, improved sidelobe measurement accuracy can also be achieved (for a fixed set of scanning tolerances) by simply attempting to measure only the relatively higher gain pattern angles, i.e., when the far field sidelobe ratio $A(k_x,k_y)/A_{max}(k_x,k_y)$ is not very small. It is the original observation of this DESAT program that this sidelobe ratio may be controlled during scan by imposing a probe pattern which discriminates against the high gain mainbeam wavenumbers, i.e., filters out the mainbeam. We are free to do this because NF scanning records the coupling product voltage between the unknown test antenna pattern in its near field and the known probe pattern in its far field. We of course must then compute the coupling product spectrum by Fourier inversion, and then normalize this coupling product spectrum by the pre-measured probe pattern spectrum, i.e., we must perform probe correction processing.

The basic coupling product expression for planar NF scanning is shown schematically in Figure 20. The value of our mainbeam-filtering probe is that it imposes a stop band in and around the mainbeam wavenumbers, i.e., it forces $A(k_x,k_y) \cdot B(k_x,k_y) \rightarrow 0$ for (k_x,k_y) in the mainbeam. This filtering increases the coupling product sidelobe ratio for all other wavenumbers, thereby minimizing the error gain. Proper probe correction processing removes the probe pattern directivity weighting throughout the entire wavenumber spectrum, leaving a highly accurately measured sidelobe pattern, but an inaccurately measured mainbeam pattern. Mainbeam patterns must subsequently be recovered using a second non-nulling broad pattern

- FAR FIELD SIDELOBE ERROR IS ALWAYS OF FORM:

$$|A_\epsilon(K_X, K_Y)| \propto \frac{(\text{CONSTANT}) \cdot |V_\epsilon(X,Y)|^2}{|A(K_X, K_Y)/A_{MAX}(K_X, K_Y)|}$$

- TO MINIMIZE $|A_\epsilon(K_X, K_Y)|$:

REDUCE $V_\epsilon(X,Y)$ BY GOOD FACILITY DESIGN

OR

DECREASE $|A_{MAX}(K_X, K_Y)|$ BY PROBE DESIGN

Figure 19. Form of the Bounding Far Field Sidelobe Error Due to Groups 1-3 Near Field Measurement Errors (Table 1)

PLANAR NEAR FIELD SCANNING

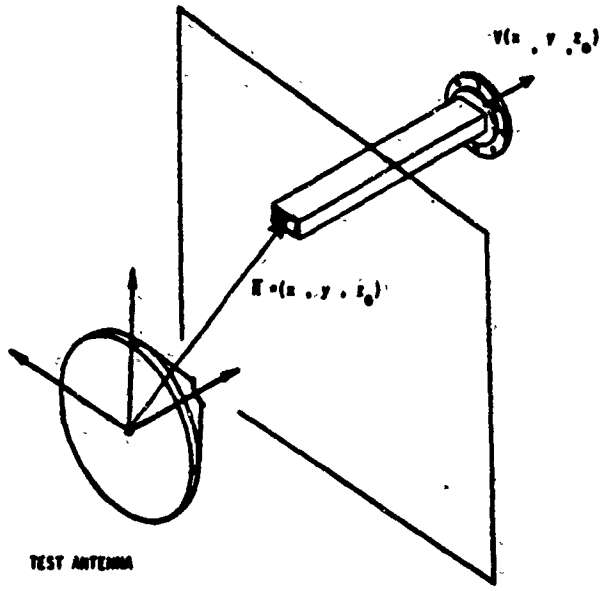

COUPLING EQUATION

$$\underbrace{A(K_x, K_y)}_{\text{TEST ANTENNA}} \cdot \underbrace{B(K_x, K_y)}_{\text{PROBE}} = \underbrace{\int_{-\infty}^{\infty}\int V(x,y,z_0)\, e^{j(K_x X + K_y Y + K_z Z)}\, dx\,dy}_{\text{VOLTAGE TRANSFORM}}$$

Figure 20. Basic Coupling Product Relation for Planar Near Field Scanning

probe. Error predictions for the remaining systematic error groups, using both standard and the nulling probe, is summarized next.

3.5.1 Probe Position Errors

Probe position errors tend to concentrate their effects in certain directions unless they are only random--then they tend to raise the average sidelobe level. For antennas with the beam steered off the z-axis, and for directions near the main beam where $\theta < \lambda/10L$ (L is the maximum antenna dimension), then the fractional error is given by Newell [8] as:

$$\left|\frac{\Delta D(\underline{K})}{D(\underline{K})}\right| \leq \frac{344}{\sqrt{\eta}} \left(\frac{\Delta(\underline{K})}{\lambda}\right)^2 \sin^2\theta_b \quad g(\underline{K}) \tag{17a}$$

for x and y position errors, and

$$\left|\frac{\Delta D(\underline{K})}{D(\underline{K})}\right| \leq \frac{43}{\sqrt{\eta}} \left(\frac{\delta_z(\underline{K})}{\lambda}\right)^2 \cos^2\theta_b g(\underline{K}) \tag{17b}$$

for the z-position errors.

For directions where $\lambda/10L < \theta < \pi/2$,

$$\left|\frac{\Delta D(\underline{K})}{D(\underline{K})}\right| \leq 13.5 \left(\frac{\Delta(\underline{K})}{\lambda}\right) \sin\theta_b \; g(\underline{K}) \tag{18a}$$

for the x and y-position errors, and

$$\left|\frac{\Delta D(\underline{K})}{D(\underline{K})}\right| \leq 13.5 \frac{\delta_z(\underline{K})}{\lambda} \cos\theta_b g(\underline{K}) \tag{18b}$$

for the z-errors.

Note η is the aperture efficiency, θ_b the angle between the z-axis and the main beam direction, Δ the Fourier transform of the x and y-position errors, and δ_z is the Fourier transform of the position error map.

Table 3 shows the magnitude and periodicity of certified position errors on the NBS scanner.

Table 3. Measured Scanner Position Errors (max) on the NBS NF Range

Type	As A Function Of	Periods (ft)	Magnitude (in)
Z	X	None	.015
Z	Y	30.0	.025
Y	X	1.34, 2.67	.005
X	Y	30.0	.025

Thirty feet is twice the scanner height and 16 inches is the separation distance between supports in the x-direction. For L = 16 feet (the ULSA maximum dimension), $\eta = 0.5$, $\theta_b = 12^\circ$, and $\lambda = 10$ cm, we can predict the far-field errors shown in Table 4. Figures 21 shows the measured Z-position error (straightness) of the NBS probe scanner as a function of scan coordinate (Y) and tower step coordinate (X).

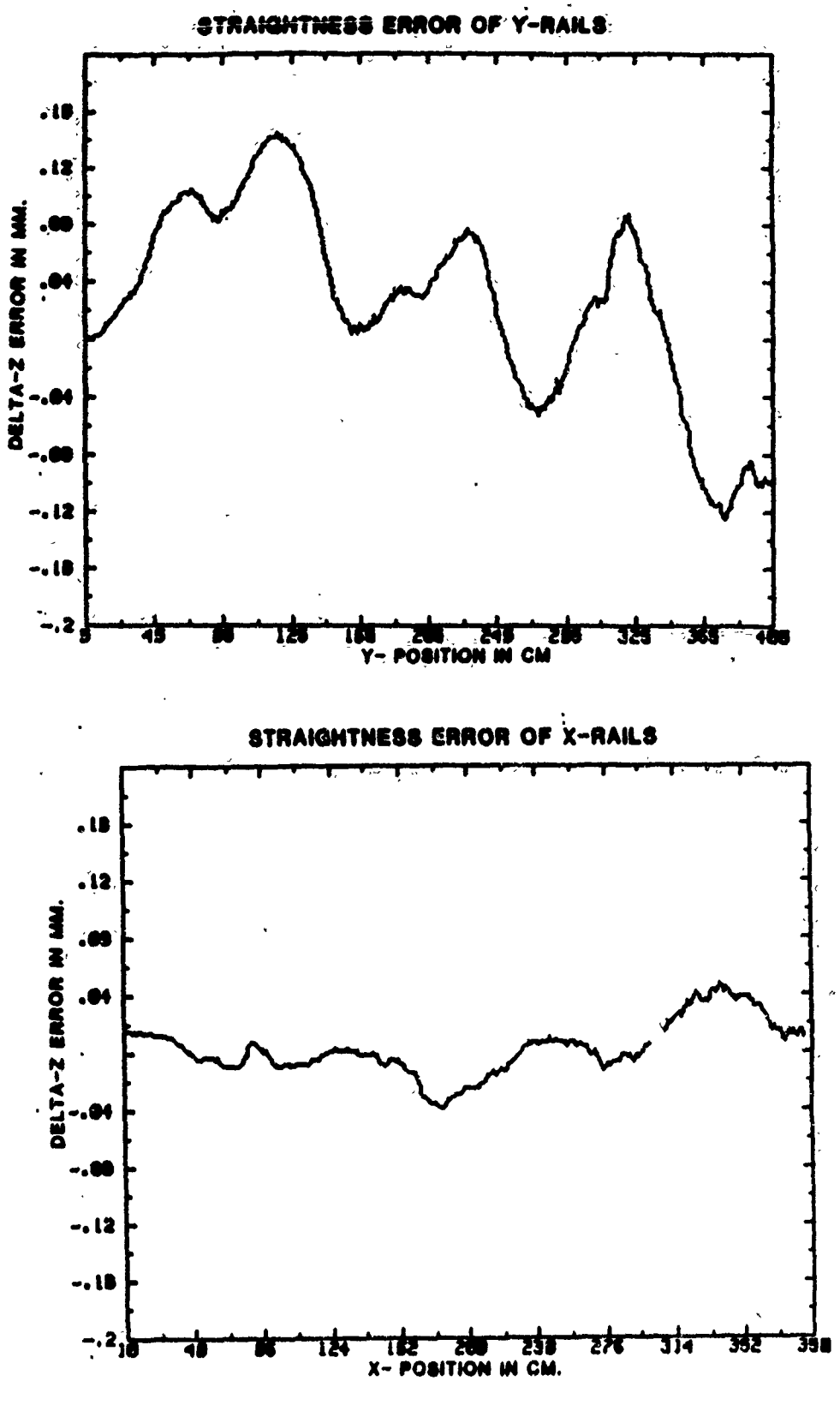

Figure 21. Measured Scanner Rail Straightness of NBS Planar Scanner

Table 4. Predicted Far Field Sidelobe Errors Due to Residual Mechanical Positioning Errors at NBS (Open-Ended Waveguide Probe)

Type	As A Function Of	Direction from Mainbeam (deg)	Error Magnitude (dB)	Sidelobe Level (dB)
Z	X	Noise	--	--
Z	Y	± 0.6	0.08	0.0
Y	X	± 7 , ±14.5	0.35	-40
			3.5	-60
X	Y	± 0.6	0.02	0.0

For the difference probe, a -40 dB sidelobe would have g(K) = 10, and a -60 dB sidelobe would have g(K) = 1000 because the probe has a 30 dB null in the direction of the main beam. Evaluating equations (17) using g(K) for the delta probe and the NBS scanner mechanical errors, Table 5 is produced.

Table 5. Predicted Far Field Sidelobe Errors due to Residual Mechanical Positioning Error at NBS (Δ-Probe)

Type	As A Function Of	Direction from Mainbeam (deg)	Error Magnitude (dB)	Sidelobe Level Under Test (dB)
Z	X	Noise	--	--
Z	Y	± 0.6	0.08	0.0
Y	X	±7 , ±14.5	0.01	-40
			0.11	-60
X	Y	±0.6	0.02	0.0

Significant error reduction at the -60 dB residual level (from 3.5 dB to .11 dB) is predicted for low sidelobe antennas tested on the NBS scanner using the mainbeam nulling probe. Section 4.3 confirms this expectation.

3.5.2 Instrumentation Errors

Amplitude and phase instrumentation errors arise from receiver nonlinearity, flexing of cables and rotary joints, source and receiver drift, and temperature drift. The drift typically amounts to about 0.5° per hour at S-band, but is usually compensated by measuring cross scans called tie scans. There is also a $2\text{-}3^{\circ}$ phase error associated with the flexing of cables to the probe and rotary joint on the NBS scanner. The periods of this error are associated with the x and y-dimensions of the scanner, and are about 15 feet in each direction. The receiver nonlinearity can be partially compensated using a calibration of the receiver. A typical value of the nonlinearity is $\mu = .01$ v/v with a spread of .005 v/v over the range 0-30 dB. Thus, .005 v/v would be the residual uncorrected receiver nonlinearity. The periods for this error will depend on the manner in which the NF amplitude falls off with scan. We expect a period of about 8 m in X and 2 m in Y for the sum and open-ended waveguide probes and 8 m in X and 1 m in Y for the difference probe. With these data, we may predict far field pattern errors due to NF receiver errors by using the equation:

$$\left|\frac{\Delta D(\underline{K})}{D(\underline{K})}\right| \leq 6U(\underline{K})g(\underline{K}) \tag{19}$$

where $U(\underline{K})$ is the Fourier transform of the residual uncorrected receiver nonlinearity. For the phase errors for $\lambda/10L \leq \theta \leq \pi/2$, the far-field errors are given by:

$$\left|\frac{\Delta D(\underline{K})}{D(\underline{K})}\right| \leq 13.5 \left(\frac{V(\underline{K})}{360}\right) g(\underline{K}) \tag{20}$$

where V(K) is the Fourier transform of the residual NF phase errors with scan.

The resulting far-field errors due to instrumentation amplitude and phase errors when measuring the DESAT arrays using both probes are predicted in Table 6.

Table 6. Predicted Far Field Sidelobe Errors for the Open-Ended Waveguide Probe due to NBS Instrumentation Inaccuracies

Type	As A Function Of	Direction from Mainbeam (deg)	Sidelobe Error (dB)		Sidelobe Level (dB)
			Δ-Probe	Σ-Probe	
Amplitude	X	±0.7	.03	0.03	0.0
	Y	±3	.005	0.3	-20.0
			0.15	3.0	-40.0
Phase	X	±1.3	.06	1.0	-20.0
	Y	±1.3	.06	1.0	-20.0

Again the predicted reduction of low sidelobe errors when scanning with the Δ-probe derives from artifically higher sidelobe level imposed on the test antenna's coupling product spectrum by the mainbeam filtering probe. Following probe correction, these sidelobes are returned to their proper level with respect to the true main beam gain as measured by a second non-nulling probe. Results of test to confirm the error immunity of the nulling probe are given in Section 4.4.

3.6 Multiple Reflection Error

Certain probe/antenna/room geometries can lead to undesirable periodic reflections in the scan plane fields. These reflections are a fundamental measurement accuracy issue because present planar transform processing codes all assume that only direct path fields are intercepting the scan plane [11]. Consequently, an initial near field testing requirement is to select an "appropriate" probe-array Z-separation distance which minimizes the magnitude of indirect path fields between probe and environment, while still satisfying field-of-view requirements from the available scan plane size.

3.6.1 First-Order Interaction

The most prevalent multipath is along the directly backscattered path between the antenna under test and the scanning probe. This first-order interaction is shown in Figure 22 which also plots the measured NF interference pattern magnitude against Z-distance separation for a selected X-Y probe location. This standing wave pattern has a p-p variation of $\lambda/2$, and is a direct measure of backscattered field strength. The primary effect of first-order interactions is on the accuracy of the far field gain. Section 4.6 gives some measured far field gain error results due to NF probe/array multipath.

3.6.2 Higher-Order Interactions

Other higher-order backscattering paths can exists between the probe and array, and these will contribute to both FF gain and sidelobe errors. These higher order fields will follow oblique propagation paths, and will create amplitude and phase errors in the scan plane voltage as a function of probe scan location for a fixed Z-separation. Consequently, to reveal the character of the multipath signal, a series of linear scans at a series of offset Z-separations are acquired as sketched in Figure 23. These scan data are then processed to form the complex average coupling product spectrum. This composite spectrum is then subtracted from the spectra of selected single probe scan data in the offset series. The resulting spectral differences reveal multipath induced sidelobe errors. This procedure has been called "scan plane survey", and test results for the DESAT arrays and probes are also given in Section 4.6.

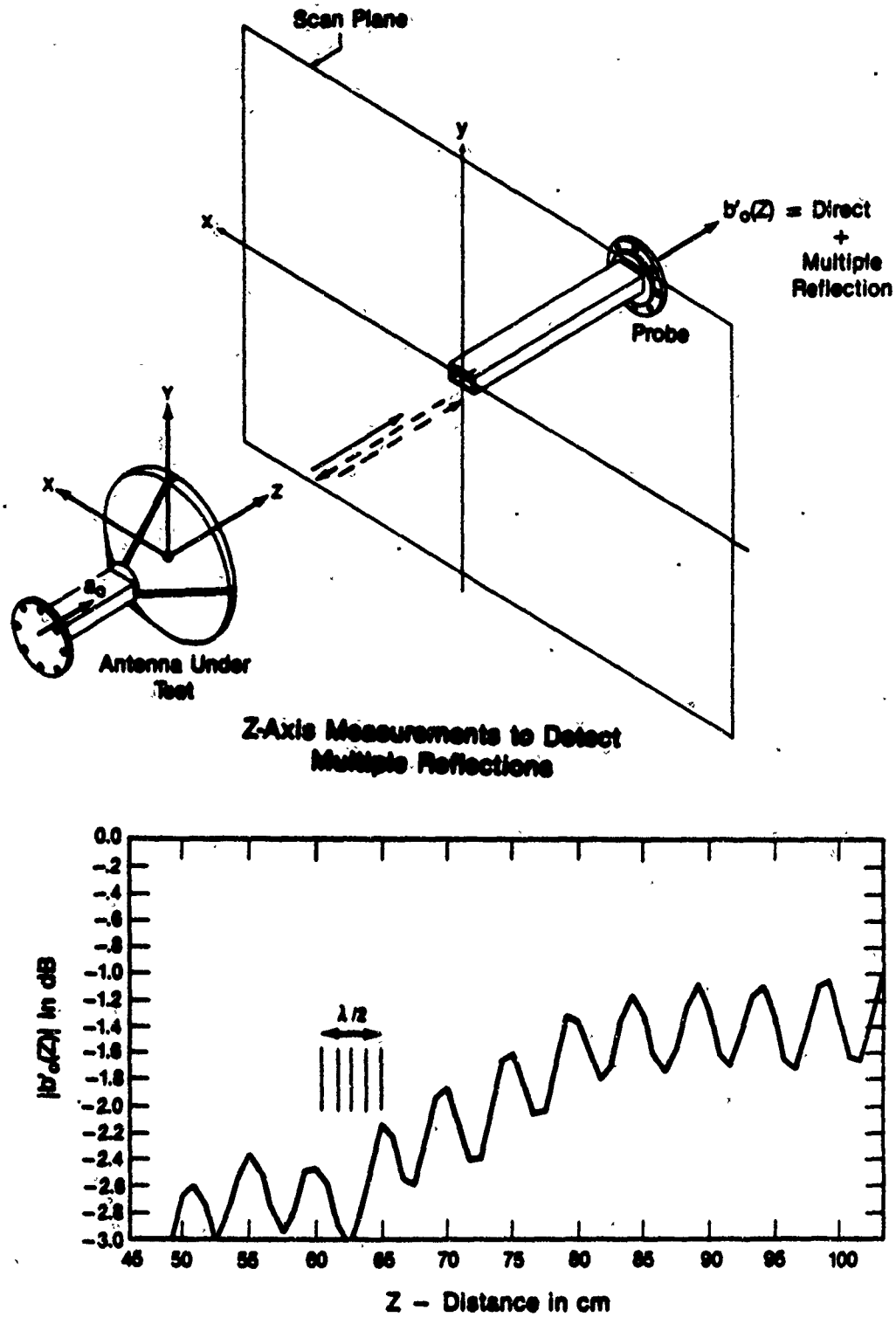

Figure 22. First-Order Multiple Reflection Error Between Probe and Test Array Produces Interference Ratio as a Function of Z at Fixed Locations in the Scan Plane

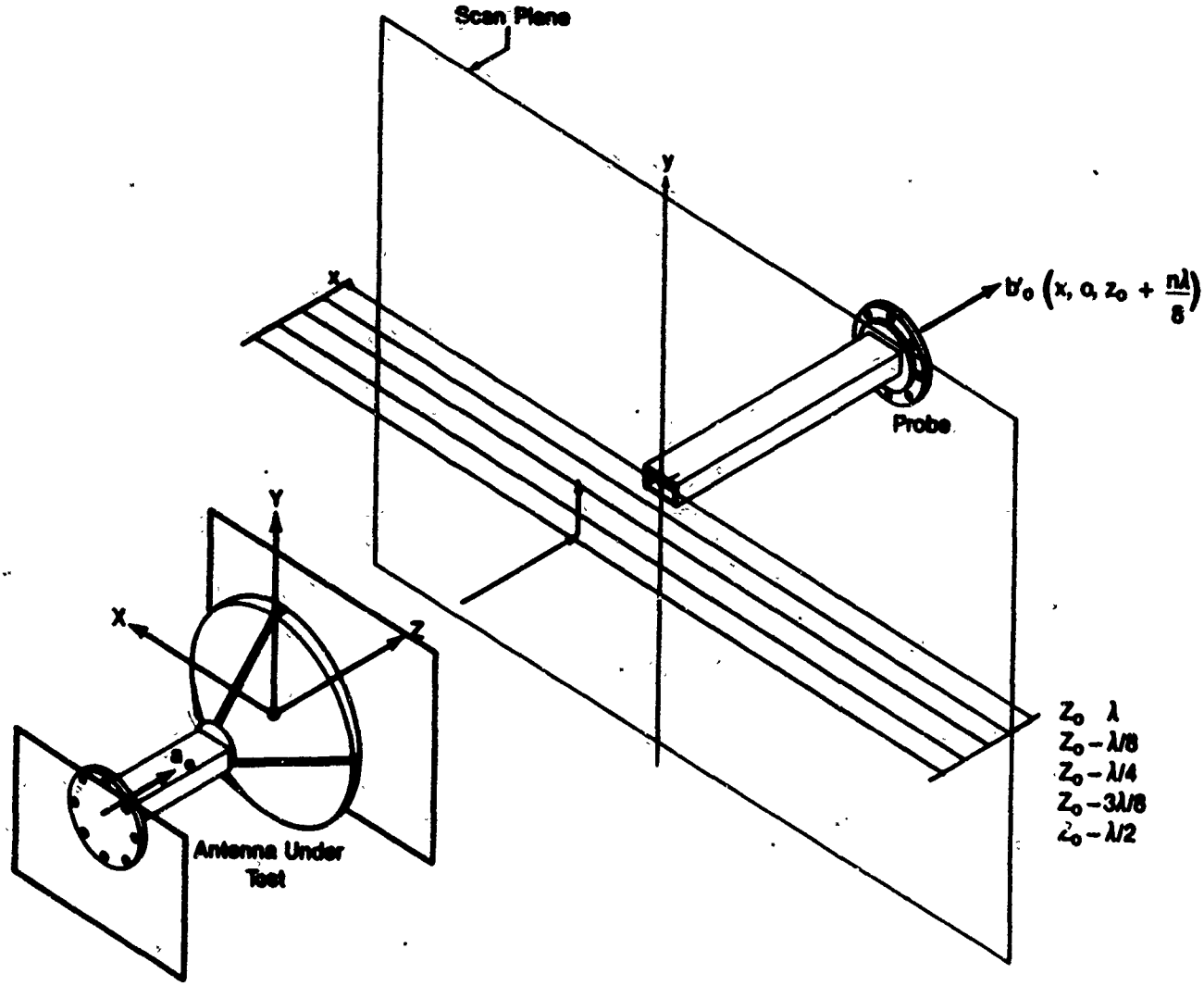

X-Axis Centerline Scans to Measure Multiple Reflections

Figure 23. Higher-Order Multiple Reflections between Probe and Array are Revealed by a Scan Plane Survey to Collect Multiple Centerline Scans at Offset Z-Separations

3.7 Random Measurement Error

Sources of random measurement error are shown in Group 4 entries in Table 1. These errors establish the repeatability limits during planar scanning, and finally limit low sidelobe measurement accuracy because they establish the RF dynamic range. These errors have always been inconsequential in previous NF measurement problems because ultralow sidelobes were not of interest. However, this DESAT program has been able to quantify some forms of random measurement error, and has shown that the new Δ-probe even has improved immunity to these forms of scan error. The following equations summarizes the bounding far field spectral error estimates (given as signal-to-noise ratios) due to residual random amplitude and phase errors from all NF sources. These expressions have been derived by Newell during the DESAT investigation [8].

Random Amplitude Error

$$\left|\frac{D(K_o)}{\epsilon_a(K)}\right| \geq \frac{\sqrt{N_e/2}}{3\sigma_a\sqrt{N/N_e}} \qquad (21)$$

where N_e is the # of NF measurement points within the effective scan area

N is the total # of NF measurement points

σ_a is the standard deviation of random amplitude error

$D(K_o)$ is the peak (mainbeam) coupling product gain

$\epsilon_a(K)$ is the noise spectrum of the random amplitude error

Random Phase Error

$$\left|\frac{D(K_o)}{\epsilon_\psi(K)}\right| \geq \frac{\sqrt{N_e/2}}{3\sigma_\psi} \qquad (22)$$

where σ_ψ is the standard deviation of random phase error

$\epsilon_\psi(K)$ is the noise spectrum of the random phase errors

In both equations, $N_e = A_e \delta_x \delta_y$, and A_e is the projected array area on the scan plane.

We may evaluate equations (21) and (22) for NF scans made with both the Σ and the Δ probe, and predict the expected signal-to-noise ratio in the FF spectra due to the single random measurement error imposed by the quantization of the NF voltage digitizers only. We further choose to reference the predicted noise power for both probes to the peak gain predicted for the Σ probe, since this normalization is always necessary for probe correction processing of Δ-probe spectra. Table 7 lists the parameters needed to evaluate equations (21, 22), and the resulting S/N_o estimates for scanning the AWACS array using both the open-ended waveguide and the Δ-probe.

Table 7. Predicted AWACS Spectral Signal-to-Noise Ratios Due Only to Random Error of Signal A/D Digitizers

Probe Type	N_e (# Samples)	N (# Samples)	σ_a (%)	σ_ψ (deg)	σ_t (rad)	S/No (dB)
Open-Ended Waveguide	2556	27775	.05	.05	.00095	82.1
Δ-Probe	1696	27775	.05	.05	.00449	93.7

In the table $\sigma_t = [\sigma_\psi^2 + \sigma_\alpha'^2]^{1/2}$ where $\sigma_\alpha' = \sigma_\alpha\sqrt{N/N_e}$ is the effective random amplitude error standard deviation, and σ_a is the known random amplitude round off error of the voltage digitizers. An effective σ_a' is used in these predictive bounds because random amplitude scanning error outside of the projected area of the test antenna on the scan plane are insignificant. This is because the scan plane phase is varying very quickly in this region, and by the principle of stationary phase, contributes little to the coupling product integral. These bounds are compared to actually measured S/N_o ratios for both probes and AWACS scanning in Section 4.5.

4.0 ULSA RESULTS FROM TWO-DIMENSIONAL NF SCANNING

This section contains the results of processing measured 2-dimensional NF scan data for the ULSA array at 3.1 Ghz. Some unclassified results from AWACS scanning is given in Section 4.5.

Processing Flow

The measured NF data is sampled in both amplitude and phase on a rectangular grid consisting of 101 rows (Y-direction) and 275 columns (X-direction) with X- and Y-spacings of 3.81 cm (.4λ) at a probe-to-array separation distance (Z-direction) of 65 cm (6.72λ). Figure 24 and 25 show perspective plots of the NF scan voltage amplitudes as measured by the open-ended waveguide probe and as measured by the Δ-probe at 3.1 Ghz. Prior to Fast Fourier Transform processing, the measured NF data is zero padded up to 128 rows by 512 columns for efficient processing and to achieve good pattern resolution in the azimuth plane. The azimuth resolution, Δk_x, is limited by the NF sample density and sample number, by the relation:

$$\frac{\Delta k_x}{k} = \frac{\lambda}{N_x \delta_x} \tag{23}$$

where k is the propagation vector ($2\pi/\lambda$)
N_x is the number of columns of NF data, and
δ_x is NF data spacing in λ in the X-direction.

Thus, a 128 x 512 transform will produce a far field angular resolution of $\Delta k_x = .005$, having at least 400 visible space samples in each principal plane pattern. This resolution (5.1 samples/deg at boresight) insures at least 4 samples over each wide-angle sidelobe. The FFT produces the so-called plane wave coupling product spectrum (PWS). The PWS is then passed to the probe-correction routine which recovers the plane wave transmitting characteristic of the ULSA, $S_{10}(K)$, by accessing previous computed probe correction coefficient files. $S_{10}(K)$ is then used to compute the ULSA array antenna far field response in two dimensions. Figure 26 is a perspective

MEASURED NF AMPLITUDE FOR OPEN-ENDED WAVEGUIDE PROBE

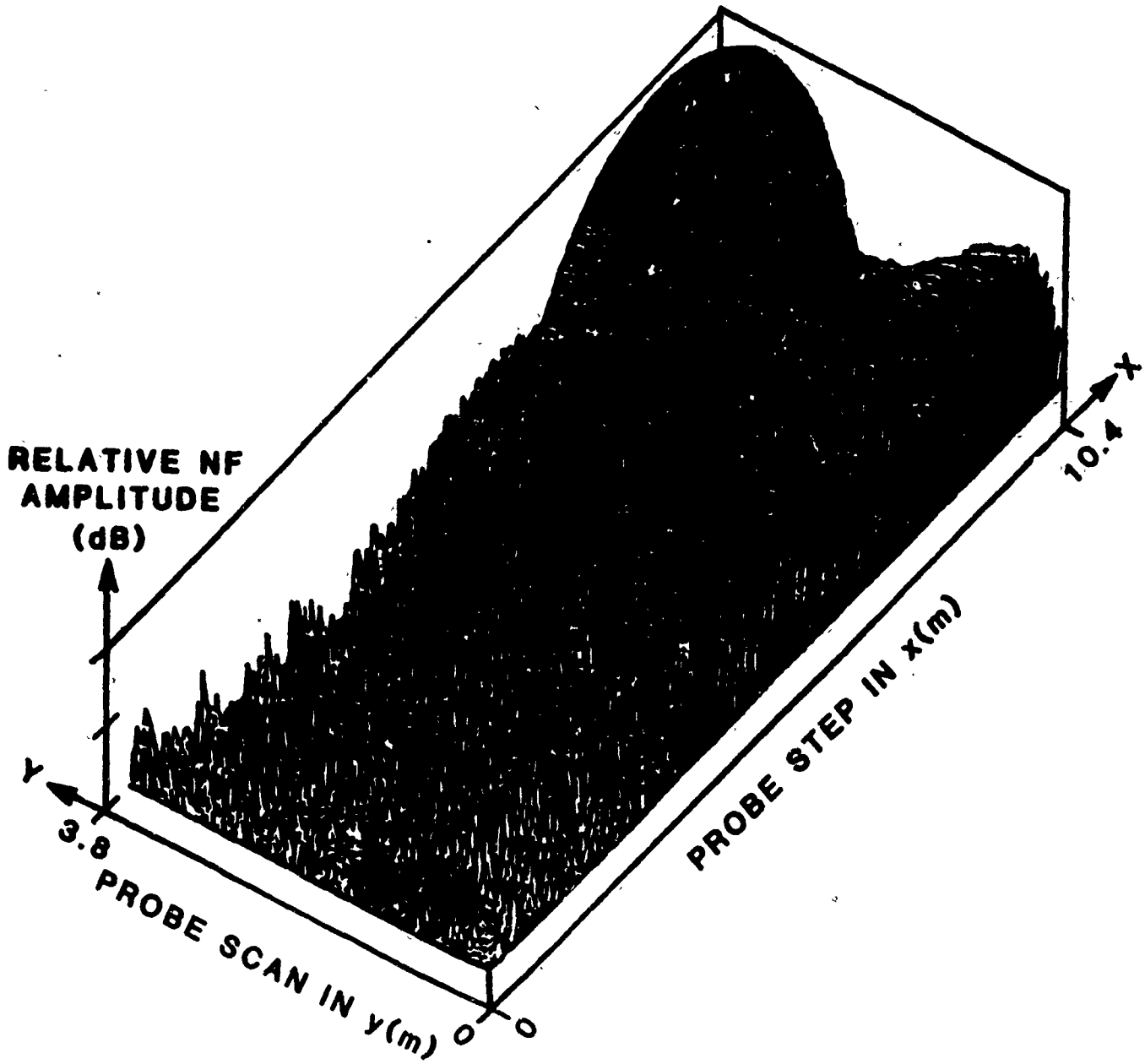

Figure 24. Measured NF Amplitude Perspective for the ULSA Array and Open-Ended Waveguide Probe Scanning at 3.1 GHz

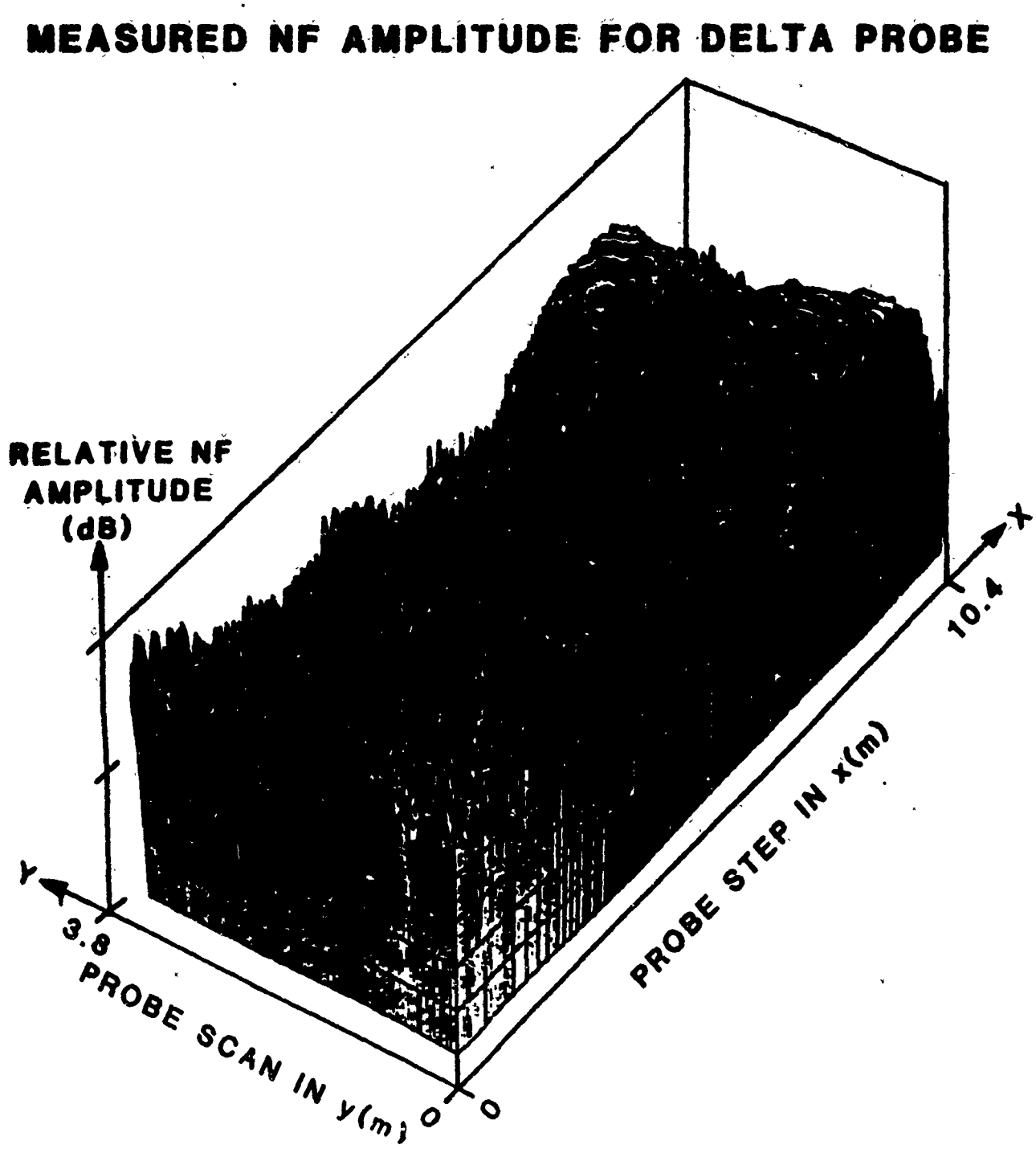

Figure 25. Measured NF Amplitude Perspective for the ULSA Array and Δ-Probe Scanning at 3.1 Ghz

plot of the final ULSA array probe-corrected far field pattern as measured by NF scanning with the open-ended waveguide probe at 3.1 Ghz.

Probe Patterns

FF probe patterns of the azimuthal vector component plotted for k_x/k for the three probes used during this program are shown overlayed on the measured ULSA array azimuth plane pattern in Figure 27. Note that the Δ-probe pattern null will reduce the mainbeam coupling product gain significantly compared to the open-ended W/G and sum probes. This reduced mainbeam coupling product gain filters the high energy content of the spectrum so that the lower wide-angle sidelobes will be artificially increased in magnitude during test, and therefore more accurately measured in the presence of known scanning errors. However, some wide angle array sidelobes may also be filtered by undesirable secondary probe pattern nulls. Such a region exists for the sum probe around $k_x/k = 0.90$ where the pattern response reaches a minimum, and the ULSA sidelobes are quite low (-50 dB). Consequently, we do not expect to measure some wide angle ULSA sidelobes accurately using the Σ probe.

ULSA centerline NF X-cuts for the three probe types are shown in Figure 28. These scan shown that the Δ-probe does reduce the dynamic range of the NF measurement. Even though the measured near fields are quite different for the three probe types, they produce the same far field pattern after probe correction to within differences associated with their intrinsic spatial frequency filtering properties. The coupling product spectrum (principal azimuth plane) for the Δ-probe and the open-ended W/G probe NF scan data (Figure 28), is shown in Figure 29.

Two-dimensional amplitude contours of the azimuthal vector component of the three probe FF patterns at 3.1 Ghz are shown in Figures 30-32. The secondary null regions are quite apparent in the Δ-probe contour of Figure 31. In fact the -20 dB contour appears to trace an figure-eight, and sidelobes which exists at these angles in the test antenna's spectrum will be filtered nearly as strongly as is the mainbeam. However, all sidelobes along the test antenna's azimuth ridge will be quite accurately recovered.

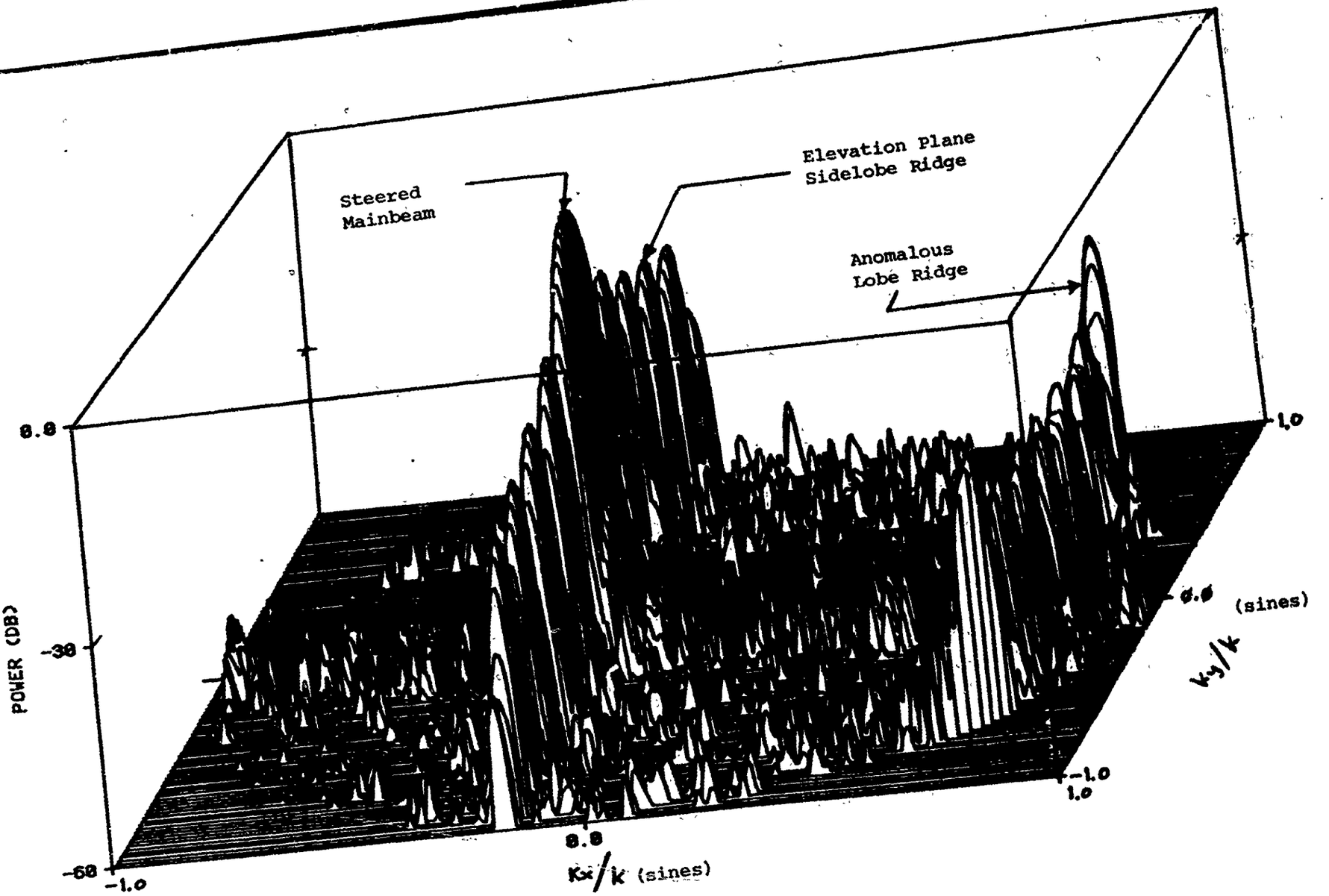

Figure 26. Perspective Plot of Probe-Corrected ULSA Array Far Field Pattern as Measured by NF Scanning with [illegible]-Ended R/G Probe at 3.1 Ghz

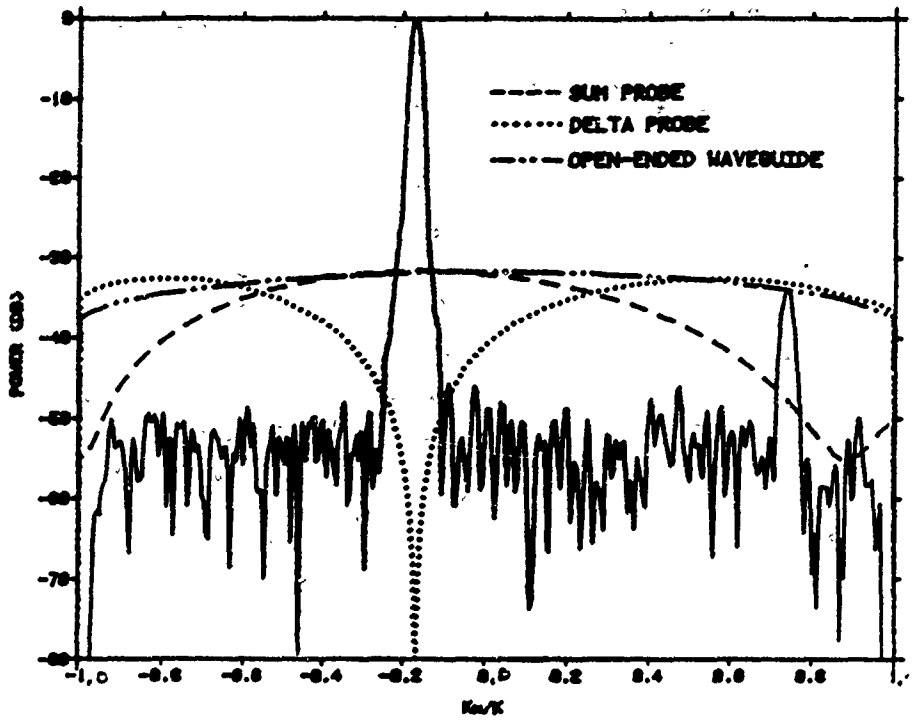

Figure 27. Far Field Probe Patterns Overlayed on the ULSA Array Pattern Computed From Transformed Probe Scan Data at 3.1 Ghz

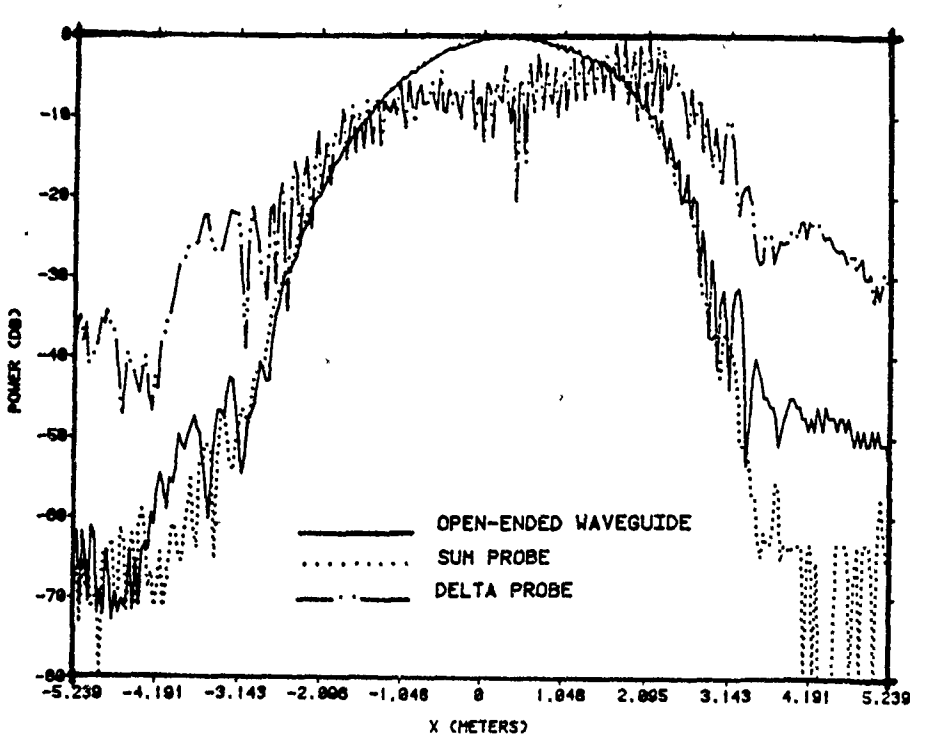

Figure 28. Centerline ULSA NF Scans Measured with the Three DESAT Probes at 3.1 Ghz

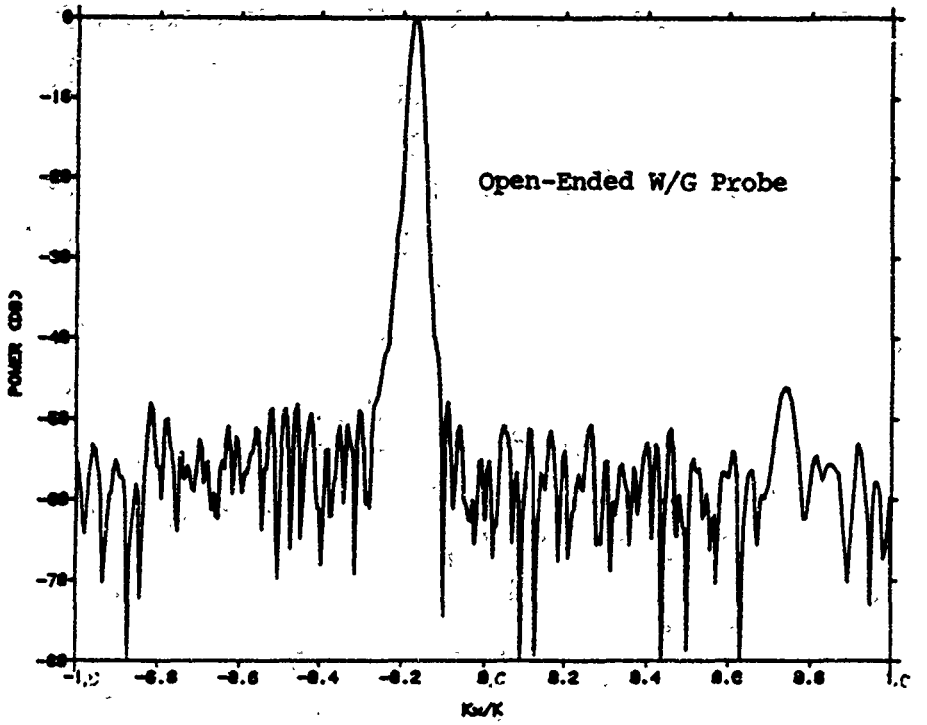

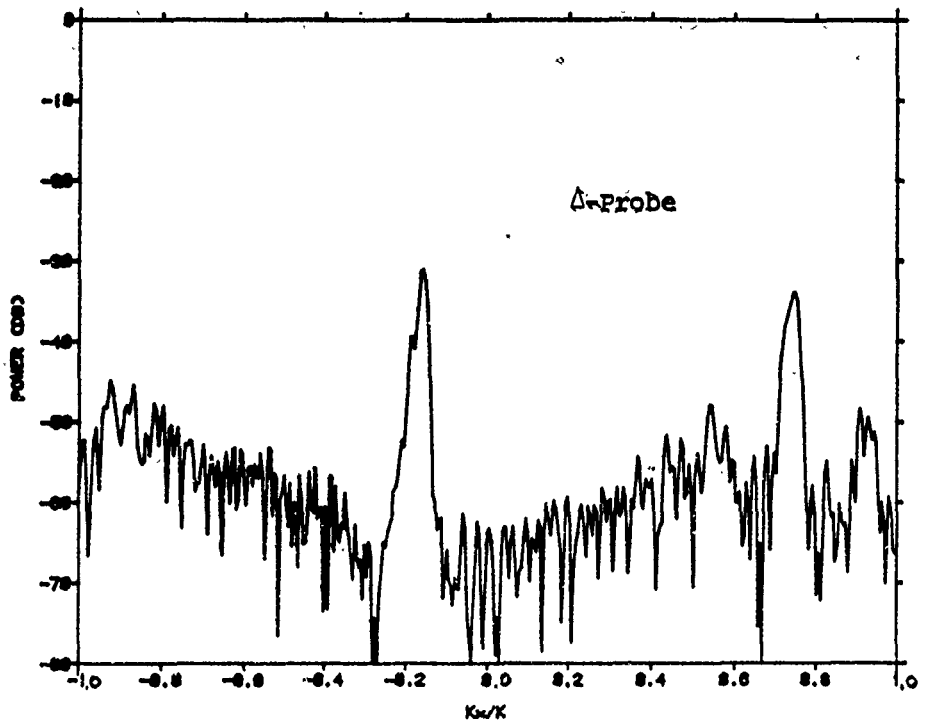

Figure 29. ULSA Coupling Product Spectrum Azimuth Plane Patterns for the NF Scans of Figure 28 (Open-Ended W/G Probe and Δ-Probe) at 3.1 Ghz

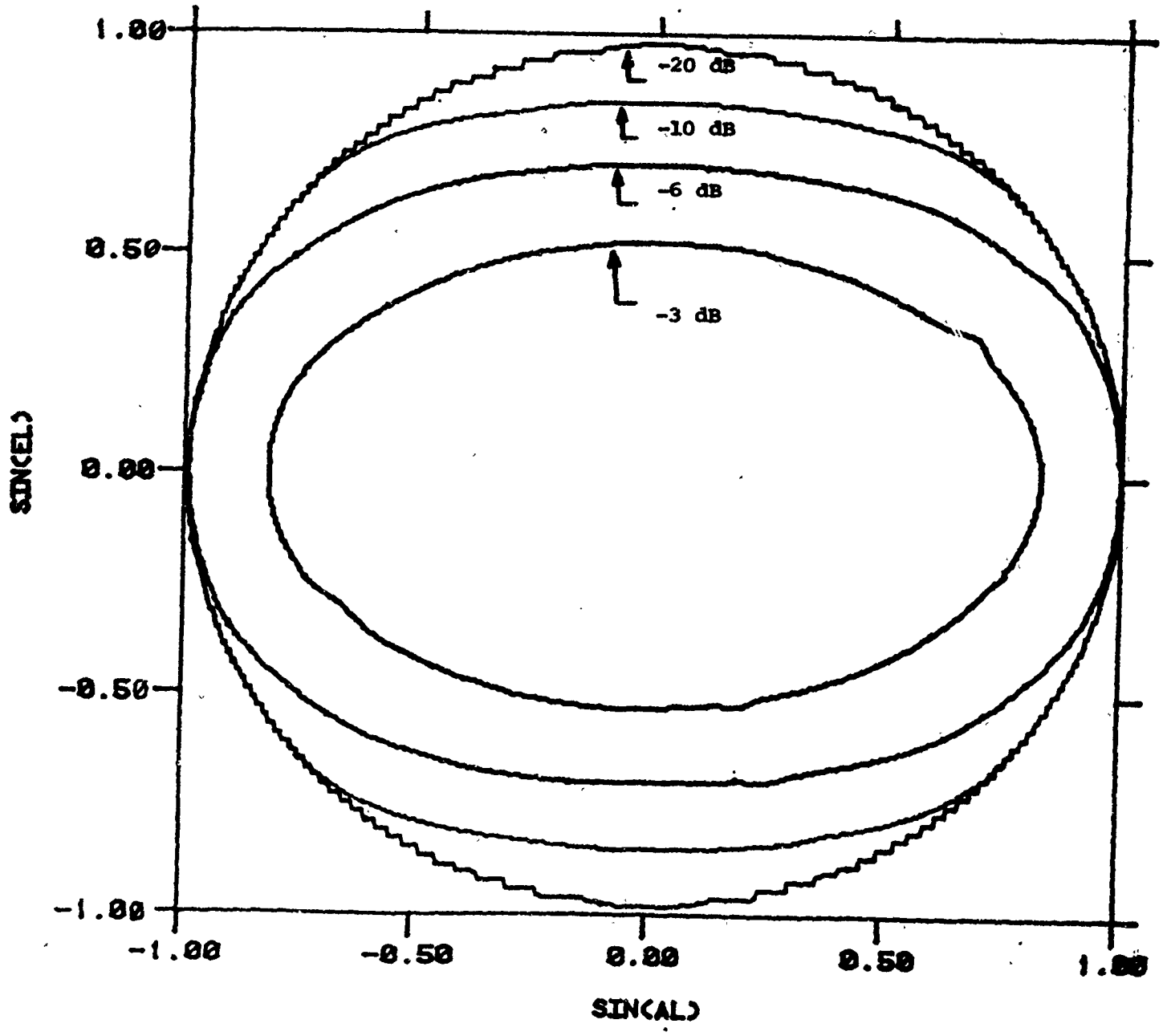

Figure 36. Equal-Amplitude Contours of the Azimuthal Far Field Pattern of the Open-Ended W/G Probe at 3.1 Ghz

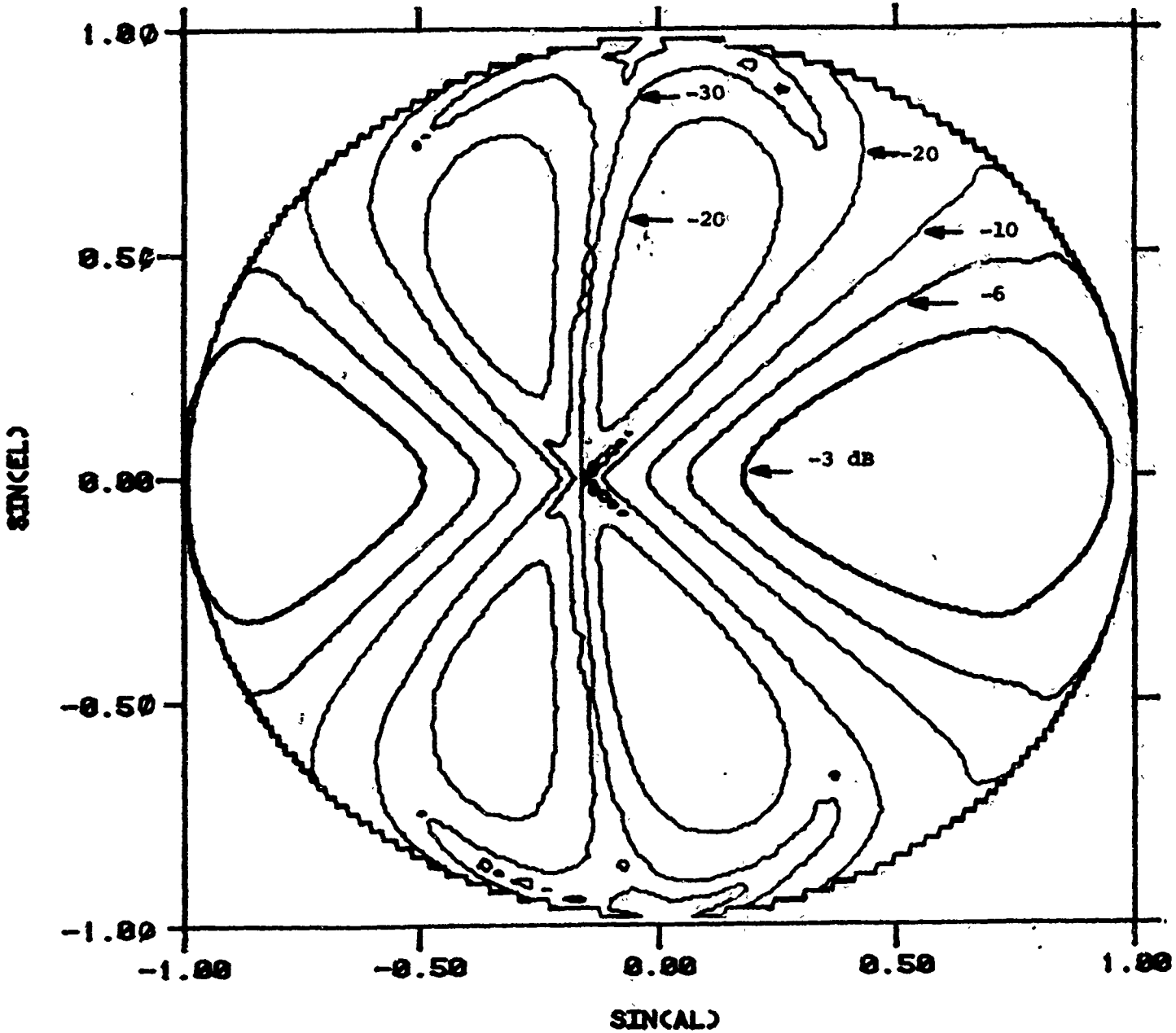

Figure 31. Equal Amplitude Contours of the Azimuthal Far Field Pattern of the Δ-Probe at 3.1 Ghz

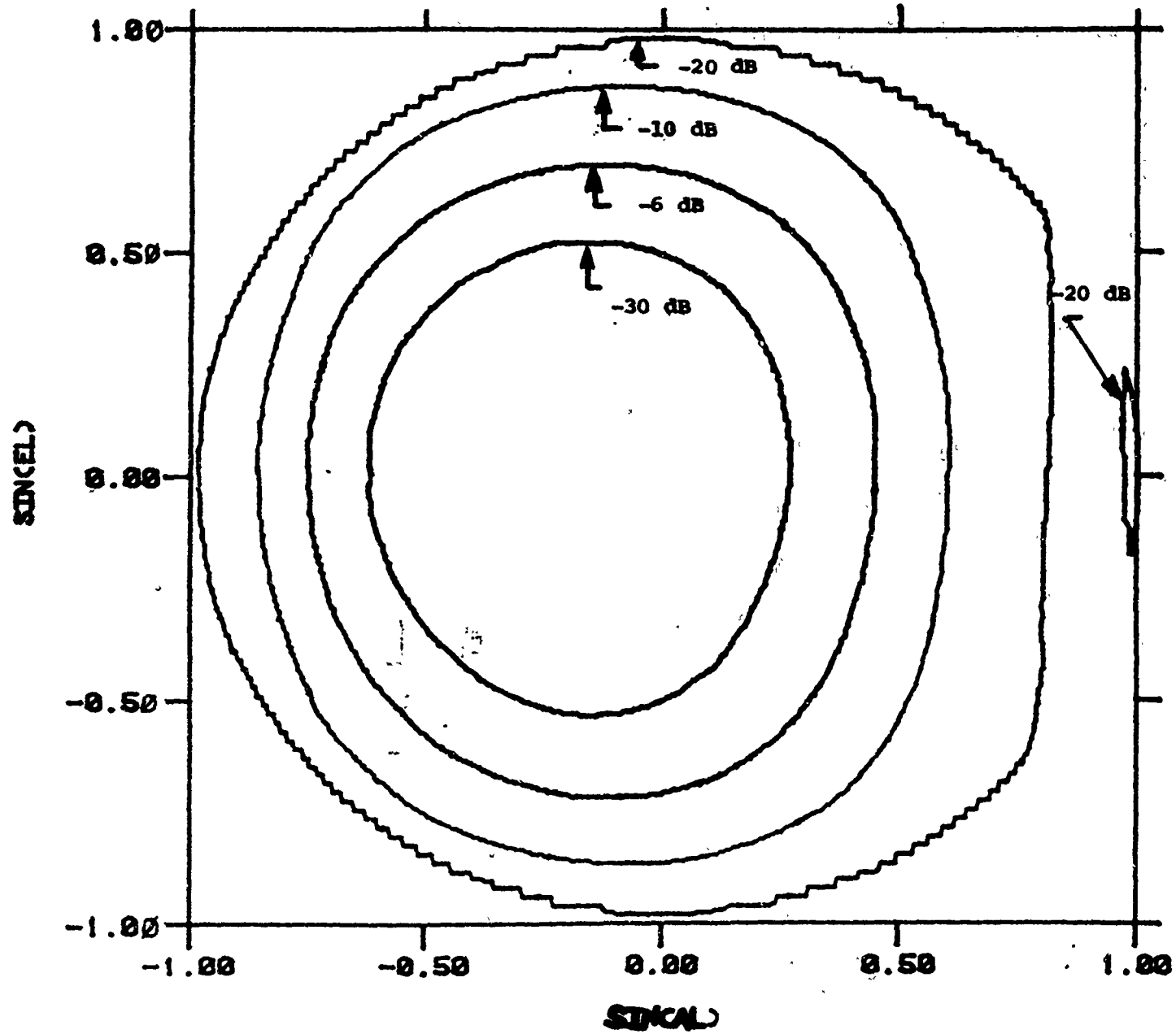

Figure 32. Equal-Amplitude Contours of the Azimuthal Far Field Pattern of the Σ-Probe at 3.1 Ghz

Similarly the Σ probe has more azimuthal directivity than does the open-ended W/G probe, and consequently we do not expect the Σ probe to recover the very wide angle azimuth plane sidelobes with the same accuracy as will the other two DESAT probes. Because the Δ-probe developed for this program is only an approximation to the ideal filtering probe, we are not surprised that secondary probe pattern nulls have imposed limitations on some regions of sidelobe measurement.

Two-dimensional amplitude contours of the elevation (cross-polarized) vector component referenced to the azimuthal vector component peak are shown for the three probes in Figures 33-35. These patterns are useful for estimating the sidelobe directions where scalar probe-correction processing error will be the largest when testing for the array's main polarization pattern. Since the peak cross-polarized response for the Δ-probe is quite high (> -5 dB) and has quadrantal symmetry as shown in Figure 34, we expect that scalar probe-correction will introduce additional measurement error in these regions*. This error has been called scalar-processing-error, and is reported from tests made on the AWACS array in [12].

4.1 Aliasing Test Results

NF centerline scans with both the Σ and Δ probes for the ULSA array at 3.1 Ghz were collected using sample spacings between .1λ (.38") and 1λ (3.81") over the entire 10.44 m in scan length. Figure 36 shows the coupling product spectrum for the Σ probe when sampling both at .1λ (top) and at 1.0λ along a centerline scan. Note the reduced field-of-view in the 1.0λ spectrum. Although these patterns are not probe-corrected, the change in the coupling product sidelobes with increasing sample spacing is a valid measure of aliasing error in the ULSA low sidelobe pattern.

---

*Using only main polarization probe correction files (equation 14a), in lieu of vector probe correction files (equation 12a).

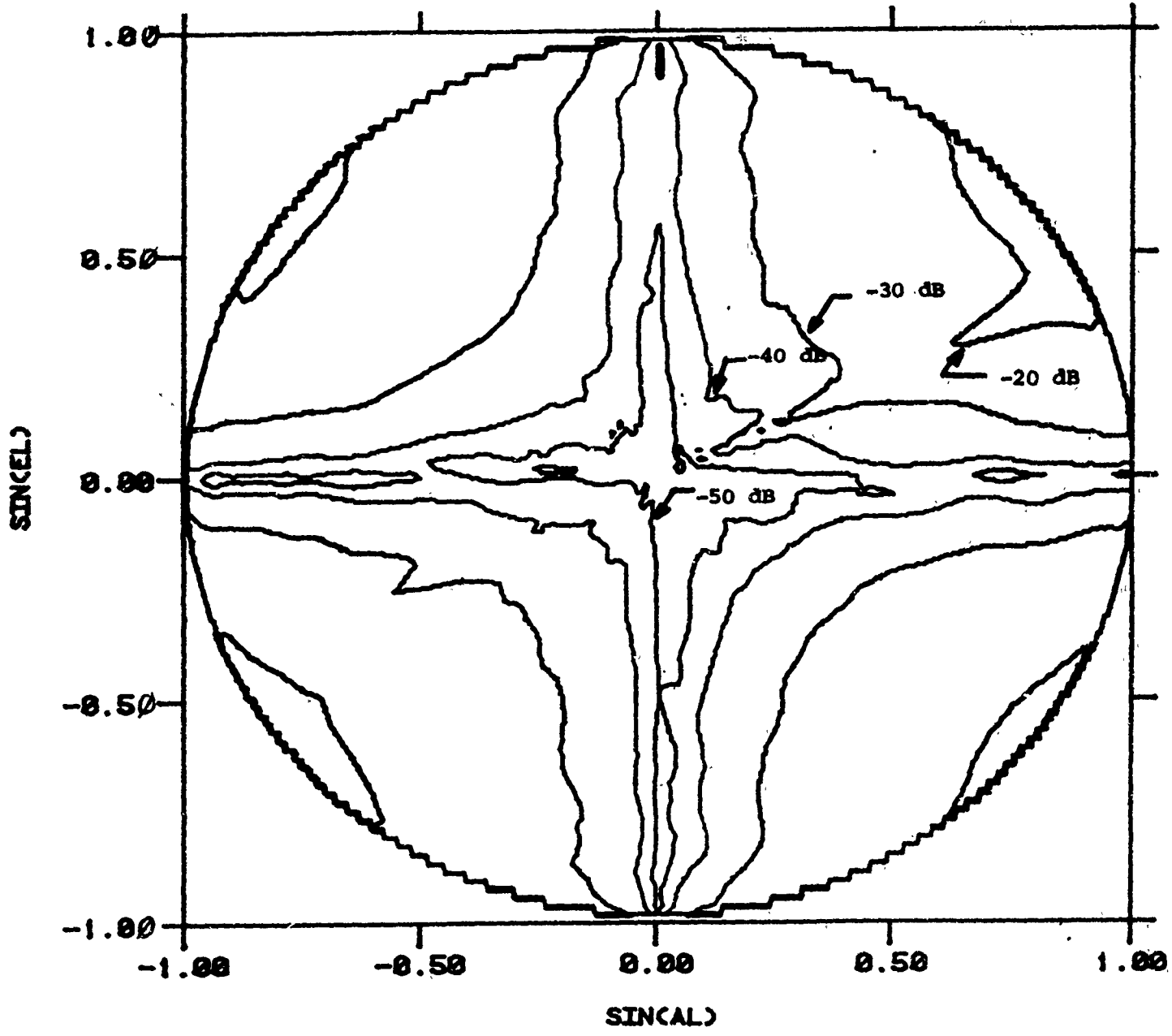

Figure 33. Equal-Amplitude Contours of the Elevation (cross-polarized) Far Field Pattern of the Open-Ended W/G Probe at 3.1 Ghz

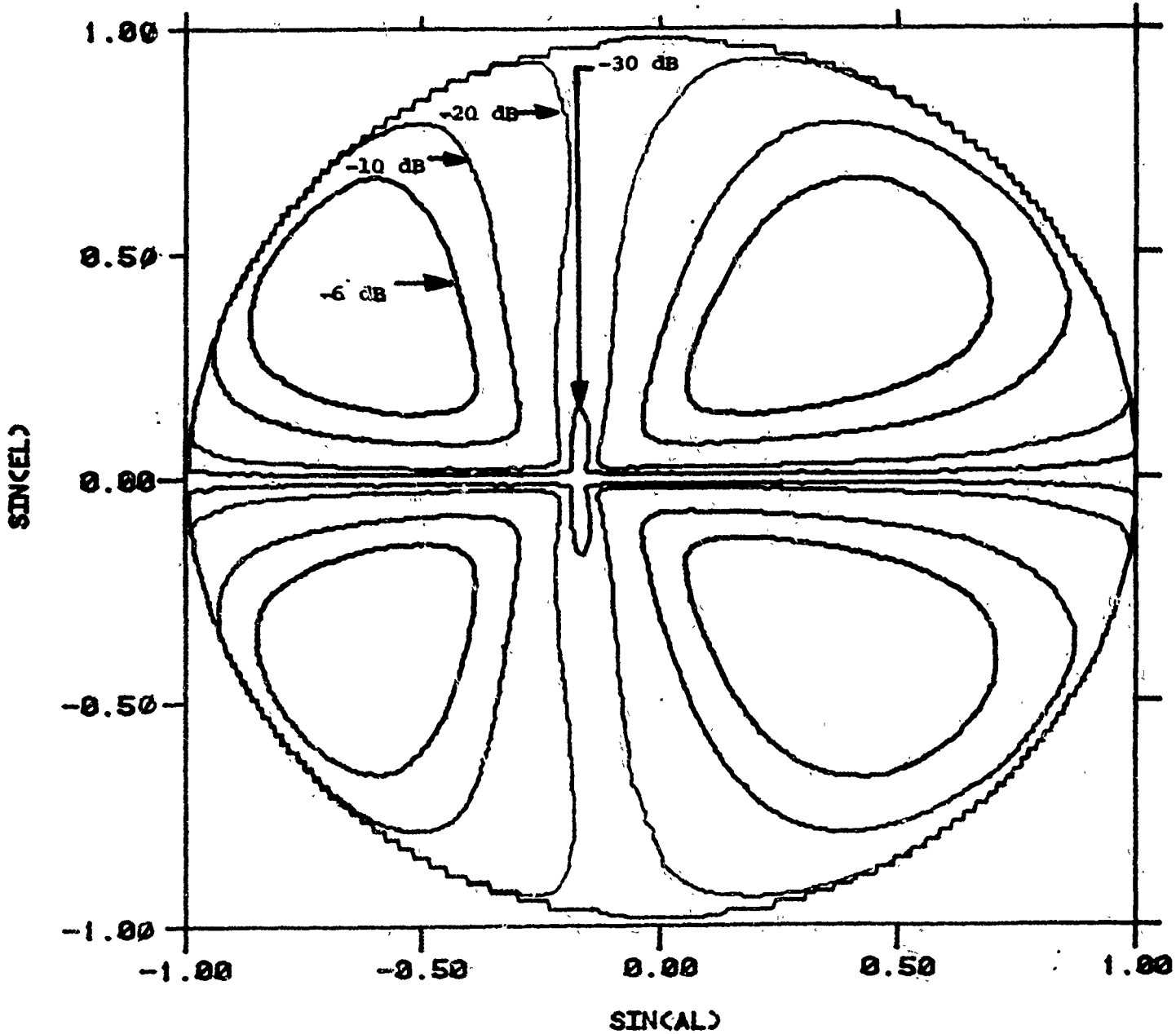

Figure 34. Equal-Amplitude Contours of the Elevation (Cross-polarized) Far Field Pattern of the Δ-Probe at 3.1 Ghz

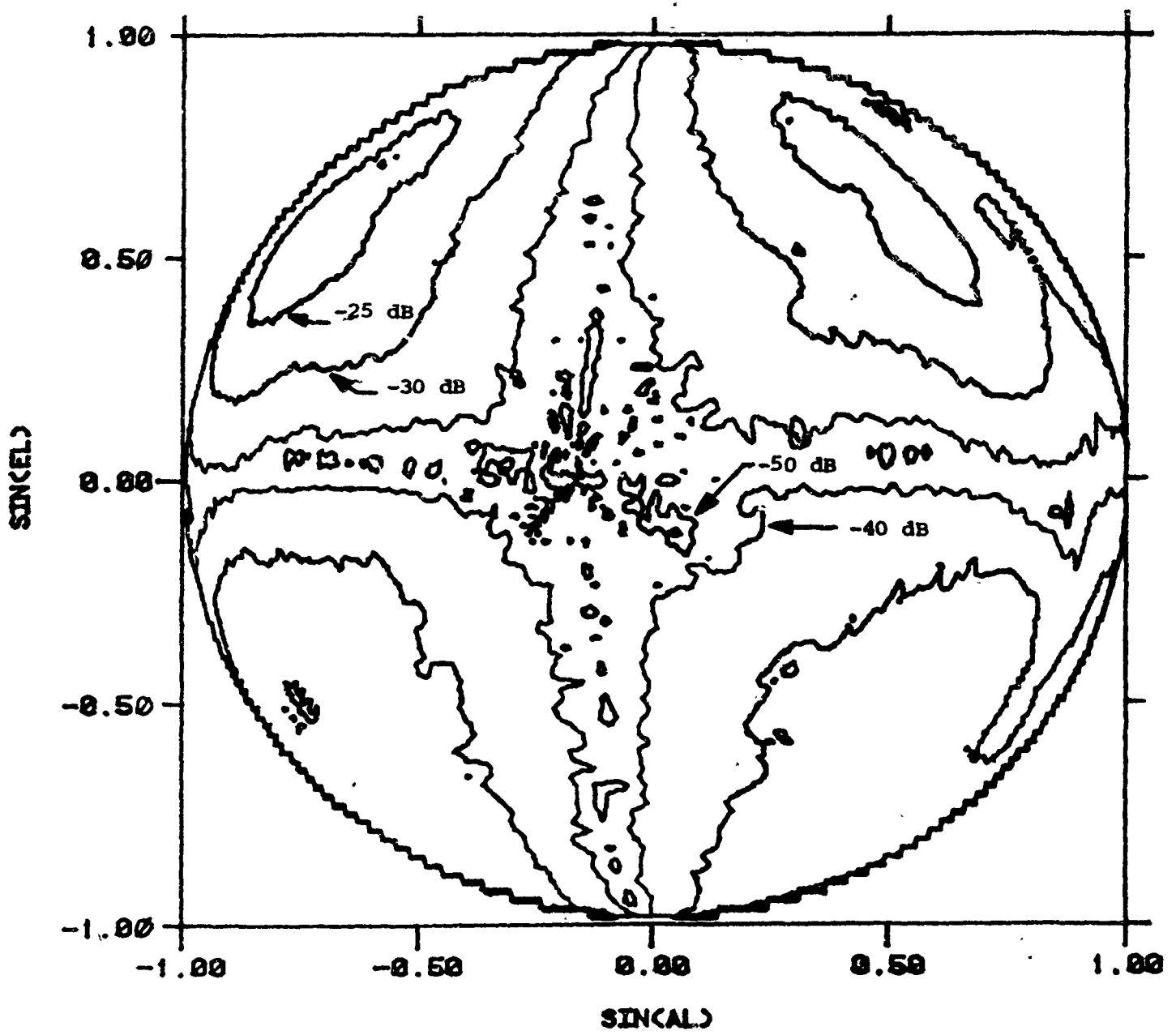

Figure 35. Equal-Amplitude Contours of the Elevation (cross-polarized) Far Field Pattern of the Σ-Probe at 3.1 Ghz

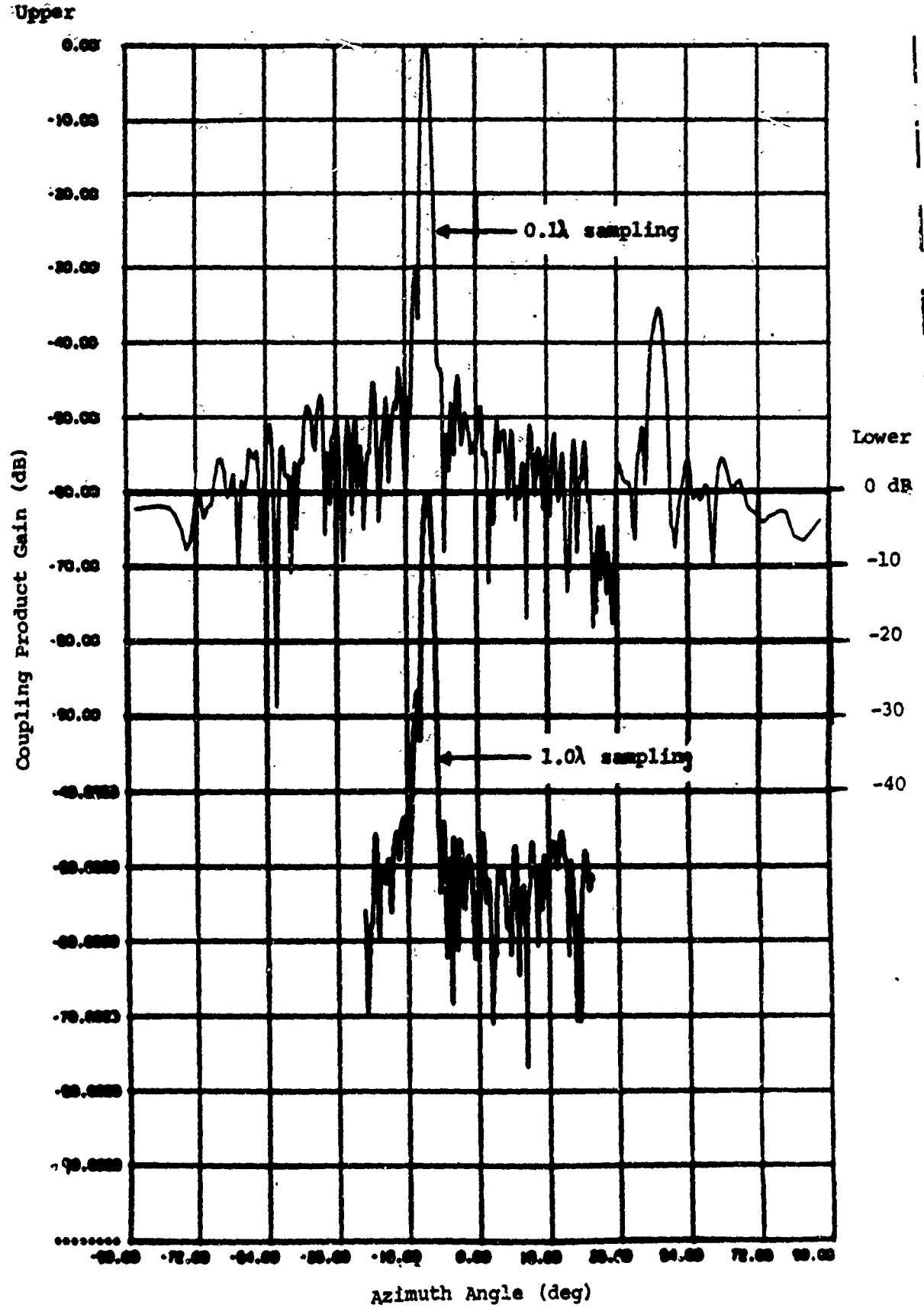

Figure 36. Coupling Product Spectrum from Centerline Scanning with the Σ-Probe and ULSA Array at 3.1 Ghz for Spacings of 1.0λ and 0.1λ

Σ-Probe Results

Figure 37 plots the summary results for the Σ probe aliasing tests. It shows the change in the measured peak sidelobe (-43.5 dB) as a function of NF sample density in the range $0.1\lambda < \Delta\chi < 1.0\lambda$. Insignificant peak sidelobe error is observed until $\lambda/2$ spacings are exceeded, and then aliasing increases peak sidelobe error by 8.5 dB compared with the reference scan peak sidelobe level. Similarly, the rms of the sidelobes in the azimuth plane (Figure 38) remains below -52 dB for NF spacings less than 0.5λ. Spacings greater than 0.5λ will add aliasing error until the measured rms sidelobes approach -49 dB at the wide sample spacings.

Δ-Probe Results

Figure 39 shows the non probe-corrected ULSA coupling product pattern as measured again at 3.1 Ghz, but using the mechanically steered Δ-probe. Probe/array separation distance was 65 cm. As with the Σ probe at wide sample spacing, the wide angle sidelobes are filtered from the coupling product spectrum--most noteably the known anomalous lobe at $+44^{\circ}$ is missing from the 1.0λ spectra. Figure 40 gives a summary of the measured change in the -46.5 dB peak sidelobe for the NF sampling increments in the range $.1\lambda < \Delta\chi < 1.0\lambda$. The 0.1λ spectrum again is considered as the reference spectrum. Measured peak sidelobes are degraded when sample spacings greater than 0.5λ are used. The apparent trend change at $.70\lambda$ is believed due to wide angle filtering of the high anomalous lobe. Figure 41 shows the changing single plane rms sidelobe level for the various sampling densities. Again the trend change at $.70\lambda$ tracks the Σ probe results, although, in general, the Δ-probe appears more sensitive to aliasing error in the low sidelobe ULSA pattern.

4.2 Scan Area Truncation Results

To compute the accuracy of sidelobe measurement under conditions of decreasing scan area size, two-dimensional scan data of adequate extent for each probe is systematically truncated prior to transform (see Figure 18), and the change in gain for a selected sidelobe is noted. Plots

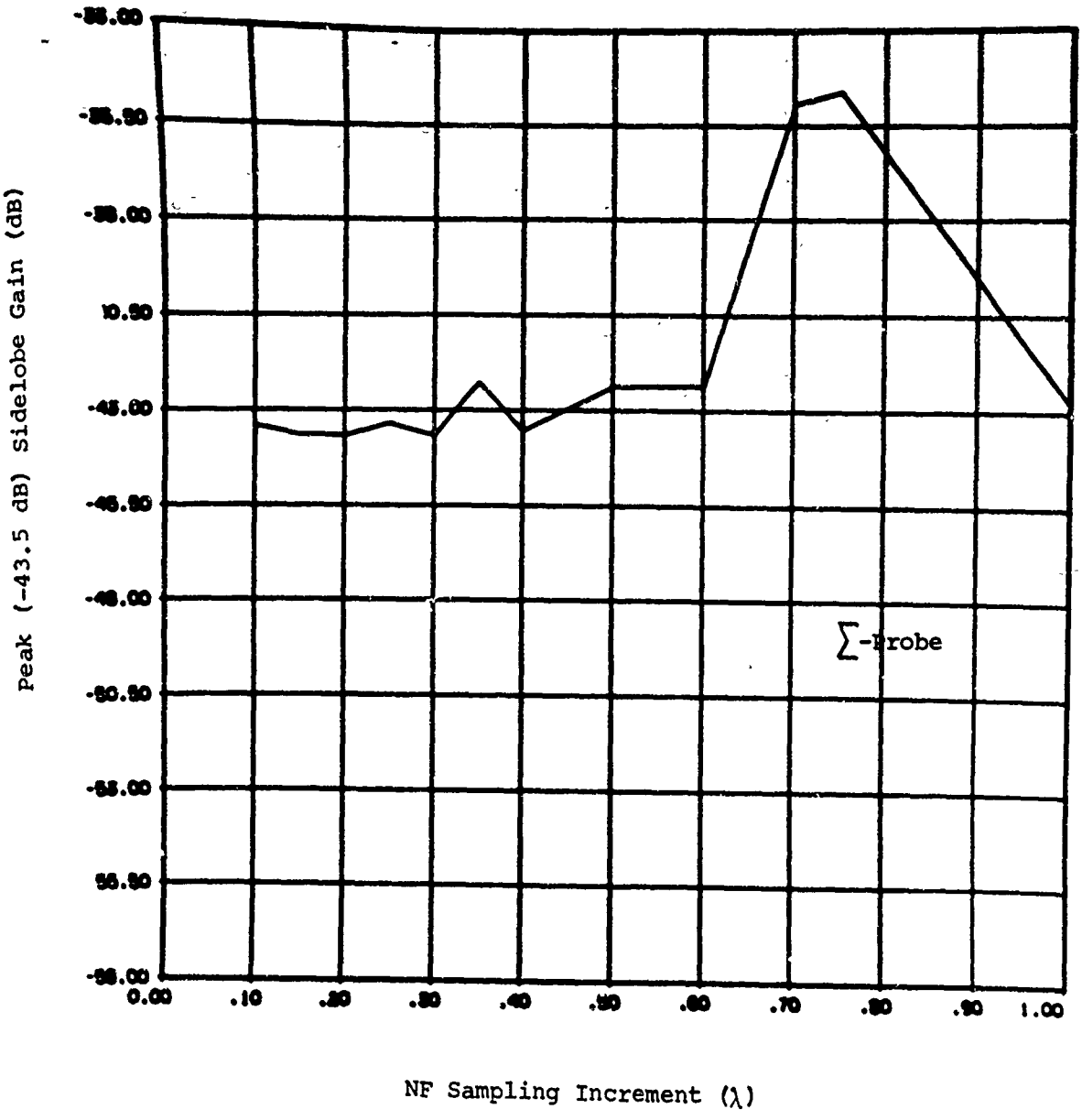

Figure 37. Summary of Peak Sidelobe Error Due to NF Aliasing for the Σ-Probe at 3.1 Ghz

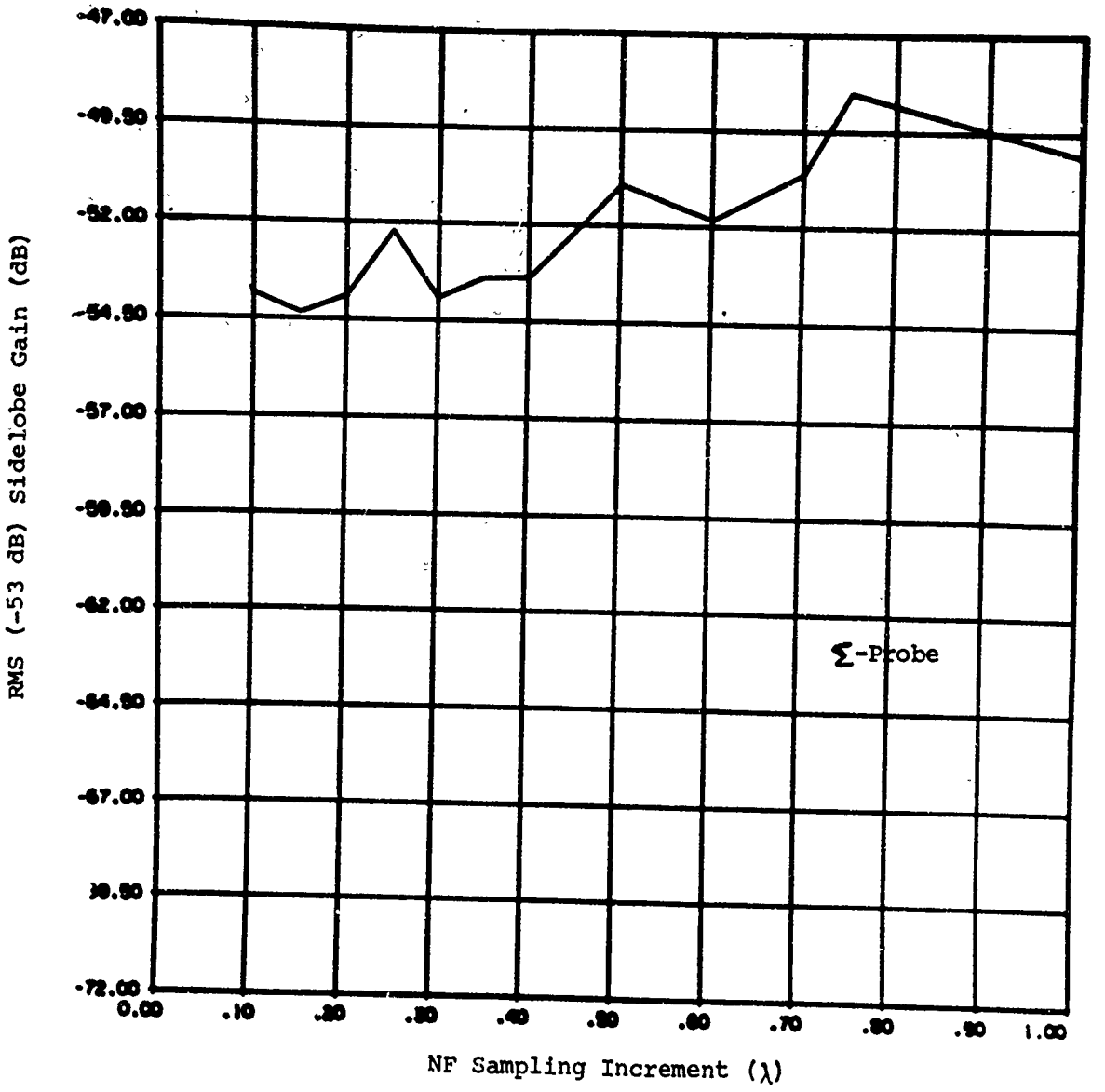

Figure 38. Summary of rms Sidelobe Error Due to NF Aliasing for the Σ-Probe and ULSA Array at 3.1 Ghz

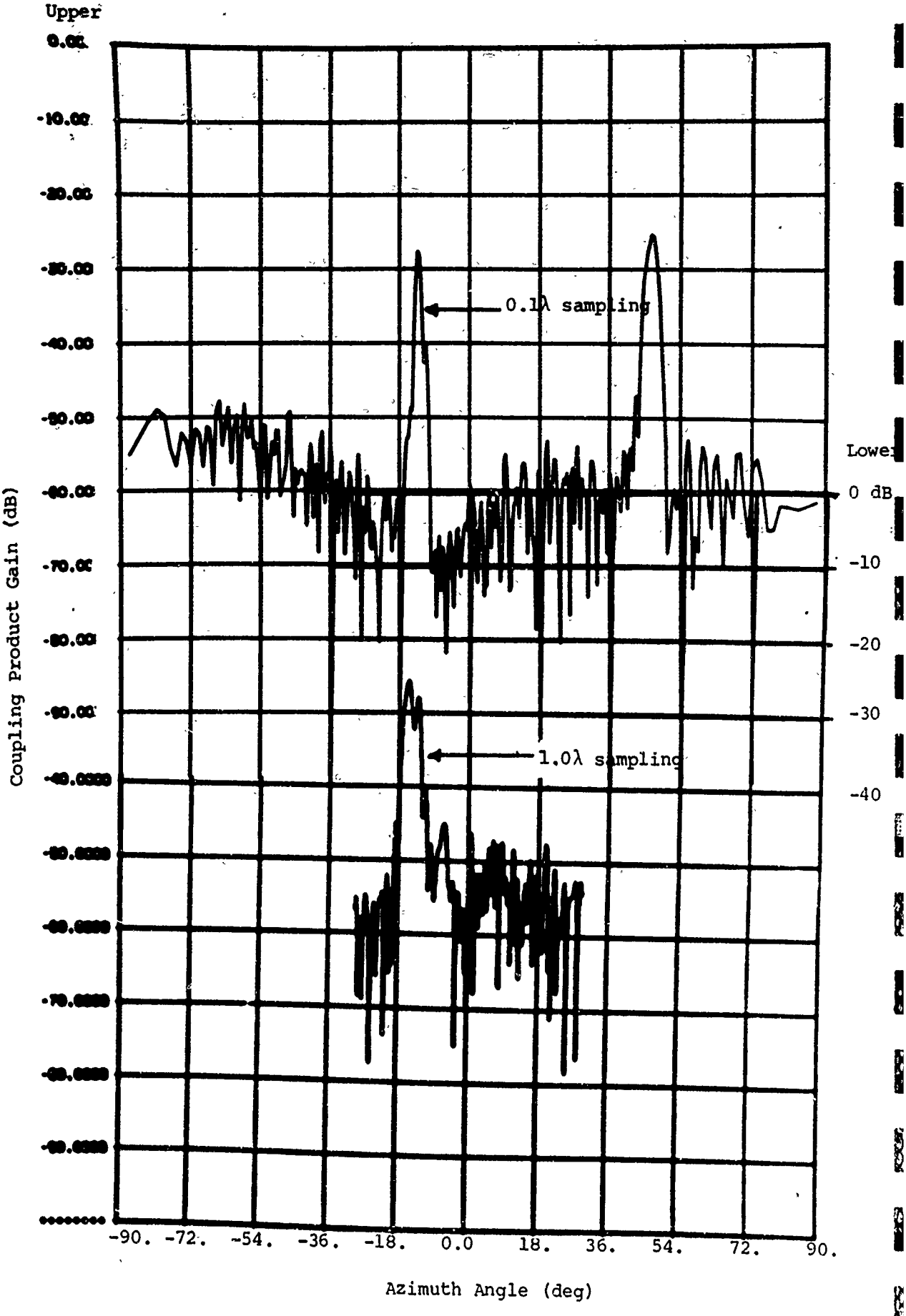

Figure 39. Coupling Product Spectrum from Centerline Scanning with the Δ-Probe and ULSA Array at 3.1 Ghz for Spacings of 1.0λ and 0.1λ

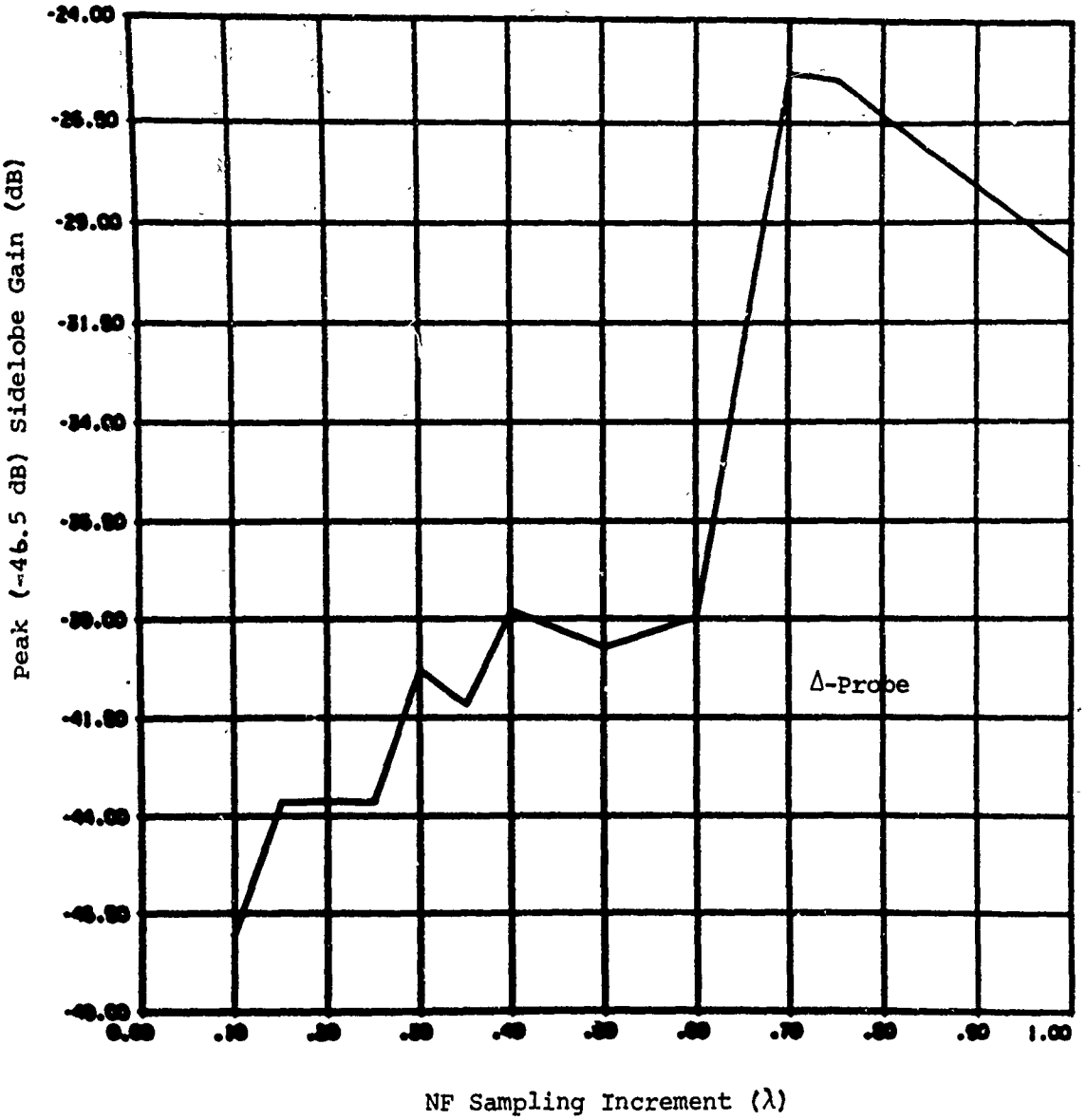

Figure 40. Summary of Peak Sidelobe Error Due to NF Aliasing for the Δ-Probe at 3.1 Ghz

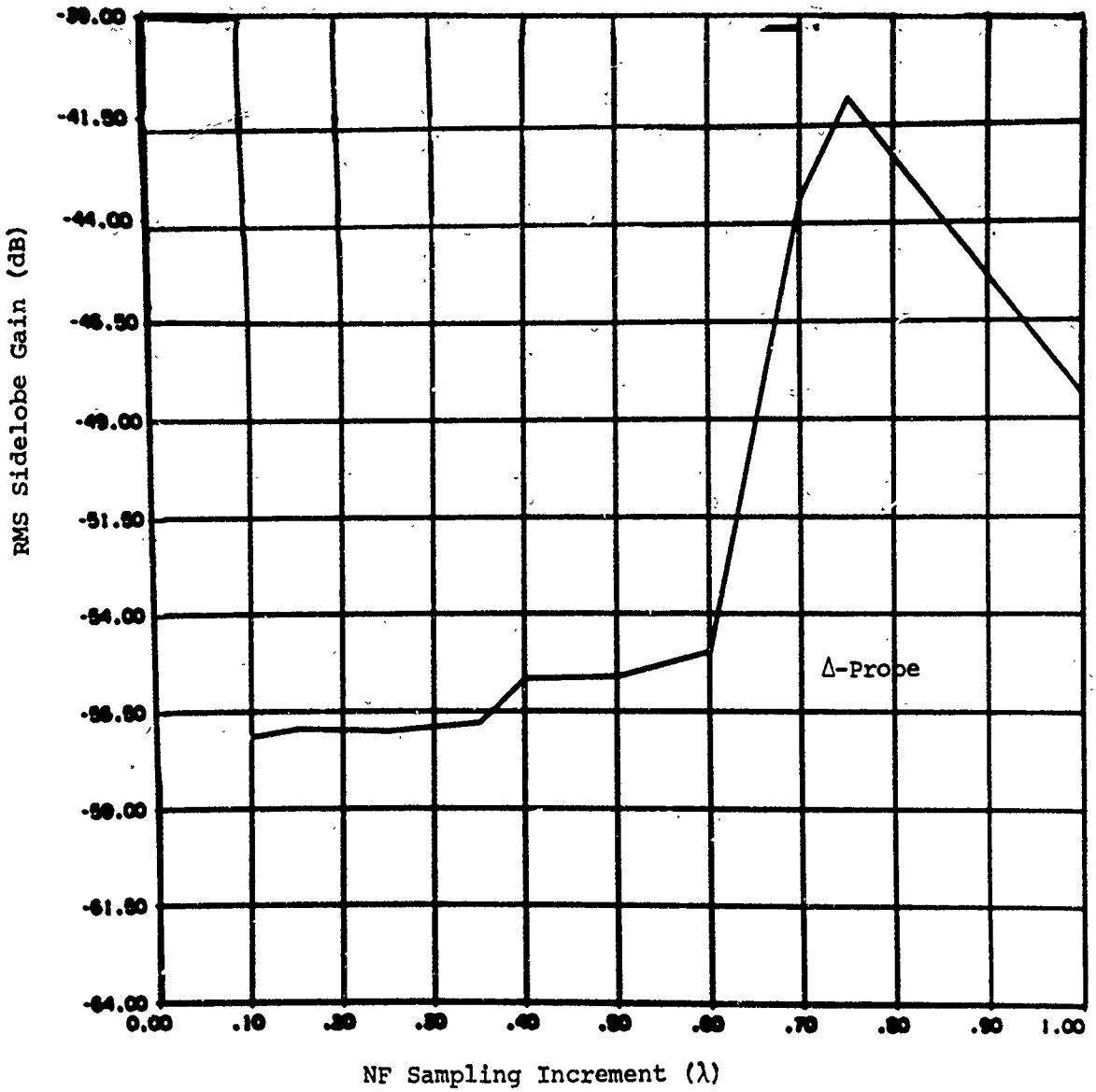

Figure 41. Summary of RMS Sidelobe Error Due to NF Aliasing for the Δ-Probe at 3.1 Ghz

of sidelobe gain change vs. normalized scan length for the three probes are summarized below. Figure 42 shows the selected ULSA sidelobes, and the three probe patterns used to measure their gain change during truncation.

For sidelobe #1 (-18.8 dbi at -37.6°), the measured gain change for all three probes is shown in Figure 43. The gain error curves converge similary because the wavenumber filtering properties of the three probes are nearly identical for that sidelobe angle.

The gain convergence curves for sidelobe #2 (-20.4 dbi at -17.6°) are shown in Figure 44. The measured sidelobe gain change for the open-ended waveguide and sum probe coverage at a normalized scan length of about 1.30, while the sidelobe gain change for the Δ-probe does not converge until a normalized scan length of 1.57 is reached. For sidelobe #2, the delta probe response is 10 dB below the response of the other two probes. Thus, the delta probe is filtering this near-in sidelobe undesirably.

The gain convergence plots for sidelobe #3 (-18.7 dbi at 65.8°), are shown in Figure 45. The sidelobe gain convergence for the open-ended waveguide and Δ-probes are nearly identical, because their far field responses are nearly identical at this sidelobe angle. The 12 dB higher full scan length sidelobe gain for the sum probe is due to its undesirably high discrimination (apparent null) at this angle. Such a probe can not be reliably used to measure wide angle low sidelobes.

Comparison to Error Bound--Σ Probe

Finally, the Yaghjian upperbound was computed for sidelobe error due to scan area truncation as shown in Figure 46. This bound selectively deletes perimeter data from an otherwise adequate two-dimensional set when scanning the ULSA array for a Z-separation distance of 65 cm. Then the angle γ_{max}, in Figure 17, is 12.2°. Selecting sidelobe #1 to be well within θ_c, and evaluating the Yaghjian error bound for Σ probe scanning, the dashed curve in Figure 46 can be generated. It shows that for truncation ratios of $L_{max}/2a > 1.3$, the Yaghjian upperbound is no greater than 3.8 dB from the -23.1 dbi true sidelobe under test, and approaches the "true" value

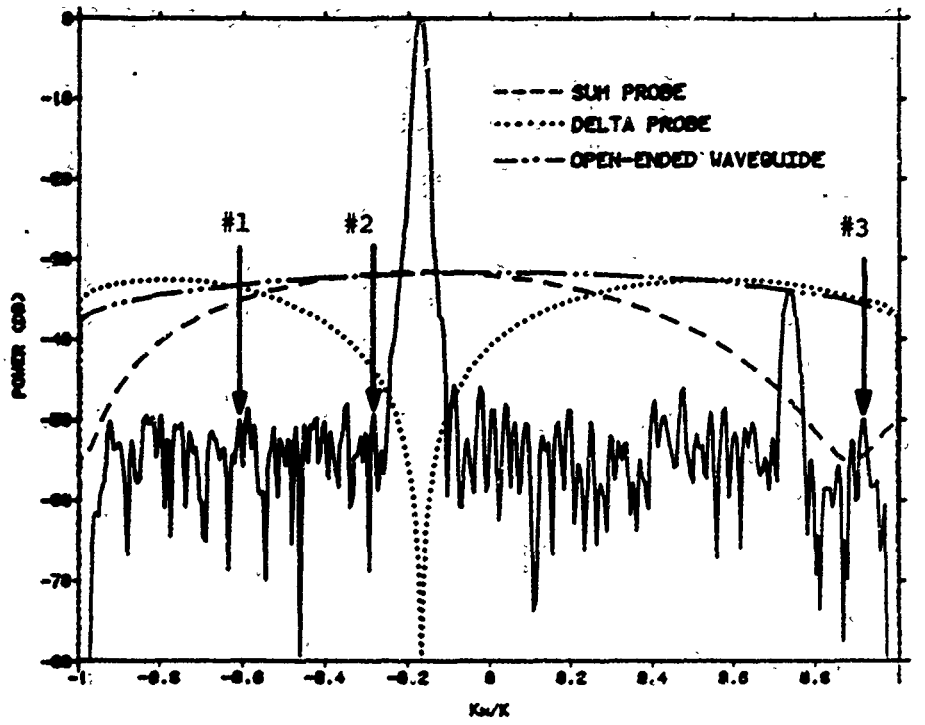

Figure 42. Sidelobes Selected (#1,2,3) for Measuring Gain Error Due to Scan Area Truncation with the Three DESAT Probes

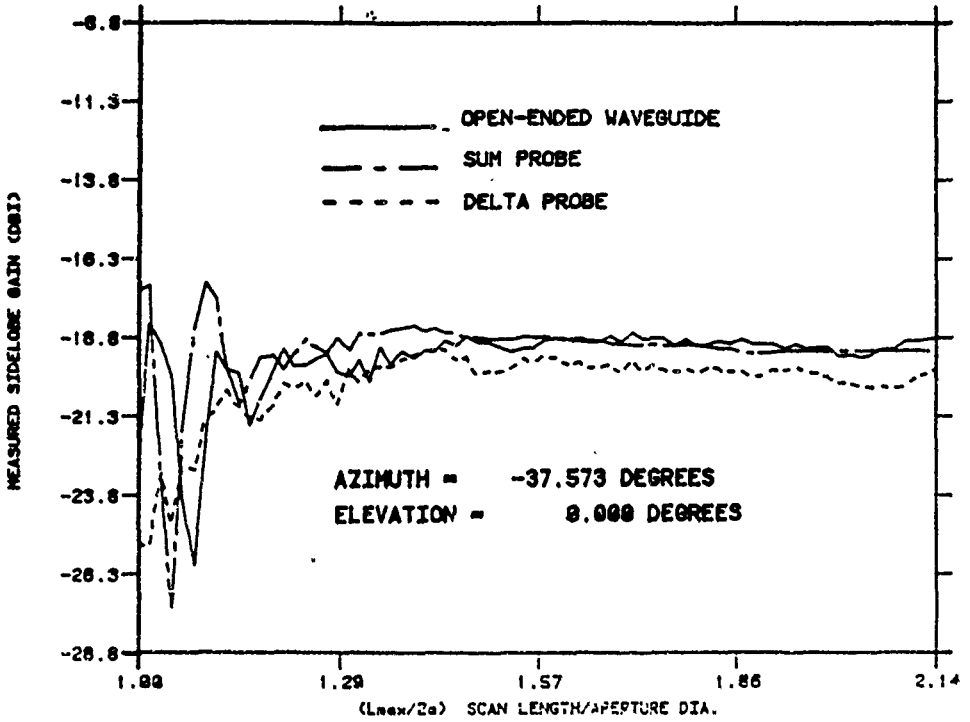

Figure 43. Measured Gain Error for Sidelobe #1 as a Function of Normalized Scan Length for the Three DESAT Probes

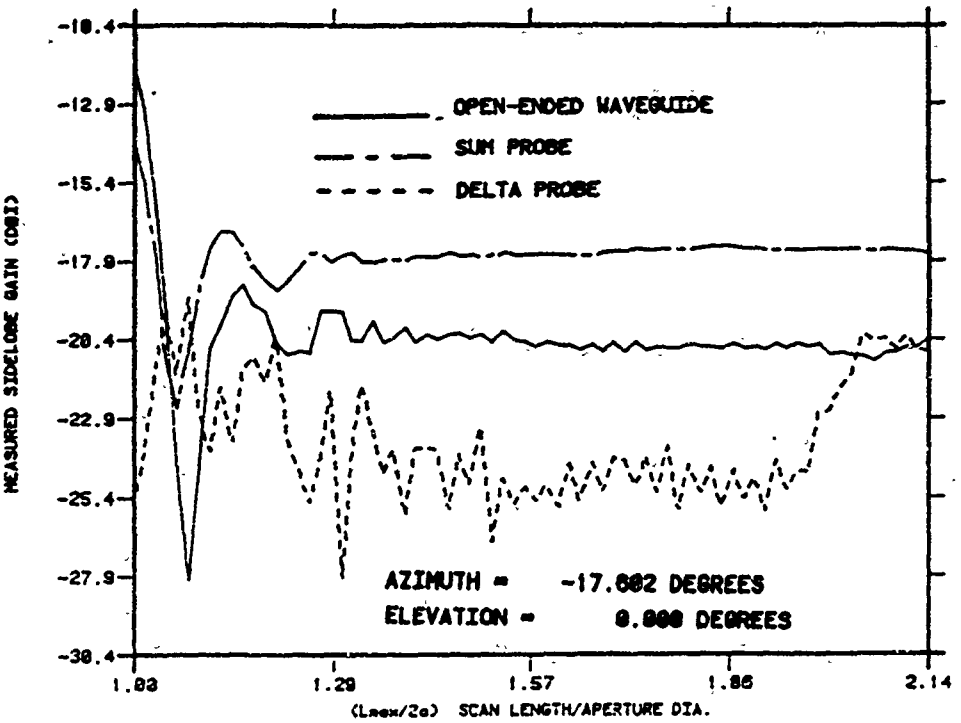

Figure 44. Measured Gain Error for Sidelobe #2 as a Function of Normalized Scan Length for the Three DESAT Probes

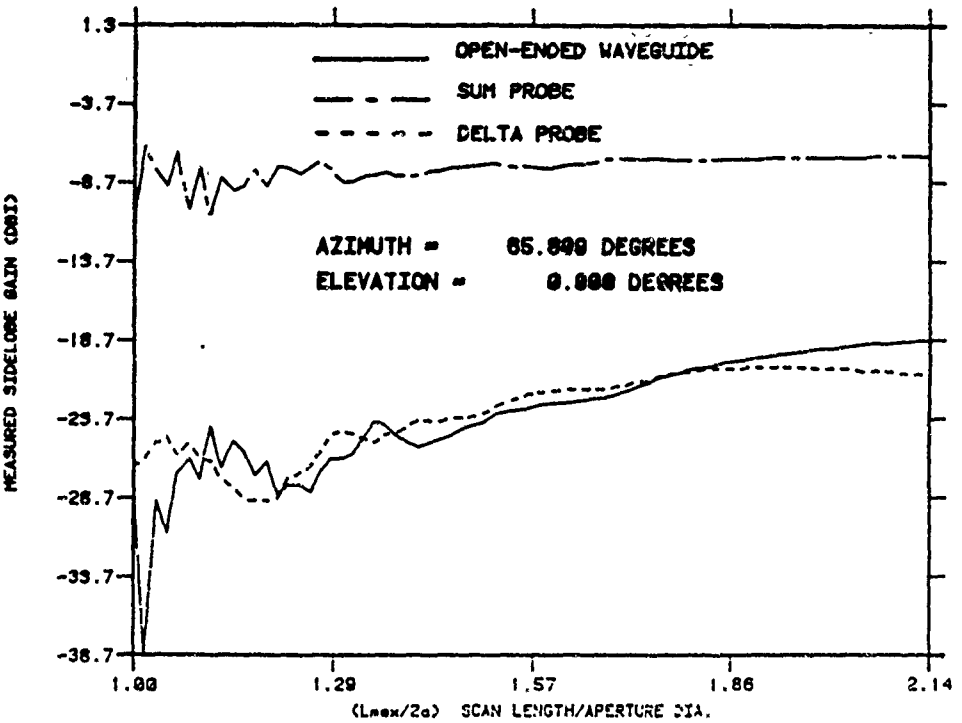

Figure 45. Measured Gain Error for Sidelobe #3 as a Function of Normalized Scan Length for the Three DESAT Probes

of -23.1 dbi for increasingly larger scan sets. At the same time, the actual sidelobe error is shown to be in the range 0.0 to +0.5 dB over the truncation range (solid curve), and always degrades (increases) the low sidelobe from its true value. These results show that two-dimensional scan lengths no larger than 30% greater than the test's antenna's maximum dimension will adequately measure low near-in sidelobes at the -23 dbi level within 0.5 dB using a directive Σ probe.

Comparison to Error Bound--Δ-Probe

Similar Δ-probe scanning tests were processed to compute the Yaghjian error bound for measurement accuracy of sidelobe #1. Figure 47 shows that the predicted error (dashed curve) exceeds the actually measured sidelobe error by at least 15 dB for truncation ratios of $L_{max}/2a > 1.3$, and never does approach the "true" sidelobe level of -23.1 dBi, even at full area scanning. Note the scale change for the "predicted gain error" axis between Figures 46 and 47. The large disparity between mesured sidelobe error and the predicted bounding estimate occurs because the bounding expression in Figure 18 is derived assuming an omni-directional, i.e., non-filtering, probe pattern. To properly use the Yaghjian bound with a filtering probe, a directivity correction for the perimeter scan fields must be applied. This has not been accomplished during DESAT testing.

4.3 Probe Z-Position Error Results

Periodic scanner z-position error is a major source of sidelobe error in any NF facility. As shown in section 3.5.1 by equations (17, 18), sidelobe error depends on the period and magnitude of Z-position error. Both Σ and Δ-probes were again scanned, and two-dimensional NF data was transformed for the coupling product spectra, and finally probe-corrected for far field antenna patterns. Two NF scan sets were measured--one containing only residual scanner position errors whose certified magnitudes are given in Table 3, and a second scan set having intentionally induced Z-probe position offset with each step of the probe tower. Three sinusoidal Z-position errors were thus induced simultaneously, in order to produce paired azimuth plane error lobes. The magnitudes (inches of tower offset in Z)

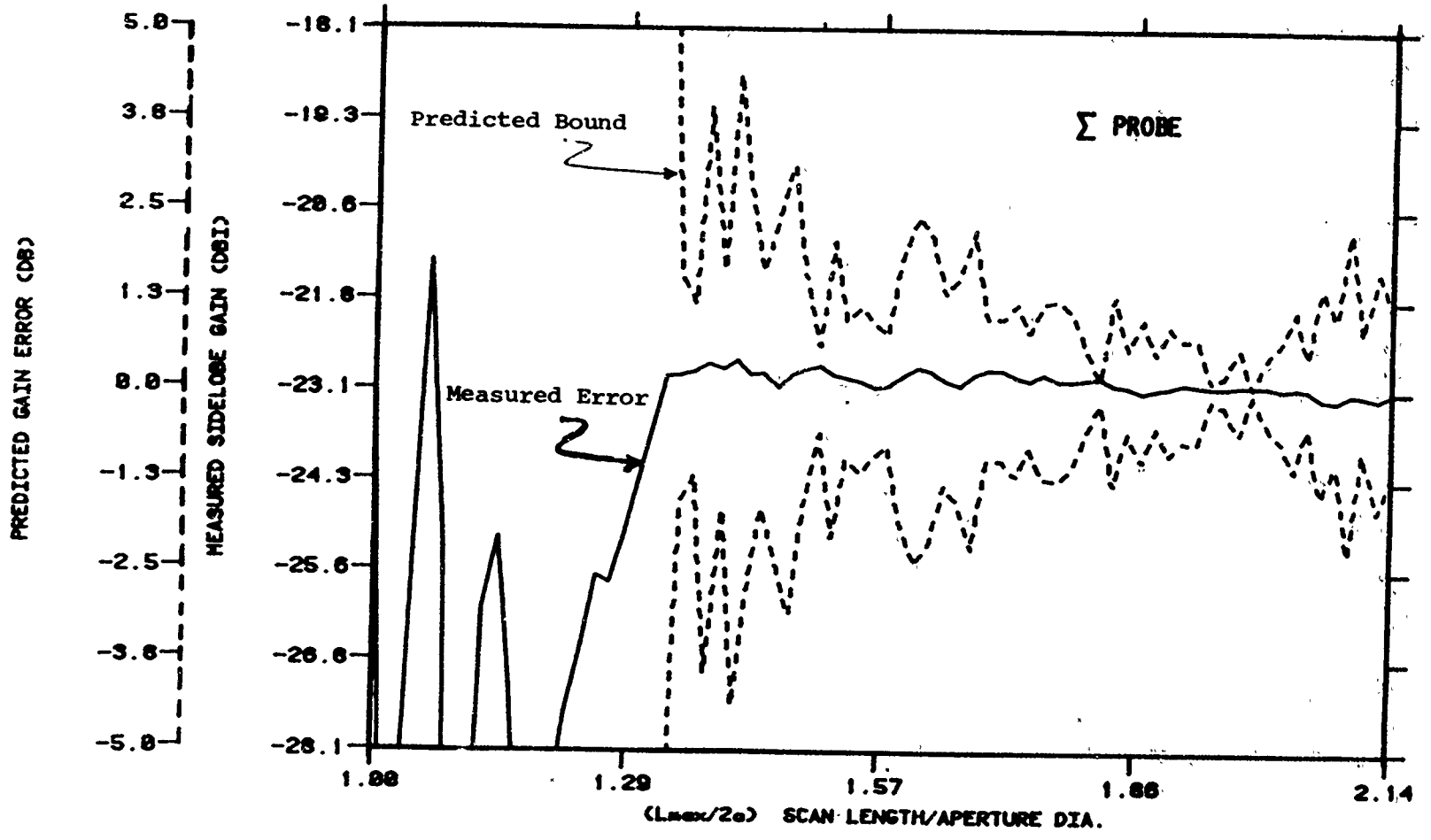

Figure 46. Comparison of the Yaghjian Upperbound for Sidelobe Error Due to Scan Area Truncation, with the Measured Error, for Sidelobe #1 and $\sum$-Probe Scanning

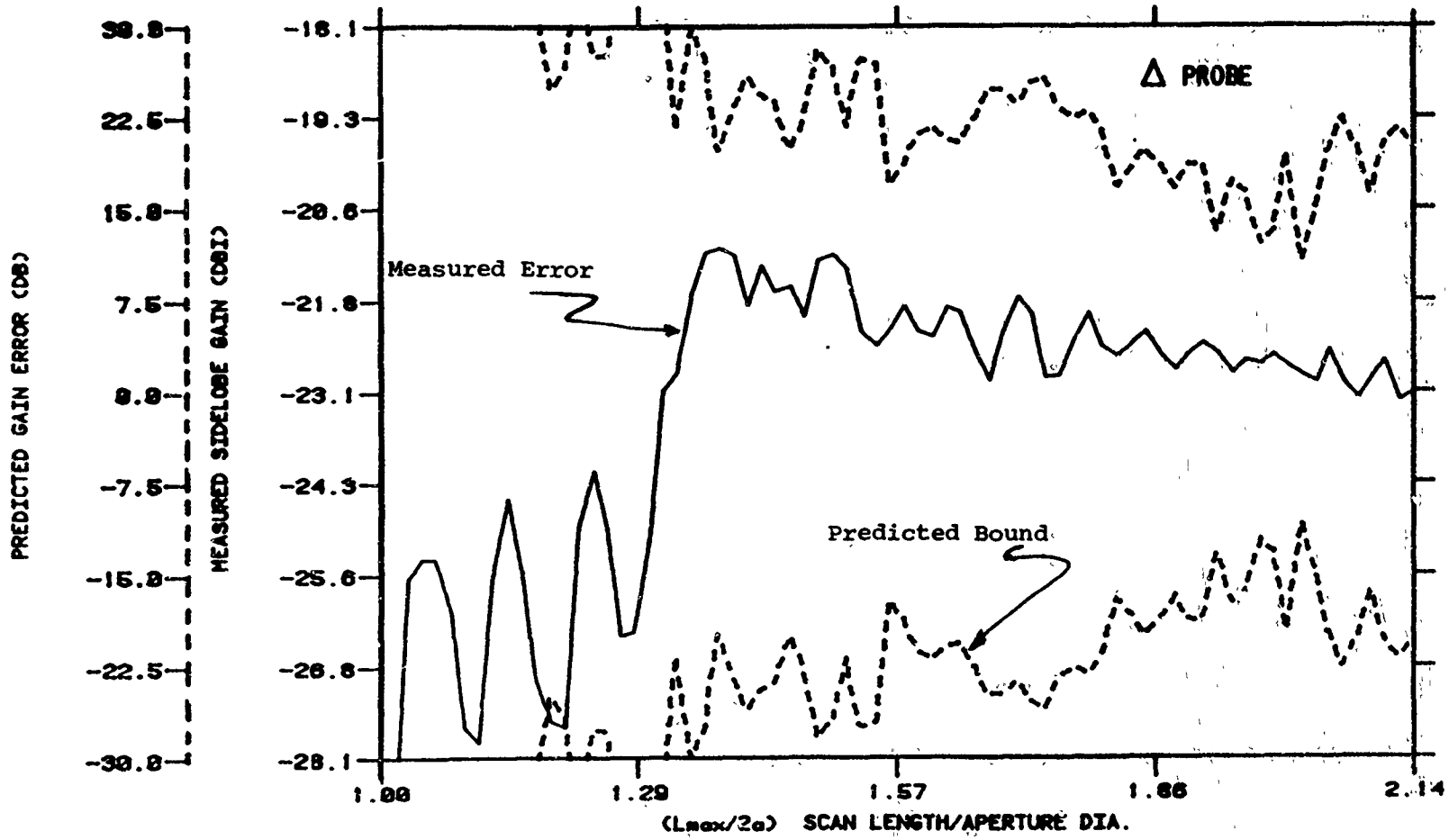

Figure 47. Comparison of the Yaghjian Upperbound for Sidelobe Error Due to Scan Area Truncation, with the Measured Error, for Sidelobe #1 and Δ-Probe Scanning

and periods of induced error are given in Table 8. In these tests, Z-position error is assumed to produce only NF phase error.

Results of scanning both probes with and without the induced position errors, are shown overlayed in the probe corrected patterns in Figure 48. The dotted patterns clearly show the systematically induced error lobes in the Σ probe overlays, but the Δ-probe overlays, following probe correction, shown no evidence of the paired error lobes to within repeatability limitations. Finally, the data in Table 9 summarizes the results of these tests, and lists both predicted and measured sidelobe ratios due to induced position error. The frequency of error in the direction of tower stepping is given as cycles/step (275 total steps), and the parenthetical values are the number of error periods in the full scan.

4.4 Receiver Amplitude Error Results

NF data measured with the open-ended W/G and Δ-probes were corrupted prior to processing in order to simulate larger receiver amplitude error than actually existed during test. The simulated amplitude error was made to vary sinusoidally with decreasing amplitude level in the direction of scan. Such an error variation is improbable with standard receivers, but it does produce the worst-case sidelobe errors in the far field, and therefore bounds the effects of any more practical NF amplitude error. The simulated error was of form:

$$A_{RX} = \frac{A}{1 + (A/A_{max} - 1)\mu} \qquad (24)$$

$$\mu = \mu_o \cos \frac{2\pi(J - J_{cen})\Delta x}{T}$$

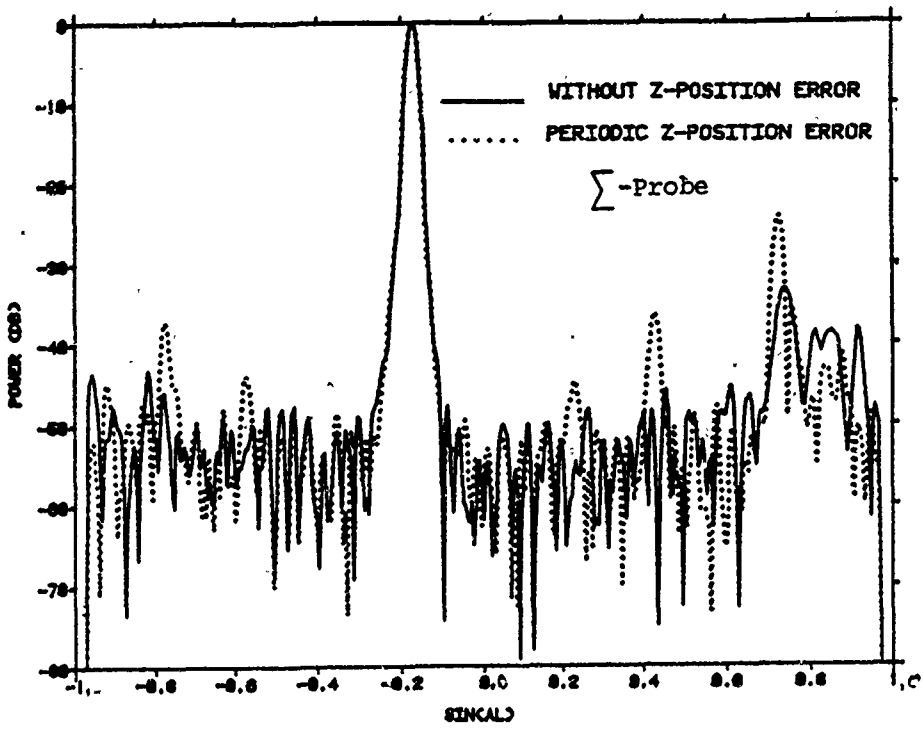

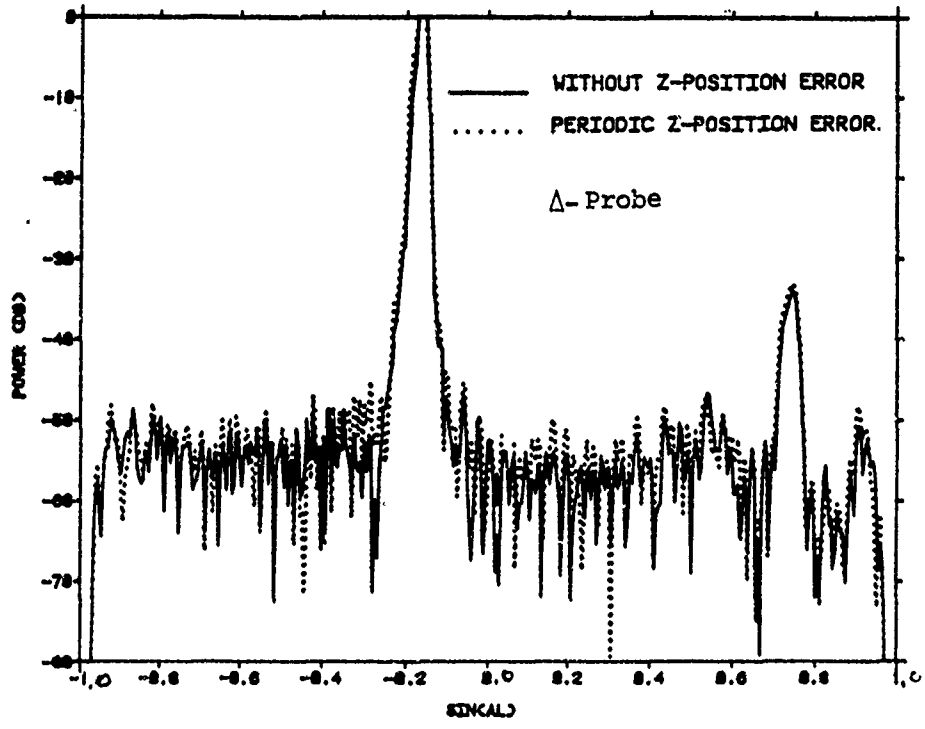

Figure 48. ULSA Azimuth Plane Pattern Computed from Σ and Δ- Probe Scanning with and without Induced Z-Position Error

Table 8. Induced Sinusoidal Z-Position Scanner Error Parameters

Z-Position Error Peak (in.)	Period (λ)	Resultant Peak NF Phase Error (Deg.)
.005	2.50	0.47
.010	1.67	0.95
.015	1.11	1.42

Table 9. Predicted and Measured Error Sidelobe Ratios Due to Induced Scanner Z-Position Errors when Scanning with Sum and Delta Probes

Z-POSITION ERROR		ERROR LOBE PEAK / UNERRORED SIDELOBE PEAK (DB)				ERROR LOBE LOCATION
FREQ CYCLE/SAMPLE	PEAK ERROR (IN)	SUM PROBE		Δ PROBE		SIDELOBE DIRECTION (Kx/K)
		PREDICTED (DB)	MEAS (DB)	PREDICTED (DB)	MEAS (DB)	
.152 (42)	.005	6.24	6.5	-22.01	<-22.	-0.57
	.005	9.15	10.0	-17.83	<-18.	0.23
.232 (64)	.010	8.18	9.1	-20.18	<-20.	-0.77
	.010	12.83	12.0	-18.65	<-19.	0.43
.356 (98)	0.15	N/A		N/A		-1.07
	0.15	8.85	9.8	-32.21	<-32	0.73

where A is the measured NF amplitude

A_{max} is the measured NF amplitude peak

μ_o is the receiver nonlinearity factor (constant)

J is the NF scan number

J_{cen} is the central NF scan number

Δx is the NF X-spacing in wavelengths, and

T is the error period in wavelengths.

Three cosinusoidal receiver amplitude errors were synthetically introduced into the measured NF data whose non-linearity factors and periodicities are given in Table 10.

Table 10. Induced Receiver Amplitude Error Parameters

Receiver Non-Linearity Factor, μ (v/v)	Error Period (λ)
.05	3.33
.10	2.00
.20	1.43

The resultant NF amplitude error distribution is quite complex since it varies as a function of both scanner X-location and relative NF amplitude level. A convenient way to display this induced error is to compute the ratio of the errored NF amplitude to the error free NF amplitude. Plots of this ratio for ULSA centerline X-cuts are shown in Figures 49 and 50 for the open-ended W/G and Δ-probes respectively. Notice that the error level is about the same in both NF amplitude ratio plots, but is at minimum magnitude for the open-ended W/G probe near the scan center. This NF error form also produces far field error which is proportional to the coupling product gain in the direction of interest. Thus, equation (19) predicts that the FF sidelobe error due to NF receiver amplitude error will be reduced by the change in g(K) imposed by the Δ-probe in the same way as was probe position error gain reduced by Δ-probe scanning.

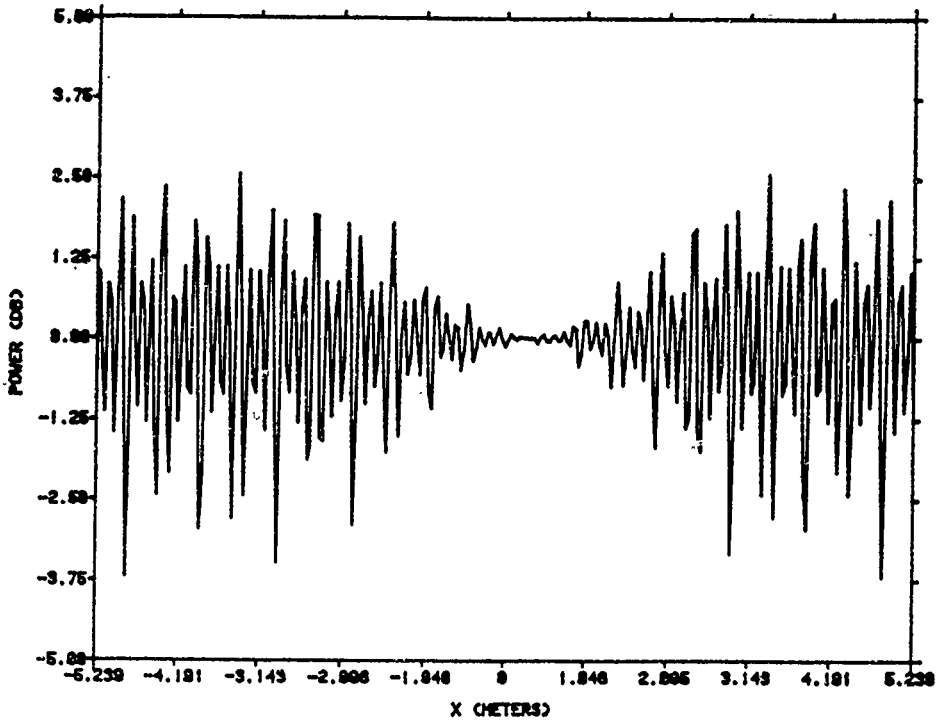

Figure 49. ULSA Centerline NF Amplitude Error Ratio Due to Induced Receiver Error as a Function of Scan for the Open-Ended W/G Probe

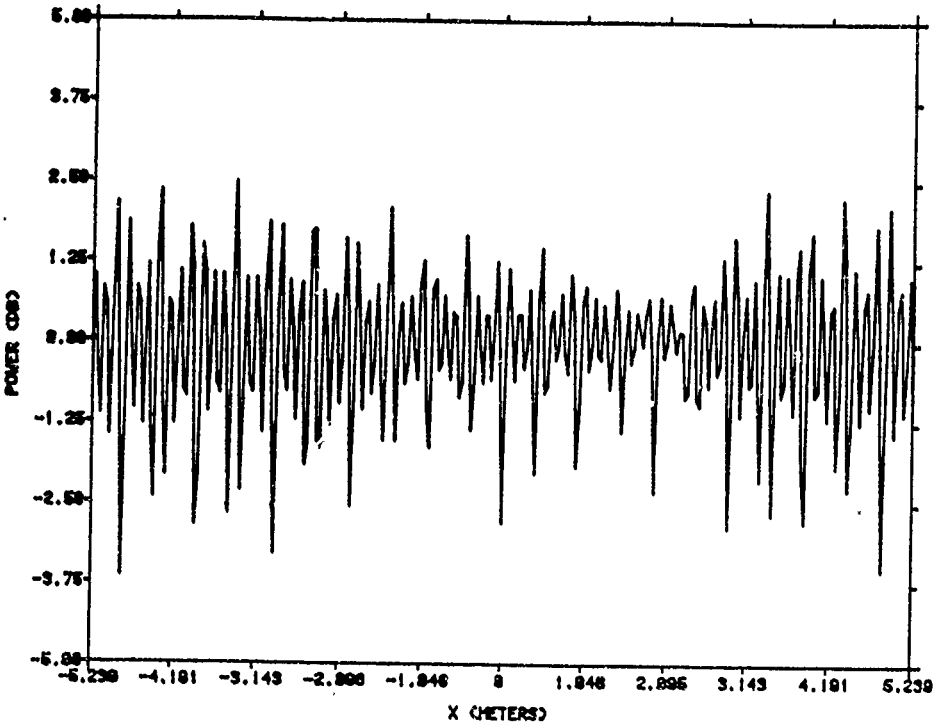

Figure 50. ULSA Centerline NF Amplitude Error Ratio Due to Induced Receiver Error as a Function of Scan for the Δ-Probe

Results showing the ULSA azimuth plane pattern with and without receiver amplitude error are shown in Figures 51 and 52 for the two probes. The receiver amplitude errors produce three pairs of echo lobes in the ULSA pattern measured with the open-ended W/G probe as shown in Figure 51. The increasing error lobe levels correspond to the increasing receiver nonlinearity. Figure 52 confirms that the Δ-probe discriminates against the effect of the receiver amplitude error at the -50 dB sidelobe level almost entirely. This same improvement is also expected for receiver phase errors, although not demonstrated herein.

4.5 Random Error Results

To certify the accuracy of measurement due to all sources of random NF error, two dimensional evanescent scanning tests were conducted with the AWACS array and the three DESAT probes. Near field spacings of 3.81 cm insured that the coupling product spectrum would extend to $(k_x/k, k_y/k) = 1.19$ at the selected test frequency, thus exposing the so-called evanescent spectrum whenever $\left[(k_x/k)^2 + (k_y/k)^2\right]^{1/2} \geq 1.0$. Because all evanescent antenna modes actually radiated by the test antenna are attenuated way below the dynamic range of the NF instrumentation only a short distance from the antenna, we do not expect to intercept evanescent fields during scanning with any probe at $Z = 35$ cm (3.85λ). Therefore, the magnitude of the uncorrelated wavenumbers in the evanescent region of the coupling product spectrum are a direct measure of far field error due to all NF random error contributors.

Evanescent spectral wavenumbers for the AWACS array are shown contoured over the viewable limits in Figures 53 and 54 as measured by NF scans with the two DESAT probes. These contours show generally a random distribution of sidelobe peaks in the region beyond the visible space limits, at or below -80 dB for the open-ended waveguide probe (Figure 53). For the Δ-probe spectrum (normalized to peak for the open-ended waveguide probe), the evanescent sidelobes have random peaks below -90 dB. However, in both contours, the random evanescent spectrum also contains sidelobe ridges which can not be a real property of the array, i.e., they do not belong to the periodic array factor, because of course the evanescent NF are

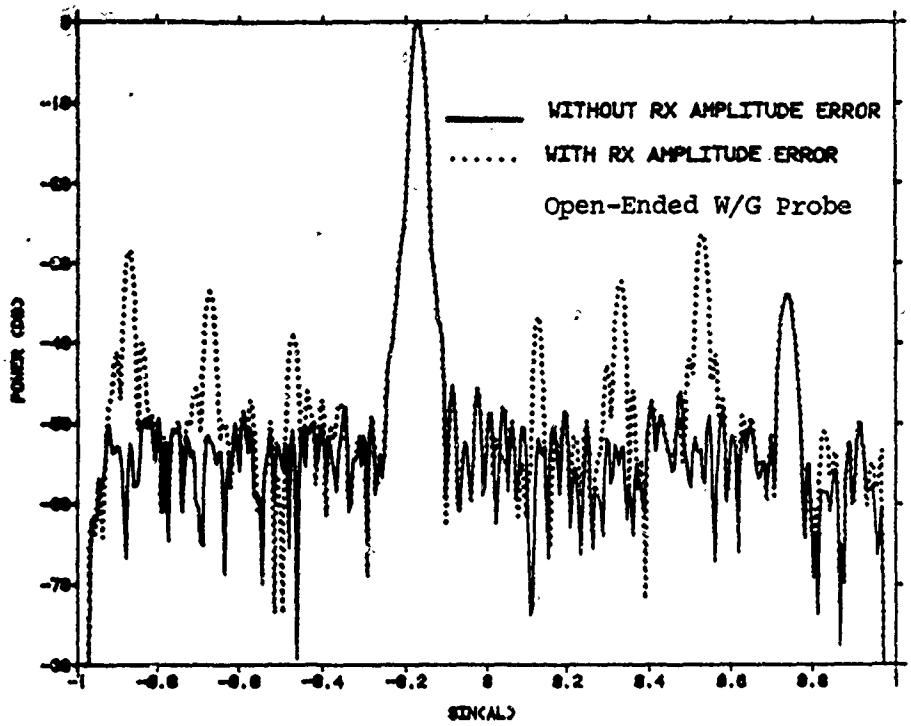

Figure 51. ULSA Azimuth Plane Pattern Computed from Open-Ended W/G Probe Data with and without Induced Receiver Error (Table 10)

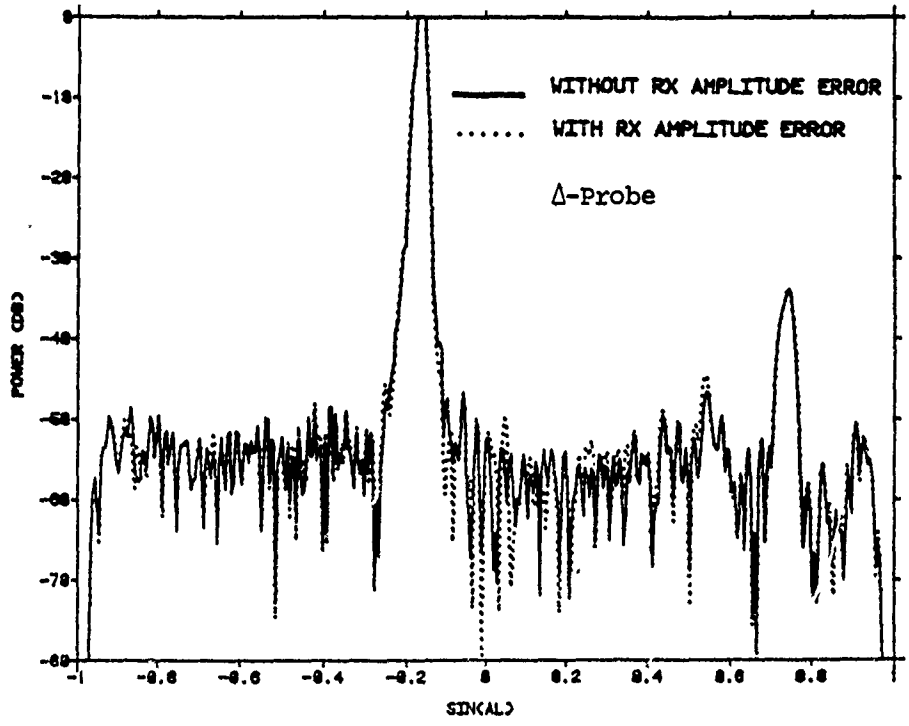

Figure 52. ULSA Azimuth Plane Pattern Computed from Δ-Probe Data with and Without Induced Receiver Error (Table 10)

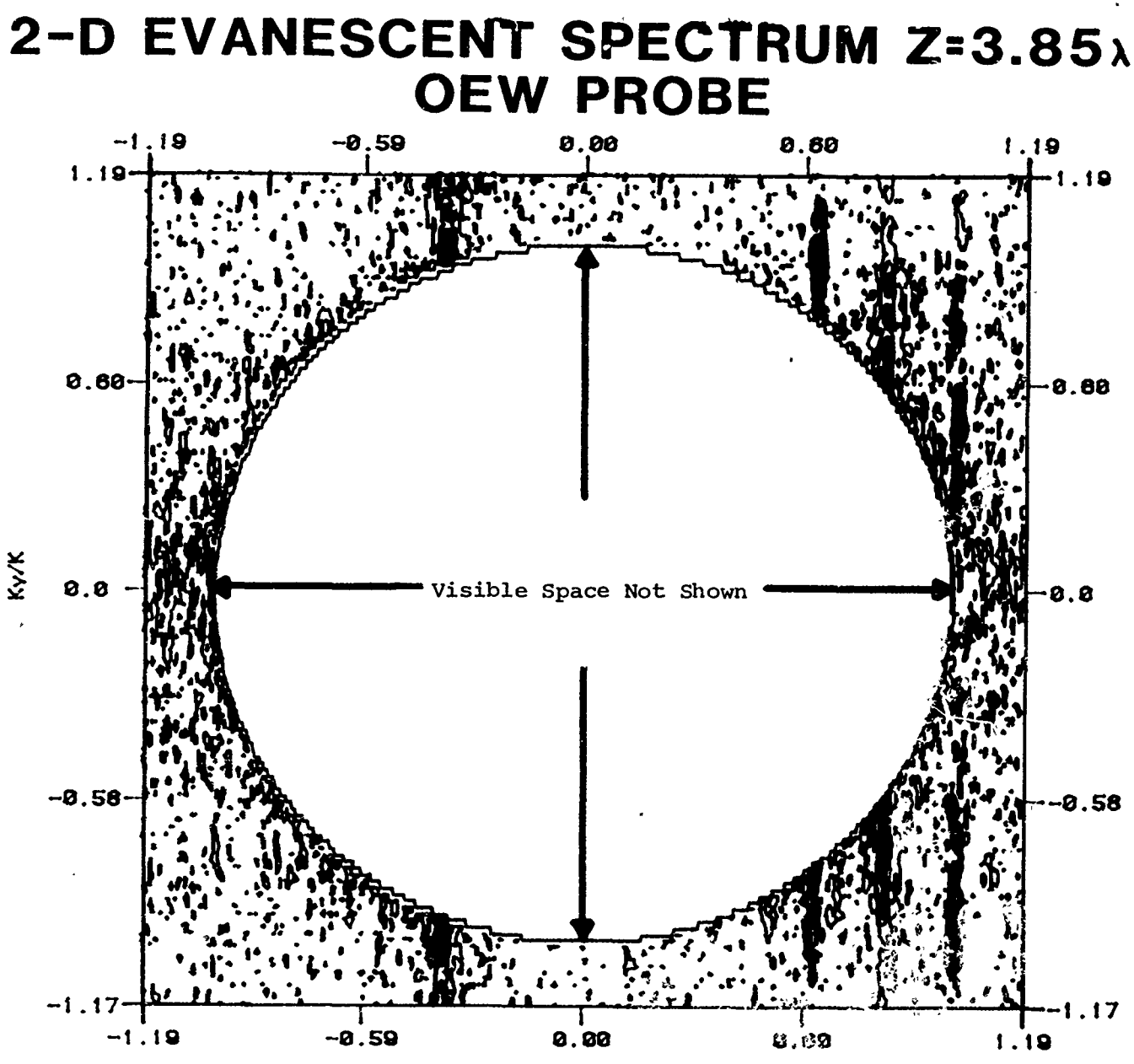

Figure 13. Evanescent Spectrum Contours Due all Sources of Random and Systematic Measurement Error, Computed from NWACS Scanning with the Open-Ended W/G Probe at 3.3 Ghz

2-D EVANESCENT SPECTRUM Z=3.85λ
DELTA PROBE

CONTOURS #	VALUE
1	-60.0000
2	-70.0000
3	-80.0000
4	-90.0000
5	-100.000

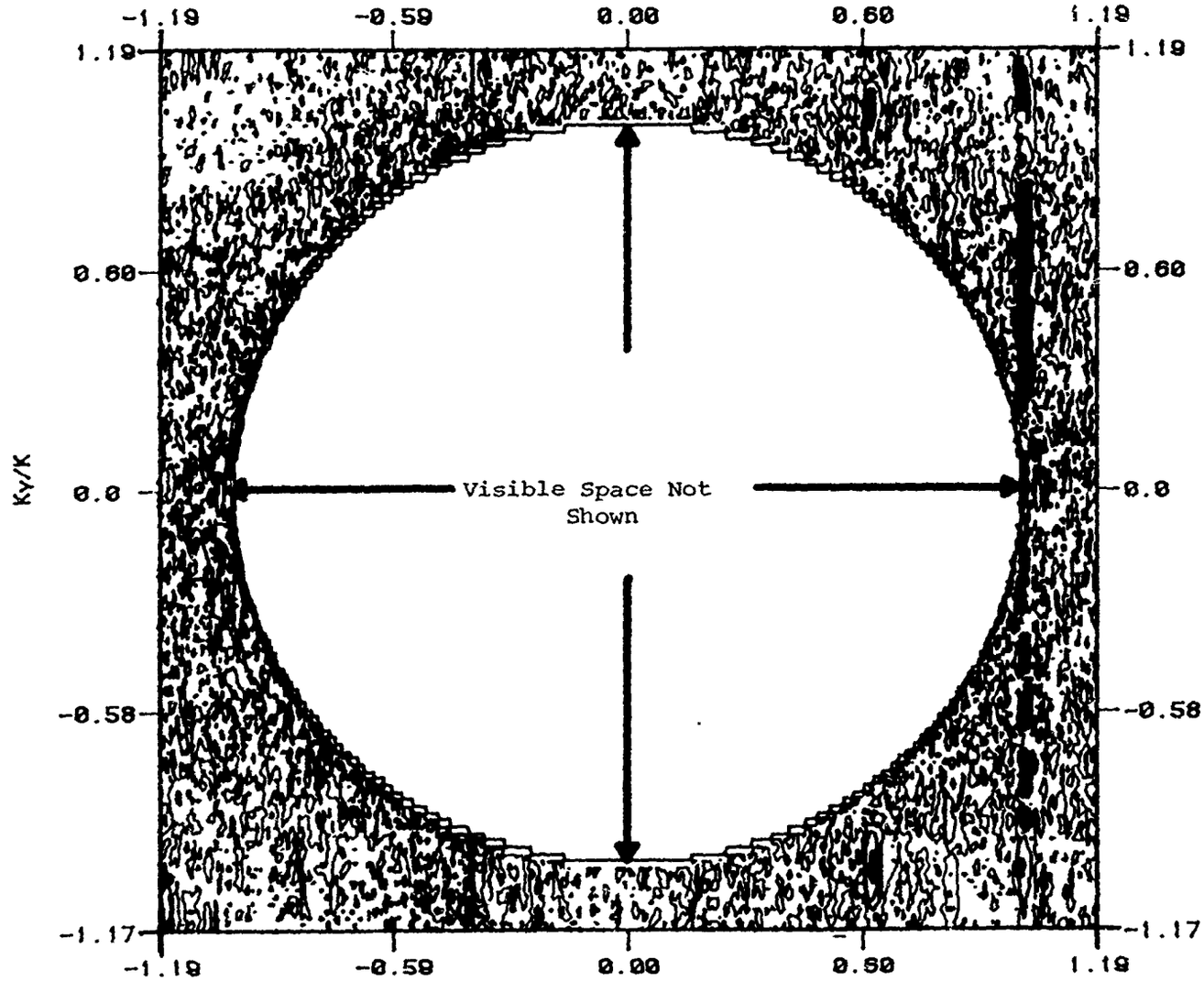

Evanescent Spectrum Contours Due to All Sources of Systematic and Random Measurement Error, Computed from AWACS Scanning with ... at 3.3 Ghz

too highly attenuated to be measured at Z = 35 cm. Therefore, these evanescent sidelobe ridges must be the result of undiagnosed periodic scan plane error--most probably due to unavoidable periodic multipath interactions. By excluding these ridge regions, we may compute the rms over all remaining evanescent wavenumbers, and present S/N_o ratios which may be compared to predictions made in section 3.7. Table 11 below contains these measured noise ratios from available results for scanning with three probes and the two DESAT arrays.

Table 11. Predicted and Measured Random Error Noise Ratios for ULSA and AWACS Scanning with Three DESAT Probes

Probe Type	Array	Signal/Noise Spectral Ratio		
		Predicted (dB)	Measured* (dB)	Measured+ (dB)
Open-ended W/G	ULSA	--	63.95	--
Σ	ULSA	--	63.91	--
Δ	ULSA	--	70.65	--
Open-ended W/G	AWACS	82.1	82.2	74.2
Δ	AWACS	93.7	94.0	89.7

* Excluding correlated evanescent lobes

\+ All evanescent space

It is concluded from these results that the bounding random error estimate for AWACS scanning closely matches the directly measured random error level*, and confirms that the major contributor to random error in the NBS DESAT facility is the roundoff error of the signal digitizers. We also conclude that the far field dynamic range of the ULSA spectrum is about 20 dB less than the AWACS spectrum, eventhough the same number of measurement points were sampled for both arrays (27775).

*As long as the magnitudes of the correlated ridge lobes are excluded from the evanescent rms.

This is because more NF sample points fall within the effective area of the higher gain AWACS than do for ULSA and by equation (21), we expect a larger S/N_o for AWACS by the ratio $\sqrt{N_e^{AWACS}/N_e^{ULSA}}$. As an aside, one could minimize the effects of random NF amplitude error for ULSA scanning by decreasing the total number of NF sample points N, i.e., reduce the size of the scan area. In this way, the ratio N/N_e in equation (21) could be held constant regardless of which array was being scanned. This test was not performed. Interestly, the total number of sample points does not affect prediction of spectral noise introduced by random NF phase error (see equation 22).

SCAT Results

The room scattering effects on far field measurement accuracy was also determined by computing the two-dimensional transform of the NF SCAT data as described in Section 3.1. It was shown there that NF SCAT scans contain, principally, undesirable random room-scattered fields, and subsequent transform processing will reveal the far field noise error spectrum. Table 12 summarizes the peak and RMS magnitudes of far field SCAT spectra from tests on AWACS using the open-ended waveguide probe. An example perspective view of a set of 95 SCAT scans, and the resulting spectrum, was shown in Figures 15 and 16.

Table 12. SCAT Spectral Error Due to Facility Room Scattering

Probe Type	Error Spectrum*	
	RMS (dB)	Peak (dB)
Open Ended W/G	-89	-68
Δ-Probe	-94	-72

*with repsect to peak coupling product gain measured with open-ended W/G probe.

The close agreement of the SCAT error spectrum RMS with measured evanescent averages in Table 11 is evidence for the utility of both random-error testing procedures, and confirms the fundamental measurement accuracy limits for AWACS testing at NBS. The -94 dB SCAT error limit (Δ-probe) is well below any AWACS sidelobe level of interest. Random room scattering effects in general are well below the AWACS sidelobe levels when measured with either probe. Figures 55 and 56 show the room-scattered error fields measured at the identical room location of probe and array, compared with the directly measured AWACS NF for the open-ended waveguide and Δ-probe respectively. Even through the NF room scattering error component in these Figures are <u>not</u> small (especially for the delta probe), the effect on far field pattern accuracy is insignificant, primarily due to the large gain of AWACS.

4.6 Multipath Results

The multipath interactions described in Section 3.6 lead to periodic scan plane errors which degrade the test antenna's mainbeam gain as well as sidelobe levels. Tests conducted with the ULSA array and the Σ and Δ-probes have quantified far field errors in gain, peak sidelobe, and RMS sidelobe due to NF multipath. First-order interactions cause constant offsets throughout the test antenna far field pattern, and are easily revealed by the Z-translation probe test (Figure 22). Higher order interactions degrade far field gain <u>and</u> sidelobe levels as a function of NF interference magnitude, frequency, and the error-free sidelobe level under test. The Δ-probe also offers increased immunity from higher order multipath interactions because it reduces the coupling product peak gain during scan. Results follow.

<u>First-Order Interactions</u>

Figure 22 showed the interference pattern due to first-order multipath between the Σ-probe and ULSA array at 3.1 Ghz. There, the λ/2 ripple has p-p magnitude of 0.6 dB, and corresponds to a second-time around scattered field strength of about 30 dB below the direct path. This multipath degrades the ULSA far field array gain <u>at all angles</u> by a constant

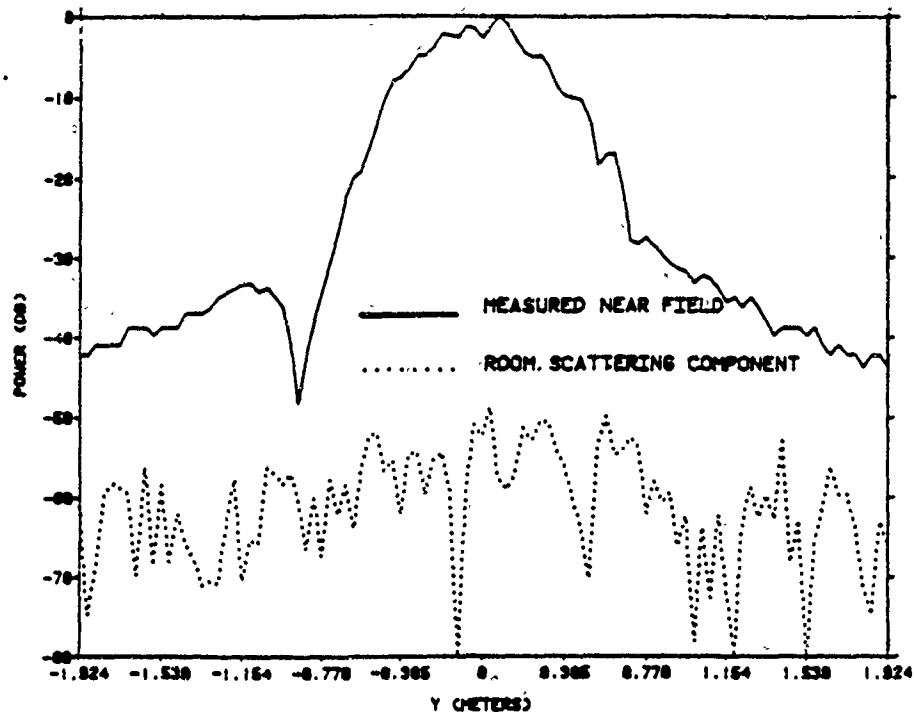

Figure 55. NF Amplitude Comparison of Measured NF to Room Scattering Component for the Open-Ended Wavequide Probe Scanning Verticlly in front of the AWACS Array

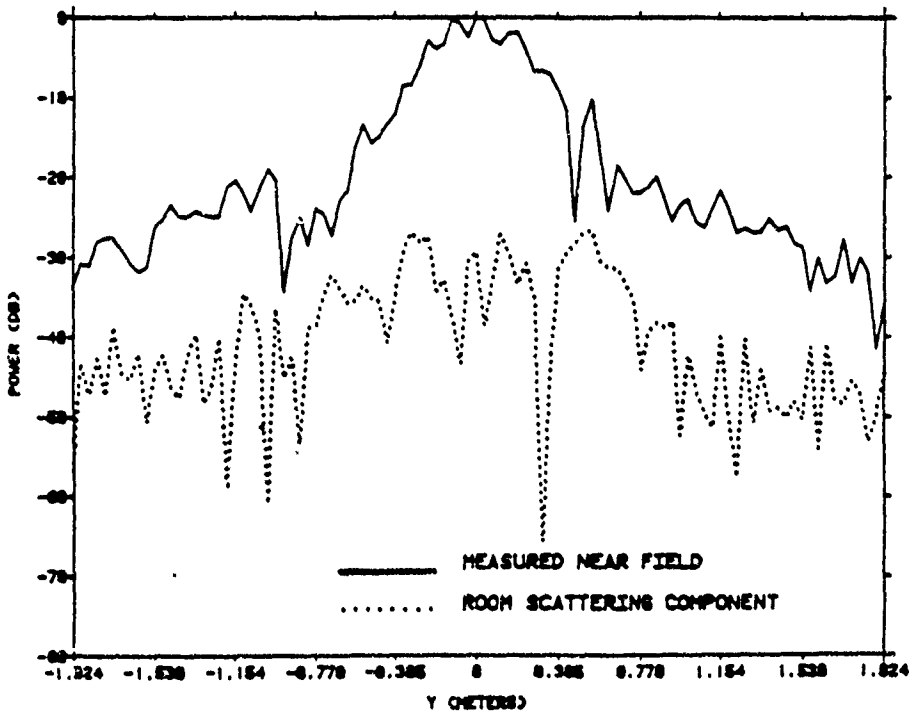

Figure 56. NF Amplitude Comparison of Measured NF to Room Scattering Component for Delta Probe Scanning Vertically in Front of the AWACS Array

offset, which, at worst, equals the NF peak ripple magnitude. Figure 57 shows the measured ULSA far field mainbeam gain error due to first-order Σ-probe multipath. The far field mainbeam gain error is accurately predicted by the periodic variation of the NF probe voltage as measured by the Z-translation test (within 0.2 dB). Figure 57 shows the peak mainbeam gain error to be ± .4dB due only to first-order near field multipath for the Σ-probe.

Higher-Order Interactions

Higher order interactions involve multiple scattering along oblique NF paths between probe and array. These interactions degrade test antenna sidelobe accuracy as a function of interaction frequency and magnitude across the scan plane for a fixed Z-separation. The higher-order interactions cause increasingly larger sidelobe errors for decreasingly smaller error-free sidelobe levels. Tests to measure the effects of higher order multipath interactions were conducted as sketched in Figure 23. Linear probe scan data at five Z-separations in the range 60 cm < ΔZ < 65 cm were measured, and transformed for the one-dimensional coupling product spectra. These five spectra were then averaged to remove the effects of multipath, and this average was then compared to each spectrum in the set of five. Figure 58 shows the change in the peak (-42.2 dB) azimuth plane sidelobe as function of increasing Z-separation as measured by the Σ and Δ-probe, and normalized to the Σ-probe sidelobe level. For no higher order interactions, the peak sidelobe would be invariant with Z-separation in the λ/2 range of separations here tested. The Δ-probe has reduced sensitivity to higher-order multiple interactions because the coupling product peak sidelobe/mainbeam gain ratio is artifically increased by the probe's filtering property.

Figure 59 shows the change in ULSA azimuth plane RMS sidelobes (-51.5 dB), as measured by both probes and normalized to the Z = 60 cm RMS sidelobe level (Σ-probe). Again, the Δ-probe shows improved immunity to the higher-order NF multipath at the artifically higher average sidelobe level of the coupling product spectrum imposed by the probe's mainbeam filter.

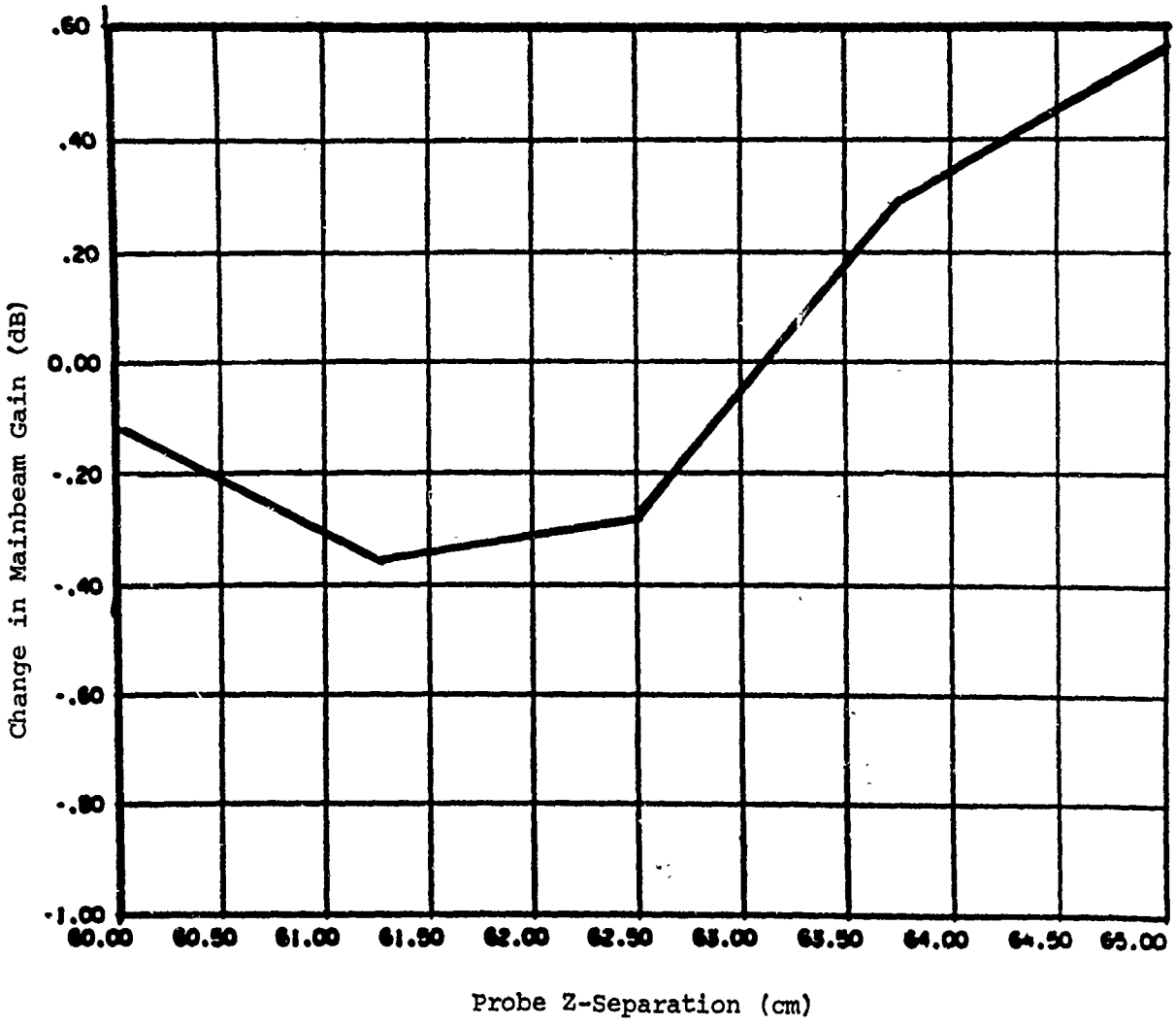

Figure 57. ULSA Mainbeam Gain Error Due to First-Order Near Field Multipath for the Σ-Probe

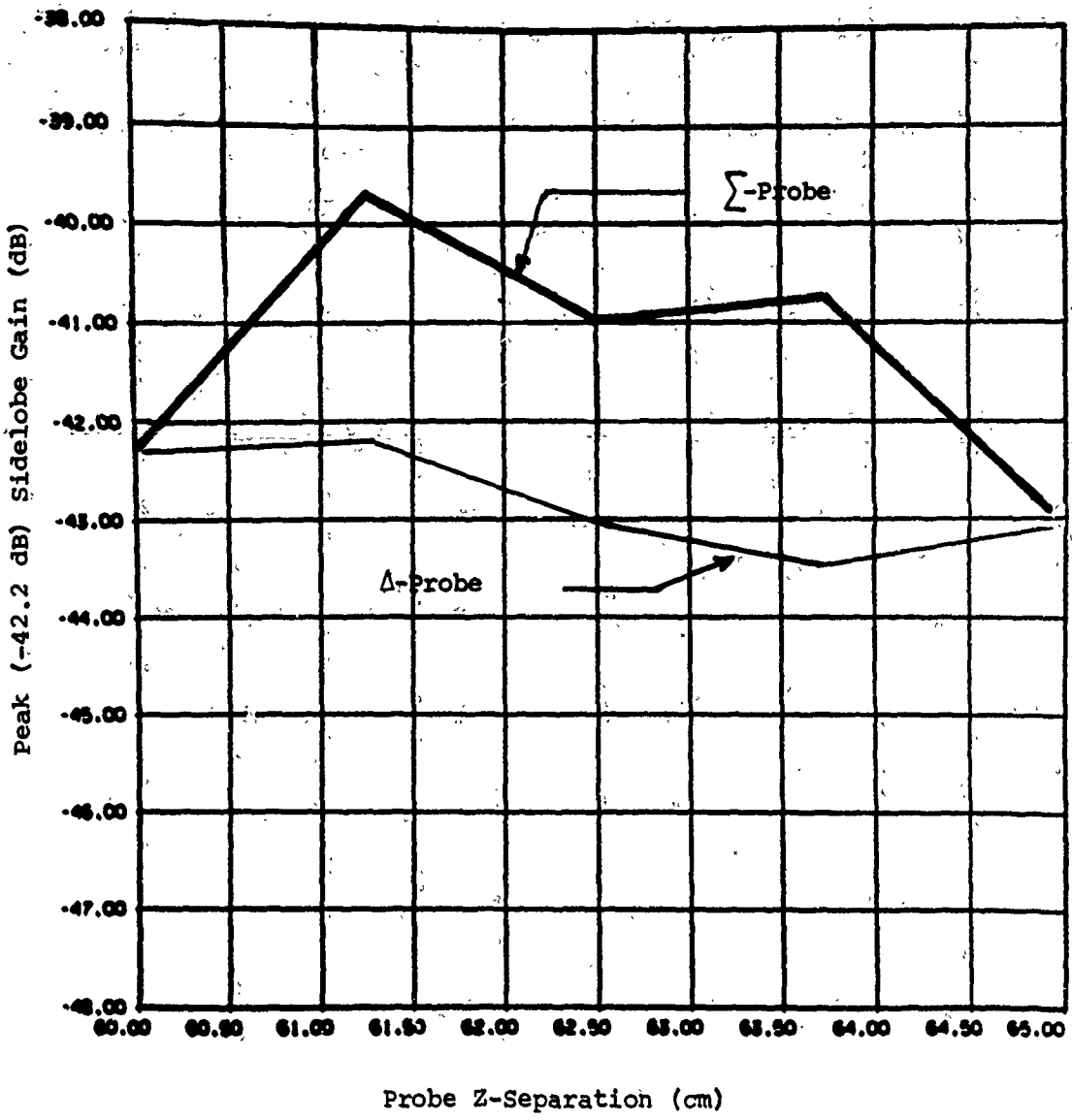

Figure 58. ULSA Azimuth Plane Peak Sidelobe Gain Change Due to Higher-Order Near Field Multipath

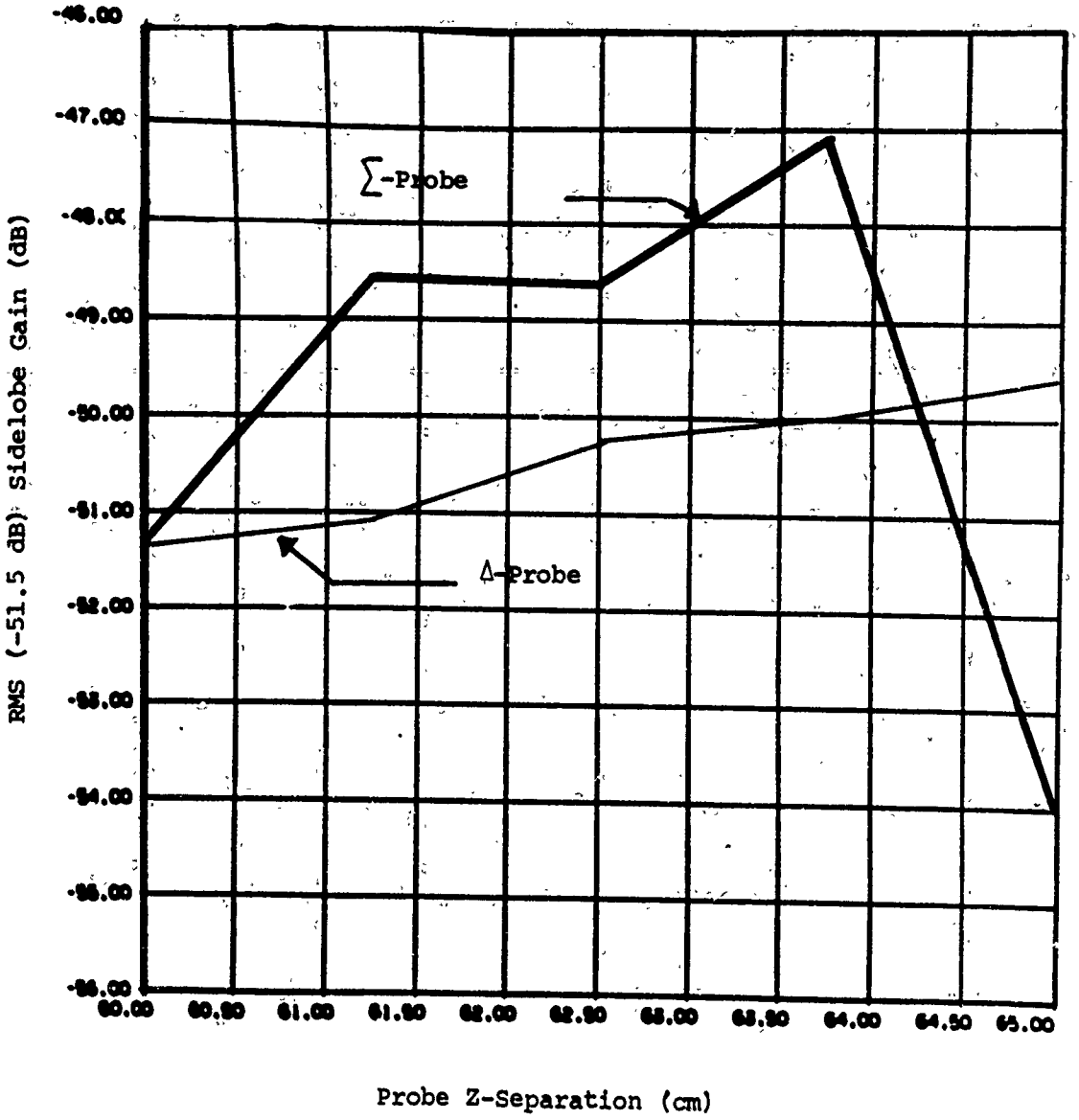

Figure 59. ULSA Azimuth Plane RMS Sidelobe Gain Change Due to Higher-Order Near Field Multipath

Figures 60 and 61 show the average coupling product spectrum and the Z = 60 cm spectrum overlayed for each probe.

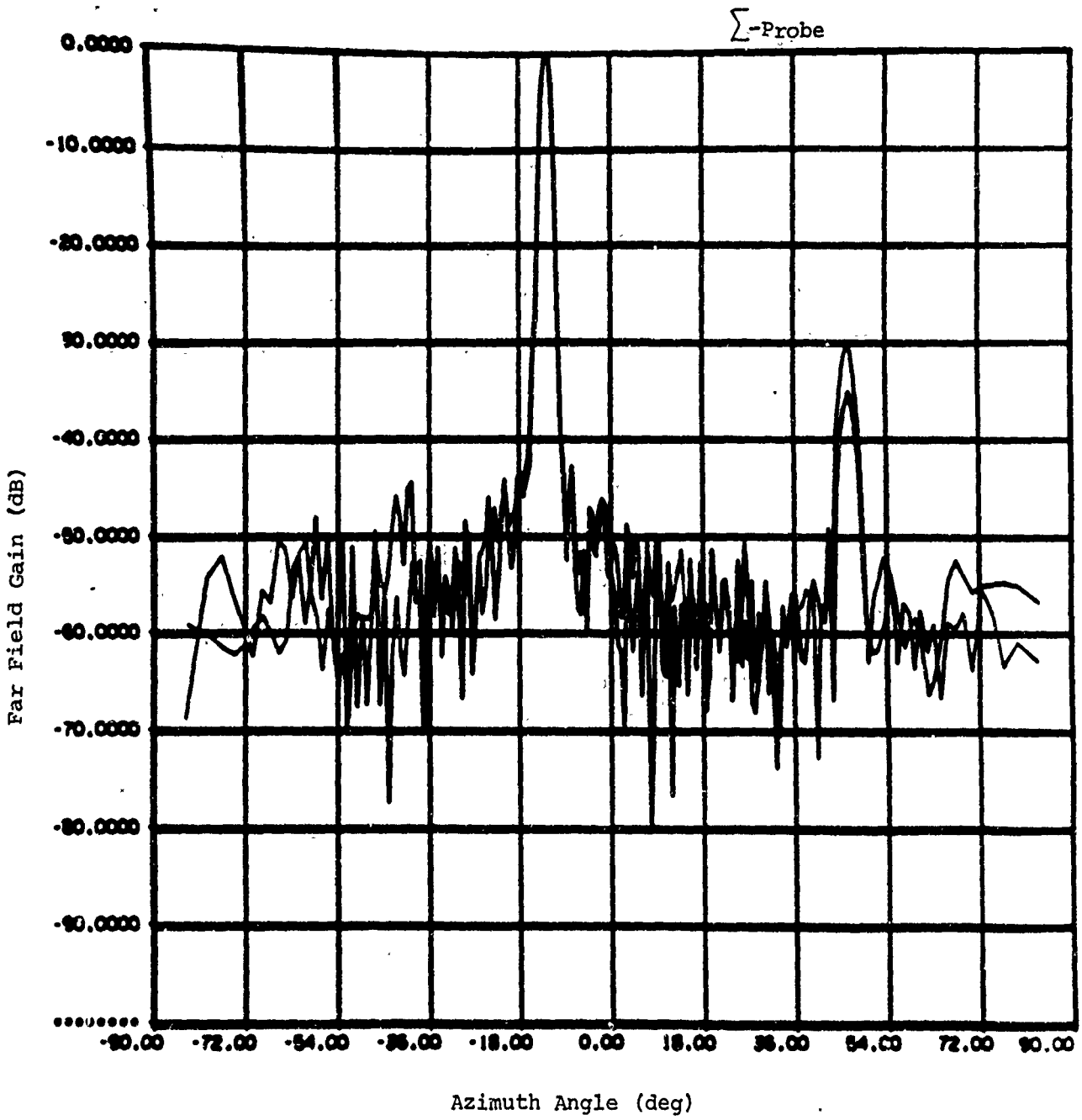

Figure 60. Five-Spectra Average Coupling-Product Pattern Overlays Measured During Tests to Quantify Higher-Order Near Field Multipath Due to Σ-Probe Scanning at 3.1 Ghz

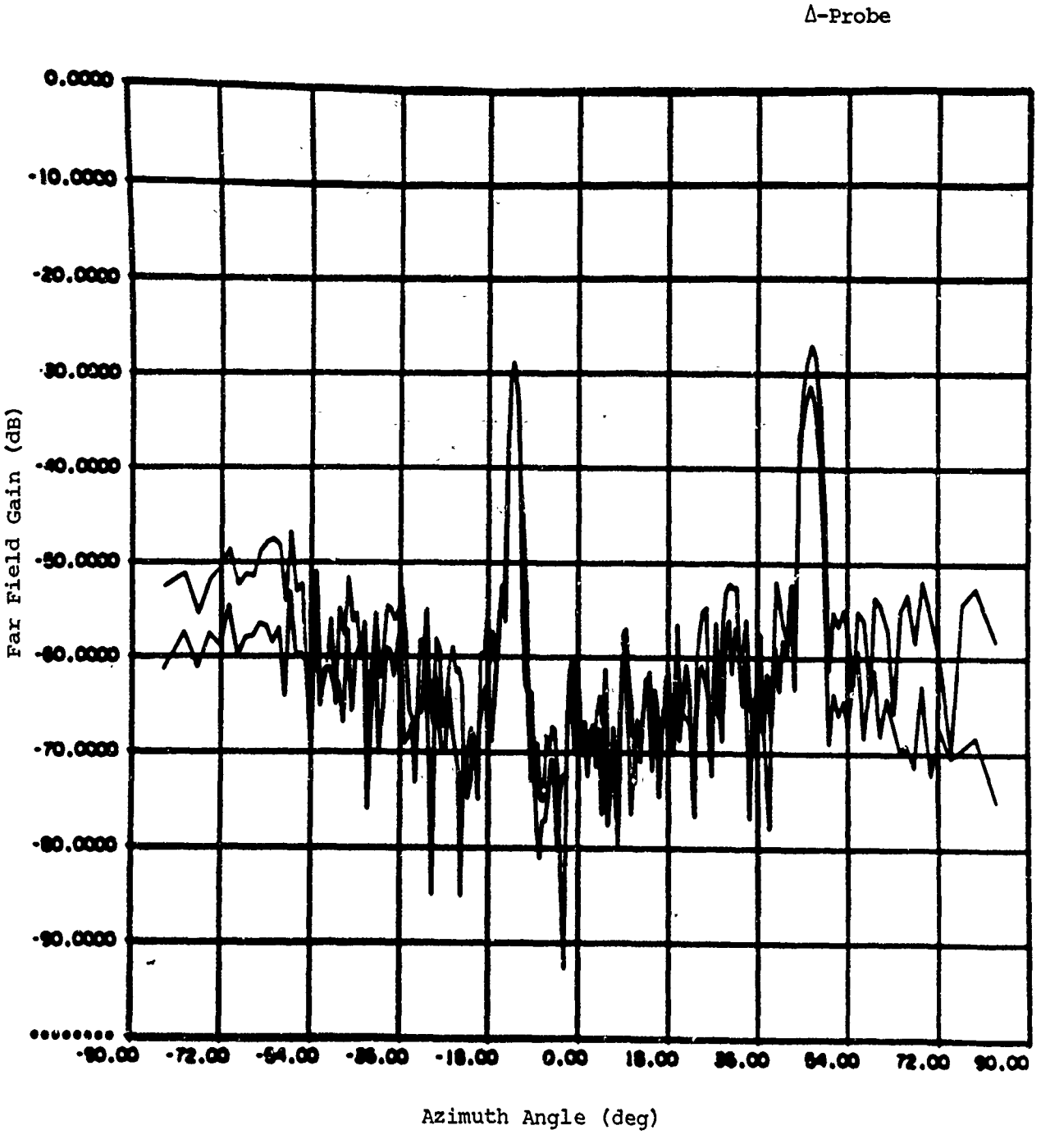

Figure 61. Five-Spectra Average Coupling Product Pattern Overlays Measured During Tests to Quantify Higher-Order Near Field Multipath Due to Δ-Probe Scanning at 3.1 Ghz

5.0 CONCLUSIONS

This report contains the results of an analytic and experimental investigation to quantify measurement accuracy when testing very low sidelobe antennas by planar near field scanning. The analytic effort has affirmed and extended the available error models for predicting far field sidelobe error due to near field error sources. These models were exercised to predict probable sidelobe error when scanning two large array antennas--the AWACS prototype array and the ULSA experimental array.

The experimental effort accomplished a complete near field pattern evaluation of both low sidelobe arrays using a standard probe and two experimental near field probes. The planar near field antenna range at the US National Bureau of Standards was modified to allow scanning of the large arrays in sections, and was the test site for all scan tests during this program.

From tests to measure the effect of controlled scanning error, it is concluded that far field sidelobe accuracy is ultimately limited by:

1. Noncompensatable scanning errors which establish the repeatability of measurement--the effect of these random errors depend both on the gain of the test antenna and on the residual tolerances of the scanning facility. At NBS, random error limits were measured to be 64 dB below the ULSA peak gain and 82.2 dB below the AWACS peak gain.

2. Multiple reflection paths which cause first-order (probe/array) and higher-order (probe/array/room) variations in the near field data. These errors are facility/probe unique, and may only be compensated by multiple scan averaging or by isolation and reduction of facility scattering sources--primarily the probe's own backscattering cross section.

3. Probe pattern directivity.

A new two-element probe, having a pattern null costeered with the test antenna's mainbeam steering angle, has been shown to improve sidelobe measurement accuracy by reducing the error gain in the coupling product sidelobe directions, but at the cost of increased error gain in the coupling

product mainbeam direction. Residual Z-position errors on the NBS scanner will cause -64 dB wide angle sidelobe errors when testing with a standard probe. However, when scanning with the new Δ-probe, an additional 30 dB of error gain reduction is possible (error level = -94 dB). Similar conclusions apply to near field receiver errors.

In summary, this DESAT Phase II investigation has shown that:

- available predictive models for estimating far field measurement accuracy remain valid for the testing of very low sidelobe antennas.
- immunity to some forms of systematic scanning errors, as well as random errors, is possible by using a main beam nulling probe. Available error models will then need modification to account for probe pattern directivity.
- a new error model for estimating the effects of random scanning error depends upon NF sample density and an independent estimate of the amplitude and phase error variance.

Finally, this research program has demonstrated measurement accuracy at pattern levels 15-20 dB lower than any previous near field antenna evaluation, and has added considerable experience to the understanding of the theory of antenna metrology errors.

REFERENCES

1. K. R. Grimm, "Final Report--Ultralow Sidelobe Planar Near Field Measurement Study", TSC-W41-142, 30 June 1982, prepared under the Defense Small Business Advanced Technology Program (DESAT)--Phase I.

2. "Near Field Directive Pattern Analyzer for Portable and Laboratory Applications", Interim Technical Report 76-Y-11164, produced by Martin Marietta Corporation for AF Avionics Laboratory under contract F33615-75-C-1173, in July 1976.

3. TSC-W41-273, "Test Plan for Ultralow Sidelobe Near Field Measurement Demonstration--DESAT II", January 1985 (Unclassified).

4. TSC-W41-331, "Preliminary RCS Results for DESAT II Transition Experiment", 18 December 1985 (Confidential).

5. "Progress Report--Ultralow Sidelobe Planar Near Field Measurement Demonstration", NBS Report 723.05, 15 June 1984.

6. A. C. Newell, M. L. Crawford, "Planar Near Field Measurements on High Performance Array Antennas", NBSIR 74-380, July 1974.

7. "Near-Zone Radar Cross-Section Technique Development," Technical Report AFAL TR-74-227, produced by Georgia Institute of Technology under contract F33615-73-C-1188, November 1974.

8. "Planar Near Field Mesurements", by A. C. Newell, 1985 Short Course notes prepared as a book preprint (National Bureau of Standards), Boulder, Co.

9. Huddleston, G. K., "Optimum Probes for Near Field Antenna Measurements on a Plane," Ph.D Dissertation, Georgia Institute of Technology, available from University Microfilms International (#7823710), Ann Arbor, Michigan, August 1978.

10. A. D. Yaghjian, "Upperbound Errors in Far Field Antenna Parameters Determined from Near-Field Measurements: Part 1-- Analysis", NBS Technical Note 667, available from DDC (#ADA014397), October 1975.

11. Kerns, David M., "Plane-Wave Scattering-Matrix Theory of Antennas and Antenna-Antenna Interactions", NBS Monograph 162, library of Congress #81-600015, June 1981.

12. "Results of Near Field Scanning Exercises with the AWACS Phased Array", TSC classified memo to be published.

Appendix A.1

CATALOG OF TEST DATA FILES

The following is a list of measured near field data files collected during Block 2 DESAT testing at NBS with both the ULSA and AWACS phased array antennas. Block 2 events occurred during the period January 1, 1985 - Novmeber 25, 1985 at NBS, Boulder, Colorado.

Also listed in this appendix are the far field probe calibration data files measured on the NBS (θ,ϕ) anechoic chamber rotator during DESAT II Block 1 testing in late 1984.

Finally, a tabulation is given of probe calibration data and processing parameters necessary for the transformation of DESAT near field probe scan data.

MEASURED NF DATA FILES

Table A.1.1

F Data ile Name	Freq	Δx (cm)	Δy (cm)	Δz (cm)	Input/Output Ratio (dB)	File Size	NF Probe	AUT	Comment
FDAY102B	F1	3.81	3.81	65	27.42	101x275	SUM (1-2)*	ULSA	RF LEAKAGE
FDAY122B	F1	3.81	3.81	65	39.88	101x275	DELTA (1-2)	ULSA	RF LEAKAGE
FDAY112B	F1	3.81	3.81	65	49.47	101x275	DELTA (1-12)	ULSA	RF LEAKAGE
FDAY902B	F2	3.81	3.81	65	28.15	101x275	OEW	ULSA	X-COMPONENT
FDAY702B	F2	3.81	3.81	65	24.64	101x275	SUM (1-3)	ULSA	
FDAY535B	F2	3.81	3.81	65	55.47	101x275	DELTA (1-3)	ULSA	NO TIE SCANS
FDAY622B	F2	3.81	3.81	65	24.64	101x275	SUM (1-3)	ULSA	Z-POSITION ERROR
FDAY752B	F2	3.81	3.81	65	55.47	101x275	DELTA (1-3)	ULSA	Z-POSITION ERROR
FDAY908B	F2	3.81	3.81	65	52.80	101x275	OEW	ULSA	Y-COMPONENT
FDAY505B	F2	3.81	3.81	65	55.47	101x275	DELTA (1-3)	ULSA	
FDAY508B	F2	3.81	3.81	65		101x275	DELTA (1-6)	ULSA	
FDAY512B	F2	3.81	3.81	65	24.64	101x275	SUM (1-3)	ULSA	
FDAY532B	F2	3.81	3.81	65	24.64	101x275	SUM (1-3)	ULSA	NO TIE SCANS
CDAY600B	F2	3.81	3.81	65	24.64	101x95	SUM (1-3)	ULSA	ROOM SCATTERING

*Cable Pair Designation

Table A.1.1 (cont'd)

NF Data File Name	Freq.	Δx (cm)	Δy (cm)	Δz (cm)	Input/Output Ratio (dB)	File Size	NF Probe	AUT	Comment
SCDAY601B	F2	3.81	3.81	65	55.47	101x95	DELTA (1-3)**	ULSA	ROOM SCATTERING
NFDAY112B	F3	3.81	3.81	35	27.54	101x275	OEW	AWACS	SCANNER ERROR
NFDAY212B	F3	3.81	3.81	37.27	27.72	101x275	OEW	AWACS	SCANNER ERROR
NFDAY405B	F3	3.81	3.81	35	27.54	101x275	OEW	AWACS	X-COMPONENT
NFDAY402B	F3	3.81	3.81	35	50.66	101x275	OEW	AWACS	Y-COMPONENT
NFDAY305B	F3	3.81	3.81	37.27	27.72	101x275	OEW	AWACS	X-COMPONENT
NFDAY302B	F3	3.81	3.81	37.27	49.34	101x275	OEW	AWACS	Y-COMPONENT
NFDAY602B	F3	3.81	3.81	35	50.06	101x275	DELTA (1-10)	AWACS	REPEATABILITY
NFDAY605B	F3	3.81	3.81	37.27	52.40	101x275	DELTA (1-10)	AWACS	
NFDAY618B	F3	3.81	3.81	35	50.06	101x275	DELTA (1-10)	AWACS	REPEATABILITY
NFSCAT500B	F3	3.81	3.81	35	27.54	101x95	OEW	AWACS	ROOM SCATTERING
NFSCAT501B	F3	7.62	3.81	35	27.54	101x48	OEW	AWACS	ROOM SCATTERING
NFSCAT610B	F3	3.81	3.81	35	50.06	101x95	DELTA (1-10)	AWACS	ROOM SCATTERING
NFRCS102B	F3	3.81	3.81	65	30.52	101x275	OEW	AWACS	W/O TARGET
NFRCS105B	F3	3.81	3.81	33*	30.52	101x275	OEW	AWACS	W/TARGET

*SCAN PLANE-TO-TARGET DISTANCE

Table A.1.1 (conclude)

NF Data File Name	Freq.	Δx (cm)	Δy (cm)	Δz (cm)	Input/Output Ratio (dB)	File Size	NF Probe	AUT	Comment
NFRCS212B	F3	3.81	3.81	70	50.50	101x275	DELTA (1-10)	AWACS	W/O TARGET
NFRCS205B	F3	3.81	3.81	38*	50.50	101x275	DELTA (1-10)	AWACS	W/TARGET

*SCAN PLANE-TO-TARGET DISTANCE

MEASURED PROBE FAR-FIELD PATTERN FILES

Table A.1.2

Data File Name	Freq.	$\Delta\Theta$ Deg.	$\Delta\Phi$ Deg.	Size	Description
TSCSNO2.SX.THETA.F1.1-2	F1	1	-5	201x37	MECHANICAL SUM - THETA COMPONENT
TSCSNO2.SX.PHI.F1.1-2	F1	1	-5	201x37	MECHANICAL SUM - PHI COMPONENT
TSCSNO2.DX.THETA.F1.1-2	F1	1	-5	201x37	MECHANICAL DELTA - THETA COMPONENT
TSCSNO2.DX.PHI.F1.1-2	F1	1	-5	201x37	MECHANICAL DELTA - PHI COMPONENT
TSCSNO2.SX.THETA.F1.1-12	F1	1	-5	201x37	ELECTRONIC SUM - THETA COMPONENT @ 12.68°
TSCSNO2.SX.PHI.F1.1-12	F1	1	-5	201x37	ELECTRONIC SUM - PHI COMPONENT @ 12.68°
TSCSNO2.DX.THETA.F1.1-12	F1	1	-5	201x37	ELECTRONIC DELTA - THETA COMPONENT @ 12.68°
TSCSNO2.DX.PHI.F1.1-12	F1	1	-5	201x37	ELECTRONIC DELTA - PHI COMPONENT @ 12.68°
TSCSNO2.SX.THETA.F2.1-3	F2	1	-5	201x37	MECHANICAL SUM - THETA COMPONENT
TSCSNO2.SX.PHI.F2.1-3	F2	1	-5	201x37	MECHANICAL SUM - PHI COMPONENT
TSCSNO2.DX.THETA.F2.1-3	F2	1	-5	201x37	MECHANICAL DELTA - THETA COMPONENT
TSCSNO2.DX.PHI.F2.1-3	F2	1	-5	201x37	MECHANICAL DELTA - PHI COMPONENT
TSCSNO2.SX.THETA.F2.1-6	F2	1	-5	201x37	ELECTRONIC SUM - THETA COMPONENT @ 9.69°
TSCSNO2.SX.PI.F2.1-6	F2	1	-5	201x37	ELECTRONIC SUM - PHI COMPONENT @ 9.69°
TSCSNO2.DX.THETA.F2.1-6	F2	1	-5	201x37	ELECTRONIC DELTA - THETA COMPONENT @ 9.69°

Table A.1.2 (cont'd)

Data File Name	Freq.	ΔΘ Deg.	ΔΦ Deg.	Size	Description
TSCSNO2.SX.THETA.F2.1-9	F2	1	-5	201x37	ELECTRONIC SUM - THETA COMPONENT @ 30.58° STYROFOAM PLUG #2 ELEMENT
TSCSNO2.SX.PHI.F2.1-9	F2	1	-5	201x37	ELECTRONIC SUM - PHI COMPONENT @ 30.58° STYROFOAM PLUG #2 ELEMENT
TSCSNO2.DX.THETA.F2.1-9	F2	1	-5	201x37	ELECTRONIC DELTA - THETA COMPONENT @ 30.58° STYROFOAM PLUG #2 ELEMENT
TSCSNO2.DX.PHI.F2.1-9	F2	1	-5	201x37	ELECTRONIC DELTA - PHI COMPONENT @ 30.58° STYROFOAM PLUG #2 ELEMENT
TSCSNO2.SX.THETA.F2.1-13	F2	1	-5	201x37	MECHANICAL SUM - THETA COMPONENT STYROFOAM PLUG #2 ELEMENT
TSCSNO2.SX.PHI.F2.1-13	F2	1	-5	201x37	MECHANICAL SUM - PHI COMPONENT STYROFOAM PLUG #2 ELEMENT
TSCSNO2.DX.THETA.F2.1-13	F2	1	-5	201x37	MECHANICAL DELTA - THETA COMPONENT STYROFOAM PLUG #2 ELEMENT - 20 dB NULL
TSCSNO2.DX.PHI.F2.1-13	F2	1	-5	201x37	MECHANICAL DELTA - PHI COMPONENT STYROFOAM PLUG #2 ELEMENT - 20 dB NULL
TSCSNO2.SX.THETA.F2.1-14	F2	1	-5	201x37	MECHANICAL SUM - THETA COMPONENT STYROFOAM PLUG #2 ELEMENT
TSCSNO2.SX.PHI.F2.1-14	F2	1	-5	201x37	MECHANICAL SUM - PHI COMPONENT STYROFOAM PLUG #2 ELEMENT
TSCSNO2.DX.THETA.F2.1-14	F2	1	-5	201x37	MECHANICAL DELTA - THETA COMPONENT STYROFOAM PLUG #2 ELEMENT 10 dB NULL
TSCSNO2.DX.PHI.F2.1-14	F2	1	-5	201X37	MECHANICAL DELTA - PHI COMPONENT STYROFOAM PLUG #2 ELEMENT 10 dB NULL
TSCSNO2.SX.THETA.F3.1-10	F3	1	-5	201X37	MECHANICAL SUM - THETA COMPONENT STYROFOAM PLUG #2 ELEMENT
TSCSNO2.SX.PHI.F3.1-10	F3	1	-5	201X37	MECHANICAL SUM - PHI COMPONENT STYROFOAM PLUG #2 ELEMENT
TSCSNO2.DX.THETA.F3.1-10	F3	1	-5	201X37	MECHANICAL DELTA - THETA COMPONENT STYROFOAM PLUG #2 ELEMENT
TSCSNO2.DX.PHI.F3.1-10	F3	1	-5	201X37	MECHANICAL DELTA - PHI COMPONENT STYROFOAM PLUG #2 ELEMENT

Table A.1.2 (conclude)

Data File Name	Freq.	ΔθDeg.	ΔφDeg.	Size	Description
SCSNO2.SX.THETA.F3.1-11	F3	1	-5	201X37	ELECTRONIC SUM - THETA COMPONENT @ 22.05°
TSCSNO2.SX.PHI.F3.1-11	F3	1	-5	201X37	ELECTRONIC SUM - PHI COMPONENT @ 22.05°
TSCSNO2.DX.THETA.F3.1-11	F3	1	-5	201X37	ELECTRONIC DELTA - THETA COMPONENT @ 22.05°
TSCSNO2.DX.PHI.F3.1-11	F2	1	-5	201X37	ELECTRONIC DELTA - PHI COMPONENT @ 22.05°
LPROBE.F2.THETA	F2	2	-5	101X37	OPEN-ENDED WAVEGUIDE - THETA COMPONENT VERTICAL POLARIZATION - WR284
LPROBE.F2.PHI	F2	2	-5	101X37	OPEN-ENDED WAVEGUIDE - PHI COMPONENT VERTICAL POLARIZATION - WR284
LPROBE.F3.THETA	F3	2	-5	101X37	OPEND-ENDED WAVEGUIDE - THETA COMPONENT VERTICAL POLARIZATION - WR284
LPROBE.F3.PHI	F3	2	-5	101X37	OPEN-ENDED WAVEGUIDE - PHI COMPONENT VERTICAL POLARIZATION - WR284

PROBE CALIBRATION DATA AND PROCESSING PARAMETERS

Table A.1.3

	MEASUREMENT FREQUENCY AND CABLE PAIR										
	F1		F2						F3		
	1-2	1-12	1-3	1-6	1-9	1-13	1-14	OEW	1-10	1-11	OEW
PROBE AXIAL RATIO (dB)	57	56	51	51	49	51	53	58	54	53	71
PROBE TILT ANGLE (DEG)	0	0	0	0	0	0	0	90.1	0	0	90.1
PROBE ON-AXIS GAIN (dB)	5.76	4.98	6.83	6.34	3.41	5.89	4.03	6.74	6.47	4.74	7.16
PROBE REFLECTION AMPLITUDE	0	0	0	0	0	0	0	0	0	0	0
PROBE REFLECTION PHASE	0	0	0	0	0	0	0	0	0	0	0
SOURCE AXIAL RATIO (dB)	51	51	68	68	68	68	68	68	66	66	68
SOURCE TILT ANGLE (DEG)	89.5	89.5	89.6	89.6	89.6	89.6	89.6	89.6	89.6	89.6	89.6
PHASE NORMALIZATION (DEG)	180	180	180	180	180	180	180	180	180	180	180
PROBE POLARIZATION SENSE	LEFT	LEFT	RIGHT	RIGHT	RIGHT	RIGHT	RIGHT	LEFT	RIGHT	RIGHT	RIGHT
SOURCE POLARIZATION SENSE	RIGHT	RIGHT	RIGHT	RIGHT	RIGHT	RIGHT	RIGHT	RIGHT	RIGHT	RIGHT	RIGHT
YAW ANGLE (DEG)	12.68	0	9.69	0	0	9.69	9.69	0	22.05	0	0
PITCH ANGLE (DEG)	0	0	0	0	0	0	0	0	0	0	0
SOURCE ON-AXIS GAIN (dB)	17.57	17.57	17.94	17.94	17.94	17.94	17.94		18.83	18.83	

Appendix A.2

Near Field Processing Software Library Description

This appendix describes the major TSC NF data processing computer programs as of August 1986. A data sheet and an example run are given for each utility. The program descriptions are arranged in alphabetical order by program name. The timing statistics are for the example run only.

ACONTOUR

DESCRIPTION: Locates and displays (via a TEKTRONIX 4662 plotter) contours of any bivariate function of x and y when values of the function are known for equal increments in x and y.

NF PROCESSING APPLICATION: Generate near field or far field amplitude and phase contour maps.

INPUT: ASCII or binary file - 512x512 maximum

OUTPUT: Contour Map Plot

TIMING:
Connect (Min)	- 32.27
CPU (Sec)	- 999.61
I/O (Sec)	- 38.26

EXAMPLE RUN: The example run is for a three value contour map of a 512x512 data matrix with the central portion (406x392) excised for regional contouring.

```
OK, ACONTOUR

ENTER FILE NAME (120 CHARACTER MAXIMUM):
FFSCOBROADF10DIF

ENTER NUMBER OF ROWS (512 MAXIMUM):
512

ENTER NUMBER OF COLUMNS (512 MAXIMUM):
512

IS FILE ASCII OR BINARY? (A/B)
B

DO YOU WISH TO USE ALL OF THE DATA IN
FFSCOBROADF10DIF
N

DO YOU WISH TO PREVIEW DATA (Y/N)
N

ENTER THE BEGINNING COLUMN # FOR THE NEW ARRAY
120

CONTINUING FOR HOW MANY COLUMNS?
273

ENTER THE BEGINNING ROW # FOR THE NEW ARRAY
106

CONTINUING FOR HOW MANY ROWS?
301

DO YOU DESIRE THINNED DATA? - Y/N
N

DO YOU WISH TO SAVE THIS ARRAY? (Y/N)
N

VALUES IN THIS FILE RANGE FROM -28.2894     TO  71.2027

DO YOU WISH TO PREVIEW DATA? (Y/N)
N

HOW MANY CONTOUR VALUES ARE TO BE PLOTTED (MAXIMUM OF 16)?
1

ENTER CONTOUR VALUES:

#  1:
0

WANT ALPHA/BETA OR AL/EL AXIS LABELS? - Y/N
Y

ALPHA/BETA OR AL/EL AXES? - AB/AE
```

```
AB

ENTER NF SPACINGS IN CM. - DELX,DELY
2.2860,2.5146

ENTER NF MEASUREMENT FREQUENCY IN GHZ
*.**


ASSIGN PLOTTER
PREPARE PAPER AND PEN
ENTER "START" TO CONTINUE
**** PAUSE
OK, AS AMLC TTY 0
OK, S

WANT REDUCED PLOT?  - (Y/N) - 9*8 INCHES NORMAL SIZE
Y

ENTER REDUCED PLOT SIZE - X,Y IN INCHES
6,6

ENTER THE PLOT TITLE - 72 CHARACTERS MAX.
F10 BROADSIDE AS BUILT SLB COVERAGE

DO WISH TO OVERLAY ADDITIONAL CONTOURS? (Y/N)
Y

VALUES IN THIS FILE RANGE FROM -28.2894     TO  71.2027

DO YOU WISH TO PREVIEW DATA? (Y/N)
N

HOW MANY ADDITIONAL CONTOURS ARE TO BE PLOTTED
(MAXIMUM OF 15)?
1

IF DESIRED, CHANGE PEN
TYPE "START" TO CONTINUE
**** PAUSE
OK, S

ENTER CONTOUR VALUES:
#  2:
10

DO WISH TO OVERLAY ADDITIONAL CONTOURS? (Y/N)
Y

VALUES IN THIS FILE RANGE FROM -28.2894     TO  71.2027

DO YOU WISH TO PREVIEW DATA? (Y/N)
N

HOW MANY ADDITIONAL CONTOURS ARE TO BE PLOTTED
(MAXIMUM OF 14)?
```

```
1

IF DESIRED, CHANGE PEN
TYPE "START" TO CONTINUE
**** PAUSE
OK, S

ENTER CONTOUR VALUES:
#  3:
20

DO WISH TO OVERLAY ADDITIONAL CONTOURS? (Y/N)
N
OK, COMO -E
```

BINFILE

DESCRIPTION: Converts ASCII files to binary files which can be read in by NFVECTOR. The ASCII files may contain a header in the first record and can be in either alternating or separated amplitude and phase format.

NF PROCESSING APPLICATION: Convert ASCII NF data files transferred over 1200 BPS modem link to binary files prior to data processing.

INPUT: ASCII Data File - maximum size 512x512

OUTPUT: Binary Data File - Alternating amplitude and phase format

TIMING:
Connect (Min)	3.87
CPU (Sec)	123.90
I/O (Sec)	8.96

EXAMPLE RUN: The example run is for a 101x275 NF scan raster of data.

```
OK, BINFILE

ENTER #ROWS, #COLS OF DATA
101,275

ENTER DATA FILE NAME
TSCPL.DAT.DAY102


COMPLEX FORMAT? (X, Y): N


BINARY FORMAT?  N


NBS FORMAT?  Y


DATA FILE HEADER
STITCH     101 PTS  ,X COMPO  02118503  ,102 DAY  TSC-ULSA F1 S H03 1-2 SEG2



NORMAL FORMAT OR SEPARATED FORMAT? - N/S
S

ENTER BINARY FILE NAME
NFDAY102

REPEAT FOR ANOTHER FILE? - Y/N
N
OK, COMO -E
```

CMPDIF

DESCRIPTION: Performs the complex difference between two antenna patterns

NF PROCESSING APPLICATION: Computes difference of scalar and vector probe-compensated far field patterns referenced to main beam peak

INPUT: Two Binary Data Files - Alternating Amplitude (voltage) and phase format

OUTPUT: Binary Data File - Magnitude of the complex difference in dB (Power)

TIMING:
Connect (Min) - 13.40
CPU (Sec) - 332.29
I/O (Sec) - 275.53

EXAMPLE RUN: The example run is for a 512x512 two-dimensional antenna pattern size.

```
OK, CMPDIF

ENTER THE NAME OF THE FIRST FILE
FFSCOSTEERF5

ENTER THE NAME OF THE SECOND FILE
FFVCOSTEERF5

ENTER MAIN BEAM PEAK VALUE IN DB
31.268

MAXIMUM DIFFERENCE AT    -66.791 DB SIDELOBE LEVEL
LOCATED AT ROW  382 COLUMN  255


ENTER DIFFERENCE FILE NAME
CMPDIFSTEERF5

OK, COMO -E
```

CONDITION

DESCRIPTION: Converts the separated output of NEWFIL to conditioned amplitude and phase files. The phase is constrained between 0^0 and 360^0 and the peak amplitude in dB can be arbitrarily referenced.

NF PROCESSING APPLICATION: Provides conditioned amplitude and phase files for input to ACONTOUR.

INPUT: NEWFIL output amplitude and phase files - ASCII or binary

OUTPUT: Conditioned amplitude and phase files - ASCII or binary

TIMING:
Connect (Min)	- 4.33
CPU (Sec)	- 164.94
I/O (Sec)	- 36.71

EXAMPLE RUN: The example run is for a 512x512 separated antenna pattern file.

```
OK, CONDITION

THIS PROGRAM CREATES NEW, CONDITIONED, FILES OF
AMPLITUDE AND PHASE


ENTER NAME OF BASE FILE:
FFSCOBROADF10

IS FILE ASCII OR BINARY  (A/B)
B

ENTER NUMBER OF ROWS:
512

ENTER NUMBER OF COLUMNS:
512

ENTER NAME OF NEW BASE FILE:
FFSCOBROADF10C


MAXIMUM AMPLITUDE =   31.220 DB
LOCATED IN ROW  256 COLUMN  256


ENTER THE PATTERN OFFSET VALUE [+OFFSET]
0
OK, COMO -E
```

LOOKFF

DESCRIPTION: Allows previewing of a rectangular subsection of complex (amplitude phase) binary data files. Previewed data can be written to a disk file.

NF PROCESSING APPLICATION: Preview selected sections of near field or far field data files.

INPUT: Binary Data File - 512x512 maximum

OUTPUT: Previewed Data

TIMING:
Connect (Min) - 3.07
CPU (Sec) - 66.92
I/O (Sec) - 40.05

EXAMPLE RUN: The example run Previews the central 256 data entries in row 256 of 512x512 far field antenna pattern file.

```
OK, LOOKFF

ENTER DATA FILE NAME
FFSCOBROADF10

ENTER THE NUMBER OF ROWS
512

ENTER THE NUMBER OF COLUMNS
512

ENTER THE ROW LIMITS
256,256

ENTER THE COLUMN LIMITS
128,384
ROW = 256 COLUMN = 128 AMPLITUDE =     0.0718 PHASE =   184.5485
ROW = 256 COLUMN = 129 AMPLITUDE =     0.0710 PHASE =   215.7850
ROW = 256 COLUMN = 130 AMPLITUDE =     0.0662 PHASE =   258.1892
ROW = 256 COLUMN = 131 AMPLITUDE =     0.0640 PHASE =   293.1441
ROW = 256 COLUMN = 132 AMPLITUDE =     0.0482 PHASE =   294.2203
ROW = 256 COLUMN = 133 AMPLITUDE =     0.0363 PHASE =   249.3552
ROW = 256 COLUMN = 134 AMPLITUDE =     0.0496 PHASE =   205.3284
ROW = 256 COLUMN = 135 AMPLITUDE =     0.0705 PHASE =   196.5911
ROW = 256 COLUMN = 136 AMPLITUDE =     0.0829 PHASE =   206.7507
ROW = 256 COLUMN = 137 AMPLITUDE =     0.0891 PHASE =   210.8492
ROW = 256 COLUMN = 138 AMPLITUDE =     0.0988 PHASE =   205.7805
ROW = 256 COLUMN = 139 AMPLITUDE =     0.1023 PHASE =   209.9927
ROW = 256 COLUMN = 140 AMPLITUDE =     0.0914 PHASE =   221.8120
ROW = 256 COLUMN = 141 AMPLITUDE =     0.0824 PHASE =   220.3962
ROW = 256 COLUMN = 142 AMPLITUDE =     0.0857 PHASE =   200.4079
ROW = 256 COLUMN = 143 AMPLITUDE =     0.0917 PHASE =   177.7186
ROW = 256 COLUMN = 144 AMPLITUDE =     0.0975 PHASE =   163.9442
ROW = 256 COLUMN = 145 AMPLITUDE =     0.1001 PHASE =   172.4952
ROW = 256 COLUMN = 146 AMPLITUDE =     0.1062 PHASE =   194.0298
ROW = 256 COLUMN = 147 AMPLITUDE =     0.1192 PHASE =   209.1093
ROW = 256 COLUMN = 148 AMPLITUDE =     0.1385 PHASE =   219.1841
  .                                                        .
  .                                                        .
  .                                                        .
ROW = 256 COLUMN = 379 AMPLITUDE =     0.0107 PHASE =    57.1185
ROW = 256 COLUMN = 380 AMPLITUDE =     0.0097 PHASE =    24.7039
ROW = 256 COLUMN = 381 AMPLITUDE =     0.0129 PHASE =    17.8568
ROW = 256 COLUMN = 382 AMPLITUDE =     0.0148 PHASE =    23.2248
ROW = 256 COLUMN = 383 AMPLITUDE =     0.0157 PHASE =    84.7299
ROW = 256 COLUMN = 384 AMPLITUDE =     0.0325 PHASE =    90.1161

WRITE SUBSECTION TO ASCII DISK FILE? - Y/N
Y

ENTER OUTPUT FILE NAME
FFSCOBROADF10R256

REPEAT FOR ANOTHER SUBSECTION? -Y/N
N
OK, COMO -E
```

LOOKPC

DESCRIPTION: Allows previewing of a rectangular subsection of alternating complex data. Previewed data can be written to a disk file.

NF PROCESSING APPLICATION: Previewed selected sections of k-space probe compensation data.

INPUT: Binary Data File - 1024x1024 maximum

OUTPUT: Previewed Data

TIMING:
Connect (Min)	4.07
CPU (Sec)	74.11
I/O (Sec)	55.74

EXAMPLE RUN: The example run Previews the central 256 data entries in row 256 of a 512x512 k-space probe compensation file for probe orientation 2.

```
OK, LOOKPC

ENTER DATA FILE NAME
COMP2.SPY1B.F10BMDJWT


COMPLEX FORMAT? (X, Y): N


BINARY FORMAT?  Y

ENTER THE ROW LIMITS
256,256

ENTER THE COLUMN LIMITS
128,384

WRITE DATA TO ASCII DISK FILE? - Y/N
N
ROW = 256 COLUMN = 128 AMPC = 0.0019 PHSC= -112.7022 AMPX= 0.2125 PHSX = -176.670
ROW = 256 COLUMN = 129 AMPC = 0.0017 PHSC=  -80.3665 AMPX= 0.2143 PHSX = -176.955
ROW = 256 COLUMN = 130 AMPC = 0.0014 PHSC=  -47.0944 AMPX= 0.2160 PHSX = -177.479
ROW = 256 COLUMN = 131 AMPC = 0.0020 PHSC=  -22.1320 AMPX= 0.2179 PHSX = -177.015
ROW = 256 COLUMN = 132 AMPC = 0.0026 PHSC=   -2.0839 AMPX= 0.2197 PHSX = -176.580
ROW = 256 COLUMN = 133 AMPC = 0.0031 PHSC=   -9.4999 AMPX= 0.2209 PHSX = -176.430
ROW = 256 COLUMN = 134 AMPC = 0.0036 PHSC=  -16.6809 AMPX= 0.2222 PHSX = -176.301
ROW = 256 COLUMN = 135 AMPC = 0.0040 PHSC=  -23.8831 AMPX= 0.2243 PHSX = -176.302
ROW = 256 COLUMN = 136 AMPC = 0.0044 PHSC=  -30.8602 AMPX= 0.2264 PHSX = -176.302
ROW = 256 COLUMN = 137 AMPC = 0.0049 PHSC=  -48.0531 AMPX= 0.2276 PHSX = -176.469
ROW = 256 COLUMN = 138 AMPC = 0.0054 PHSC=  -65.1937 AMPX= 0.2287 PHSX = -176.639
ROW = 256 COLUMN = 139 AMPC = 0.0052 PHSC=  -73.5540 AMPX= 0.2299 PHSX = -176.833
ROW = 256 COLUMN = 140 AMPC = 0.0046 PHSC=  -77.4988 AMPX= 0.2311 PHSX = -177.036
ROW = 256 COLUMN = 141 AMPC = 0.0043 PHSC=  -81.2162 AMPX= 0.2322 PHSX = -177.148
ROW = 256 COLUMN = 142 AMPC = 0.0045 PHSC=  -84.3685 AMPX= 0.2328 PHSX = -176.952
ROW = 256 COLUMN = 143 AMPC = 0.0047 PHSC=  -87.4558 AMPX= 0.2334 PHSX = -176.759
ROW = 256 COLUMN = 144 AMPC = 0.0045 PHSC=  -82.7096 AMPX= 0.2343 PHSX = -176.643
ROW = 256 COLUMN = 145 AMPC = 0.0041 PHSC=  -73.6529 AMPX= 0.2352 PHSX = -176.571
ROW = 256 COLUMN = 146 AMPC = 0.0037 PHSC=  -64.7591 AMPX= 0.2362 PHSX = -176.500
ROW = 256 COLUMN = 147 AMPC = 0.0036 PHSC=  -80.8741 AMPX= 0.2370 PHSX = -176.459
ROW = 256 COLUMN = 148 AMPC = 0.0037 PHSC=  -98.9748 AMPX= 0.2377 PHSX = -176.420
 .                                                                        .
 .                                                                        .
 .                                                                        .
ROW = 256 COLUMN = 376 AMPC = 0.0028 PHSC= -358.5897 AMPX= 0.2203 PHSX = -180.310
ROW = 256 COLUMN = 377 AMPC = 0.0025 PHSC= -355.4053 AMPX= 0.2189 PHSX = -180.583
ROW = 256 COLUMN = 378 AMPC = 0.0022 PHSC= -352.1181 AMPX= 0.2174 PHSX = -180.865
ROW = 256 COLUMN = 379 AMPC = 0.0026 PHSC= -339.3691 AMPX= 0.2171 PHSX = -180.812
ROW = 256 COLUMN = 380 AMPC = 0.0030 PHSC= -324.9158 AMPX= 0.2169 PHSX = -180.711
ROW = 256 COLUMN = 381 AMPC = 0.0032 PHSC= -322.1191 AMPX= 0.2158 PHSX = -181.211
ROW = 256 COLUMN = 382 AMPC = 0.0033 PHSC= -319.3790 AMPX= 0.2145 PHSX = -181.801
ROW = 256 COLUMN = 383 AMPC = 0.0028 PHSC= -265.1925 AMPX= 0.2136 PHSX = -181.850
ROW = 256 COLUMN = 384 AMPC = 0.0023 PHSC= -238.6542 AMPX= 0.2124 PHSX = -181.763

REPEAT FOR ANOTHER SUBSECTION? - Y/N
N
OK, COMO -E
```

LPRINT

DESCRIPTION: Reads nominal theta and phi components of far field data produced from probe pattern measurements and combines them to produce two new files of actual theta and phi components correcting for source antenna polarization. The AZ/EL or AL/EP components of the probe receiving pattern are obtained using a vector coordinate transformation. This data is interpolated for equal spacing in k_x and k_y. This program applies to an antenna mount whose rotation is defined as follows. Theta varies from -90 to 90 degrees and phi varies from 0 to -180 degrees in the coordinate system of the probe, which is 0 to 180 degrees for the head axis of the model mount. The probe pattern can be mechanically translated in elevation (Tilt) or azimuth (Yaw).

NF PROCESSING APPLICATION: Preparation of probe compensation data

INPUT: ASCII files - measured probe far field theta and phi components

OUTPUT: Probe compensation data

TIMING:
Connect (Min)	- 9.93
CPU (Sec)	- 563.79
I/O (Sec)	- 57.37

EXAMPLE RUN: The example run computes k-space probe compensation coefficient for a linear waveguide probe. The probe coefficients are used to compensate a 128x512 coupling product.

```
OK, LPRINT

ENTER DATA IDENTIFIER FOR THIS RUN
LPROBE.F3

SCALAR OR VECTOR PROCESSING DATA SET? - S/V
V

ENTER NROW,NCOL,DELX,DELY,FREQ,ARMIN,ARMAX,ACMIN,ACMAX
101,37,-5,2,3.3,0,-180,-90,90



THETA POINTS USED IN PROCESSING =   101
PHI POINTS USED IN PROCESSING =    37
PHI SPACING =      -5.000 DEGREES
THETA SPACING =      2.000 DEGREES
THETA PLOTTING INTERVAL =      0.000 TO   -180.000 DEGREES
PHI PLOTTING INTERVAL =    -90.000 TO     90.000 DEGREES



ENTER NROWD,NCOLD,NRMOD,NCMOD,NSKIPR,THETO,PHIO,TLT
101,37,1,1,0,-100,0,0


THETA POINTS PER SCAN =   101
PHI POINTS PER SCAN =    37
THETA DATA MULTIPLE =     1
PHI DATA MULTIPLE =     1
DATA POINTS SKIPPED IN THETA DIRECTION =     0
INITIAL THETA VALUE OF PROBE DATA =  -100.0000
INITIAL PHI VALUE OF PROBE DATA =     0.0000
PROBE PHYSICAL ELEVATION TILT ANGLE =     0.0000



ENTER AZIMUTHAL PHYSICAL TILT ANGLE FOR PROBE
0.00


PROBE AZIMUTHAL TILT ANGLE =     0.0000 DEGREES



ENTER AXRP,TLTP,GP,REFLA,REFLP,AXRS,TLTS,PHSNRM
71,90.1,7.16,0,0,68,89.6,180

ENTER PROBE POLARIZATION SENSE
RIGHT
```

```
ENTER SOURCE ANTENNA POLARIZATION SENSE
RIGHT


PROBE AXIAL RATIO =    71.0000 DB
PROBE TILT ANGLE =    90.1000 DEGREES
PROBE ON-AXIS GAIN =     7.1600 DBI
PROBE REFLECTION AMPLITUDE =     0.0000
PROBE REFLECTION PHASE =     0.0000 DEGREES
SOURCE ANTENNA AXIAL RATIO =    68.0000 DB
SOURCE ANTENNA TILT ANGLE =    89.6000 DEGREES
S02'(0) PHASE REFERENCE =   180.0000 DEGREES
PROBE POLARIZATION SENSE = RIGHT HAND
SOURCE ANTENNA POLARIZATION SENSE = RIGHT HAND



PROBE CIRCULAR POLARIZATION RATIO AMPLITUDE =      0.99944
PROBE CIRCULAR POLARIZATION RATIO PHASE =      3.14508 RADIANS
PROBE CIRCULAR POLARIZATION RATIO (RECT) =       -0.99943       -0.00349
PROBE LINEAR POLARIZATION RATIO (RECT) =        0.00175        0.00028
SOURCE ANTENNA CIRCULAR POL. AMPLITUDE =      0.99920
SOURCE ANTENNA CIRCULAR POL. PHASE =      3.12763 RADIANS
SOURCE ANTENNA CIRCULAR POL. RATIO (RECT) =       -0.99911        0.01395
SOURCE ANTENNA LINEAR POL. RATIO (RECT) =        0.00698       -0.00040



ON-AXIS NORMALIZATION FACTOR (RECT) =       -0.99999       -0.00000
ON-AXIS NORMALIZATION FACTOR AMPLITUDE =      0.99999
ON-AXIS NORMALIZATION FACTOR PHASE =   -179.99979
PSI =      3.13636
ACONST =      0.00000
BCONST =     -0.00068



ENTER SUM OR DIFFERENCE PATTERN - S/D
S


                    ********************************
                    *** SUM PATTERN PROCESSING ***
                    ********************************
```

```
ENTER IR2TON,IC2TON,NR1,NC1,DX,DY
128,512,128,512,3.8100,3.8100

SELECT A,E OR ALPHA,EPSILON INTERPOLATION (ELECTRIC/MAGNETIC)
ELECTRIC


NFVECTOR ROWS INCLUDING ZERO-PADDING =   128
NFVECTOR COLUMNS INCLUDING ZERO-PADDING =   512
FILTER ROW LENGTH =   128
FILTER COLUMN LENGTH =   512
NEAR FIELD X-SPACING =      3.81000 CM.
NEAR FIELD Y-SPACING =      3.81000 CM.



ENTER NOMINAL THETA COMPONENT PATTERN FILE NAME
LPROBE.F3.THETA


THETA COMPONENT PATTERN FILE HEADER
NORMALIZ   101 PTS  ,X COMPO  08068411  ,106 DAY  NBS LIN PROBE 01 03300 YX THET

      -90.000       90.000        0.035       -1.745       101          5         96

                                THETA COMPONENT CENTRAL COLUMN

MAXIMUM AMPLITUDE =      1.002 AT POINT NO.    50


ANGLES OR INDICES
    -92.00    -90.00    -88.00    -86.00    -84.00    -82.00    -80.00    -78.00
    -68.00    -66.00    -64.00    -62.00    -60.00    -58.00    -56.00    -54.00
    -44.00    -42.00    -40.00    -38.00    -36.00    -34.00    -32.00    -30.00
    -20.00    -18.00    -16.00    -14.00    -12.00    -10.00     -8.00     -6.00
      4.00      6.00      8.00     10.00     12.00     14.00     16.00     18.00
     28.00     30.00     32.00     34.00     36.00     38.00     40.00     42.00
     52.00     54.00     56.00     58.00     60.00     62.00     64.00     66.00
     76.00     78.00     80.00     82.00     84.00     86.00     88.00     90.00


AMPLITUDES IN DB
```

```
-7.21    -6.97    -6.69    -6.35    -6.04    -5.82    -5.61    -5.46
-4.43    -4.22    -3.96    -3.77    -3.60    -3.47    -3.29    -3.09
-2.04    -1.85    -1.68    -1.52    -1.40    -1.28    -1.17    -1.06
-0.43    -0.37    -0.30    -0.23    -0.18    -0.12    -0.07    -0.04
-0.05    -0.07    -0.11    -0.15    -0.21    -0.27    -0.35    -0.44
-1.01    -1.13    -1.24    -1.39    -1.55    -1.71    -1.90    -2.06
-3.07    -3.25    -3.43    -3.62    -3.84    -4.06    -4.27    -4.46
-5.44    -5.62    -5.83    -6.13    -6.33    -6.60    -6.88    -7.12


PHASES IN DEGREES
 118.90   116.65   115.46   114.36   113.36   113.11   112.60   111.95
 108.36   107.86   107.56   107.20   107.30   106.50   106.15   105.35
 103.06   102.85   102.95   102.60   102.80   102.55   102.10   101.90
 100.95   100.65   100.35   100.45   100.15   100.15   100.20   100.15
 100.20   100.65   100.20   100.40   100.55   100.10   100.45   100.35
 101.45   101.30   101.81   101.45   101.65   102.15   101.90   102.25
 104.30   104.70   105.35   105.86   105.80   106.26   106.95   107.85
 110.80   110.95   112.00   112.40   113.79   114.55   116.23   117.53

AMP=  0.4358     TO    1.000     VOLTS.  (   7.2 DB.)

PLOT AXES?  N

PLOT AMPLITUDE? N

PLOT PHASE? N

MAXIMUM AMPLITUDE FOR Y-COMPONENT =      1.002

        0.000    -180.000       -0.087       0.000        37          1     .    37

                                THETA COMPONENT CENTRAL ROW

MAXIMUM AMPLITUDE =      1.002 AT POINT NO.     1


ANGLES OR INDICES
    0.00     -5.00    -10.00    -15.00    -20.00    -25.00    -30.00    -35.00
  -60.00     -65.00    -70.00    -75.00    -80.00    -85.00    -90.00    -95.00
 -120.00    -125.00   -130.00   -135.00   -140.00   -145.00   -150.00   -155.00
 -180.00


AMPLITUDES IN DB
  -39.78    -20.24    -14.69    -11.36     -9.00     -7.24     -5.82     -4.65
   -1.20     -0.83     -0.53     -0.26     -0.13     -0.04     -0.02     -0.06
```

```
    -1.31     -1.79     -2.42     -3.14     -3.98     -4.98     -6.22     -7.74
   -39.78


PHASES IN DEGREES
    105.80    100.22    101.95    101.15    100.55    100.35    100.65    100.65
    100.35    100.25    100.20    100.20    100.35    100.05    100.00    100.20
    100.00     99.75     99.90    100.00    100.40    100.20     99.95    100.25
    285.80

AMP=  0.1025E-01 TO   0.9980     VOLTS.  (  39.8 DB.)


PLOT AXES?  N


PLOT AMPLITUDE? N


PLOT PHASE? N

ENTER NOMINAL PHI COMPONENT PATTERN FILE NAME
LPROBE.F3.PHI


PHI COMPONENT PATTERN FILE HEADER
NORMALIZ   101 PTS  ,Y COMPO  08068405  ,113 DAY  NBS LIN PROBE 01 03300 YY PHI
```

COL#	REFAMP	PREFP	ACORRP	PCORRP	REFAMT	PREFT
1	1.0000	0.0000	1.0000	-100.0000	0.0053	-7.3989
2	0.9957	0.0034	0.9996	-99.7475	0.0924	-0.4201
3	0.9839	0.0069	0.9961	-99.7448	0.1788	-0.2146
4	0.9646	0.0105	0.9947	-99.7912	0.2639	-0.1426
5	0.9379	0.0142	0.9943	-99.9379	0.3469	-0.1055
6	0.9041	0.0182	0.9920	-99.8331	0.4274	-0.0826
7	0.8634	0.0226	0.9922	-99.6809	0.5045	-0.0669
8	0.8161	0.0274	0.9922	-99.8272	0.5779	-0.0552
9	0.7627	0.0328	0.9924	-99.8194	0.6468	-0.0461
10	0.7034	0.0392	0.9935	-99.8119	0.7108	-0.0388
11	0.6388	0.0467	0.9936	-99.8062	0.7694	-0.0325
12	0.5693	0.0561	0.9879	-99.6476	0.8222	-0.0272
13	0.4955	0.0681	0.9898	-99.4843	0.8686	-0.0224
14	0.4179	0.0845	0.9872	-99.7181	0.9085	-0.0181
15	0.3371	0.1086	0.9919	-99.9954	0.9415	-0.0142
16	0.2538	0.1483	0.9863	-100.1042	0.9673	-0.0104
17	0.1685	0.2277	0.9796	-98.8252	0.9857	-0.0069
18	0.0819	0.4736	0.9686	-101.7272	0.9967	-0.0034

PHI COMPONENT CENTRAL COLUMN

MAXIMUM AMPLITUDE = 1.002 AT POINT NO. 1

ANGLES OR INDICES

-92.00	-90.00	-88.00	-86.00	-84.00	-82.00	-80.00	-78.00
-68.00	-66.00	-64.00	-62.00	-60.00	-58.00	-56.00	-54.00
-44.00	-42.00	-40.00	-38.00	-36.00	-34.00	-32.00	-30.00
-20.00	-18.00	-16.00	-14.00	-12.00	-10.00	-8.00	-6.00
4.00	6.00	8.00	10.00	12.00	14.00	16.00	18.00
28.00	30.00	32.00	34.00	36.00	38.00	40.00	42.00
52.00	54.00	56.00	58.00	60.00	62.00	64.00	66.00
76.00	78.00	80.00	82.00	84.00	86.00	88.00	90.00

AMPLITUDES IN DB

-52.14	-52.13	-56.25	-57.01	-60.50	-65.35	-57.78	-55.81
-57.02	-55.04	-50.58	-52.70	-50.23	-47.96	-49.36	-44.46
-48.62	-52.71	-50.95	-47.80	-53.35	-52.05	-46.57	-42.79
-49.15	-48.17	-46.93	-50.47	-50.75	-43.76	-45.34	-43.96
-49.12	-45.20	-47.87	-45.83	-49.12	-52.30	-47.90	-47.20
-48.18	-43.10	-45.72	-49.17	-49.22	-46.19	-43.10	-44.85
-45.24	-45.75	-52.12	-45.96	-45.62	-51.02	-51.27	-57.35
-45.32	-46.37	-44.45	-48.71	-52.80	-56.08	-54.01	-52.08

PHASES IN DEGREES

69.24	68.68	356.73	145.22	4.63	71.49	35.35	317.45
170.45	218.91	260.28	268.36	286.94	251.17	278.65	283.86
284.18	328.75	312.30	328.60	280.55	249.57	272.30	308.44
302.35	336.66	303.53	301.10	309.74	268.51	303.32	309.75
281.42	324.64	275.95	281.63	250.04	276.53	265.61	269.51
291.63	265.80	279.83	324.96	341.54	303.16	280.74	285.65
291.19	300.48	290.64	230.60	255.58	220.93	199.80	227.78
290.04	257.83	284.10	255.25	234.79	292.31	315.25	254.17

AMP= 0.5000E-03 TO 0.7962E-02 VOLTS. (24.0 DB.)

PLOT AXES? N

PLOT AMPLITUDE? N

PLOT PHASE? N

19 0.0053 172.6012 1.3223 -122.2017 1.0000 0.0000

CORRECTED PHI COMPONENT CENTRAL COLUMN

MAXIMUM AMPLITUDE = 0.930 AT POINT NO. 1

ANGLES OR INDICES

-92.00	-90.00	-88.00	-86.00	-84.00	-82.00	-80.00	-78.00
-68.00	-66.00	-64.00	-62.00	-60.00	-58.00	-56.00	-54.00
-44.00	-42.00	-40.00	-38.00	-36.00	-34.00	-32.00	-30.00
-20.00	-18.00	-16.00	-14.00	-12.00	-10.00	-8.00	-6.00
4.00	6.00	8.00	10.00	12.00	14.00	16.00	18.00
28.00	30.00	32.00	34.00	36.00	38.00	40.00	42.00
52.00	54.00	56.00	58.00	60.00	62.00	64.00	66.00
76.00	78.00	80.00	82.00	84.00	86.00	88.00	90.00

AMPLITUDES IN DB

-45.63	-45.42	-53.09	-45.65	-50.74	-47.99	-48.22	-55.79
-44.86	-46.32	-49.59	-50.97	-56.16	-46.76	-53.36	-48.54
-55.21	-49.79	-53.19	-51.44	-49.20	-46.42	-50.28	-48.97
-53.72	-47.85	-60.59	-50.88	-49.98	-47.13	-65.06	-53.92
-50.72	-50.16	-50.74	-53.53	-45.68	-47.93	-48.52	-49.61
-57.21	-45.26	-52.15	-51.64	-48.30	-62.24	-47.07	-51.39
-51.56	-53.80	-55.32	-43.09	-45.60	-45.24	-43.97	-47.46
-48.25	-45.98	-46.01	-47.74	-47.87	-56.29	-65.44	-49.61

PHASES IN DEGREES

159.97	159.13	153.85	195.34	170.15	180.85	163.33	180.00
198.01	213.63	242.87	225.62	244.10	252.78	252.11	314.40
239.75	154.16	161.64	112.97	196.81	212.31	256.19	19.55
172.16	127.02	148.93	174.81	163.93	273.26	66.17	47.41
205.93	93.84	223.43	255.17	219.89	194.69	229.44	237.40
212.98	283.97	276.29	131.10	127.02	16.62	312.67	310.13
326.12	350.80	208.95	249.02	272.95	225.69	217.02	209.22
328.79	280.46	323.05	268.65	237.75	220.65	192.54	256.26

AMP= 0.5346E-03 TO 0.7857E-02 VOLTS. (23.3 DB.)

PLOT AXES? N

PLOT AMPLITUDE? N

PLOT PHASE? N

MAXIMUM AMPLITUDE FOR THE PHI COMPONENT = 0.930

COL#	REFAMP	PREFP	ACORRP	PCORRP	REFAMT	PREFT
20	0.0924	179.5799	1.0034	-102.5631	0.9957	0.0034
21	0.1788	179.7854	0.9906	-101.3184	0.9839	0.0069
22	0.2639	179.8574	0.9783	-100.2976	0.9646	0.0105
23	0.3469	179.8945	0.9834	-100.6073	0.9379	0.0142
24	0.4274	179.9174	0.9765	-100.1863	0.9041	0.0182
25	0.5045	179.9331	0.9845	-99.8180	0.8634	0.0226
26	0.5779	179.9448	0.9826	-100.1594	0.8161	0.0274
27	0.6468	179.9539	0.9834	-100.0486	0.7627	0.0328
28	0.7108	179.9612	0.9828	-99.8922	0.7034	0.0392
29	0.7694	179.9674	0.9835	-99.7854	0.6388	0.0467
30	0.8222	179.9728	0.9854	-99.7812	0.5693	0.0561
31	0.8686	179.9776	0.9865	-99.5766	0.4955	0.0681
32	0.9085	179.9819	0.9862	-99.8217	0.4179	0.0845
33	0.9415	179.9858	0.9874	-99.6158	0.3371	0.1086
34	0.9673	179.9896	0.9851	-99.6131	0.2538	0.1483
35	0.9857	179.9931	0.9852	-99.6591	0.1685	0.2277
36	0.9967	179.9966	0.9860	-99.5567	0.0819	0.4736
37	1.0000	-180.0000	1.0000	-99.9999	0.0053	172.6015

PHI COMPONENT RADIATED POWER = 0.73138
THETA COMPONENT RADIATED POWER = 1.44685
NORMALIZED TOTAL RADIATED POWER = 2.17823
DIRECTIVITY = 5.76908
DIRECTIVITY = 7.61107 DBI

CORRECTED THETA COMPONENT CENTRAL COLUMN

MAXIMUM AMPLITUDE = 0.932 AT POINT NO. 50

ANGLES OR INDICES

-92.00	-90.00	-88.00	-86.00	-84.00	-82.00	-80.00	-78.00
-68.00	-66.00	-64.00	-62.00	-60.00	-58.00	-56.00	-54.00
-44.00	-42.00	-40.00	-38.00	-36.00	-34.00	-32.00	-30.00
-20.00	-18.00	-16.00	-14.00	-12.00	-10.00	-8.00	-6.00
4.00	6.00	8.00	10.00	12.00	14.00	16.00	18.00
28.00	30.00	32.00	34.00	36.00	38.00	40.00	42.00
52.00	54.00	56.00	58.00	60.00	62.00	64.00	66.00
76.00	78.00	80.00	82.00	84.00	86.00	88.00	90.00

AMPLITUDES IN DB

```
    -7.22     -6.97     -6.69     -6.35     -6.04     -5.82     -5.61     -5.46
    -4.43     -4.22     -3.96     -3.77     -3.60     -3.47     -3.29     -3.09
    -2.04     -1.85     -1.68     -1.52     -1.40     -1.28     -1.17     -1.06
    -0.43     -0.37     -0.30     -0.23     -0.18     -0.12     -0.07     -0.04
    -0.05     -0.07     -0.11     -0.15     -0.21     -0.27     -0.35     -0.44
    -1.01     -1.13     -1.24     -1.39     -1.55     -1.71     -1.90     -2.06
    -3.07     -3.25     -3.43     -3.62     -3.84     -4.06     -4.27     -4.46
    -5.44     -5.62     -5.83     -6.13     -6.33     -6.60     -6.88     -7.12


PHASES IN DEGREES
    18.90     16.65     15.46     14.36     13.36     13.11     12.61     11.95
     8.36      7.86      7.56      7.20      7.30      6.50      6.15      5.35
     3.05      2.85      2.95      2.60      2.80      2.55      2.10      1.90
     0.95      0.65      0.35      0.45      0.15      0.15      0.20      0.15
     0.20      0.65      0.20      0.40      0.55      0.10      0.45      0.35
     1.45      1.30      1.80      1.45      1.65      2.15      1.90      2.25
     4.30      4.70      5.35      5.85      5.80      6.26      6.95      7.85
    10.79     10.95     12.00     12.40     13.79     14.55     16.23     17.53

AMP= 0.4358     TO    1.000     VOLTS.  (   7.2 DB.)

PLOT AXES?  N

PLOT AMPLITUDE? N

PLOT PHASE? N

                                CORRECTED THETA COMPONENT CENTRAL ROW

MAXIMUM AMPLITUDE =      0.932 AT POINT NO.      1


ANGLES OR INDICES
      0.00     -5.00    -10.00    -15.00    -20.00    -25.00    -30.00    -35.00
    -60.00    -65.00    -70.00    -75.00    -80.00    -85.00    -90.00    -95.00
   -120.00   -125.00   -130.00   -135.00   -140.00   -145.00   -150.00   -155.00
   -180.00


AMPLITUDES IN DB
    -55.07    -21.39    -15.31    -11.81     -9.38     -7.53     -6.06     -4.87
     -1.28     -0.88     -0.56     -0.32     -0.15     -0.05     -0.02     -0.05
     -1.26     -1.74     -2.32     -3.01     -3.84     -4.82     -6.01     -7.47
    -55.07
```

PHASES IN DEGREES

189.17	359.81	359.91	359.94	359.96	359.97	359.97	359.98
359.99	359.99	359.99	360.00	360.00	360.00	0.00	0.00
0.01	0.01	0.01	0.02	0.02	0.02	0.03	0.03
9.17							

AMP= 0.1764E-02 TO 0.9980 VOLTS. (55.1 DB.)

PLOT AXES? N

PLOT AMPLITUDE? N

PLOT PHASE? N

CORRECTED THETA COMPONENT FILE HEADER
SOURCE ANTENNA POLARIZATION CORRECTED THETA DATA LPROBE.F3

CORRECTED PHI COMONENT FILE HEADER
SOURCE ANTENNA POLARIZATION CORRECTED PHI DATA LPROBE.F3

AMPLITUDES FOR THETA COMPONENT ORIENTATION 1

1	1	0.000	-1.745	0.000	1.000	1.000	-0.000	0.073	0.001	-0.000
1	2	0.000	-1.710	0.000	1.000	1.000	-0.009	0.069	-0.000	0.001
1	3	0.000	-1.676	0.000	1.000	1.000	-0.018	0.060	-0.000	0.000
1	4	0.000	-1.641	0.000	1.000	1.000	-0.031	0.054	0.000	0.001
1	5	0.000	-1.606	0.000	1.000	1.000	-0.033	0.045	-0.001	-0.000
1	6	0.000	-1.571	0.000	1.000	1.000	-0.040	0.044	0.000	0.000
1	7	0.000	-1.536	0.000	1.000	1.000	-0.046	0.040	-0.001	-0.000
1	8	0.000	-1.501	0.000	1.000	1.000	-0.052	0.042	-0.002	-0.000
1	9	0.000	-1.466	0.000	1.000	1.000	-0.063	0.044	0.000	-0.001
1	10	0.000	-1.431	0.000	1.000	1.000	-0.075	0.044	0.001	-0.001
1	11	0.000	-1.396	0.000	1.000	1.000	-0.090	0.046	0.001	0.001
1	12	0.000	-1.361	0.000	1.000	1.000	-0.104	0.043	-0.000	0.000
1	13	0.000	-1.326	0.000	1.000	1.000	-0.120	0.044	-0.000	-0.000
1	14	0.000	-1.292	0.000	1.000	1.000	-0.137	0.039	-0.000	-0.001
1	15	0.000	-1.257	0.000	1.000	1.000	-0.151	0.038	0.000	-0.000
1	16	0.000	-1.222	0.000	1.000	1.000	-0.168	0.037	-0.000	0.001
1	17	0.000	-1.187	0.000	1.000	1.000	-0.182	0.035	-0.000	0.001
1	18	0.000	-1.152	0.000	1.000	1.000	-0.201	0.035	-0.000	0.002
:										:
1	101	0.000	1.745	0.000	1.000	1.000	-0.003	0.071	-0.001	0.001
16	1	-1.309	-1.745	0.168	0.308	0.250	-0.059	-0.058	0.337	0.152
:										:

16	86	-1.309	1.222	-0.330	0.420	0.259	-0.097	-0.042	0.509	0.061
16	87	-1.309	1.257	-0.298	0.395	0.259	-0.089	-0.046	0.496	0.065
16	88	-1.309	1.292	-0.266	0.371	0.259	-0.085	-0.046	0.486	0.068
16	89	-1.309	1.326	-0.234	0.349	0.259	-0.085	-0.045	0.475	0.071
16	90	-1.309	1.361	-0.201	0.328	0.259	-0.081	-0.044	0.465	0.072
16	91	-1.309	1.396	-0.168	0.308	0.259	-0.077	-0.047	0.450	0.076
16	92	-1.309	1.431	-0.134	0.292	0.259	-0.074	-0.045	0.439	0.077
16	93	-1.309	1.466	-0.101	0.278	0.259	-0.069	-0.046	0.423	0.082
16	94	-1.309	1.501	-0.067	0.267	0.259	-0.062	-0.042	0.408	0.082
16	95	-1.309	1.536	-0.034	0.261	0.259	-0.059	-0.043	0.393	0.090
16	96	-1.309	1.571	0.000	0.259	0.259	-0.056	-0.046	0.380	0.098
16	97	-1.309	1.606	0.034	0.261	0.259	-0.052	-0.049	0.366	0.109
16	98	-1.309	1.641	0.067	0.267	0.259	-0.051	-0.053	0.357	0.122
16	99	-1.309	1.676	0.101	0.278	0.259	-0.054	-0.054	0.351	0.129
16	100	-1.309	1.710	0.134	0.292	0.259	-0.054	-0.058	0.347	0.141
16	101	-1.309	1.745	0.168	0.308	0.259	-0.057	-0.056	0.339	0.155
	-90.000		90.000		0.035	-1.745		101	5	96

AZIMUTH COMPONENT CENTRAL COLUMN

MAXIMUM AMPLITUDE = 0.930 AT POINT NO. 1

ANGLES OR INDICES

-92.00	-90.00	-88.00	-86.00	-84.00	-82.00	-80.00	-78.00
-68.00	-66.00	-64.00	-62.00	-60.00	-58.00	-56.00	-54.00
-44.00	-42.00	-40.00	-38.00	-36.00	-34.00	-32.00	-30.00
-20.00	-18.00	-16.00	-14.00	-12.00	-10.00	-8.00	-6.00
4.00	6.00	8.00	10.00	12.00	14.00	16.00	18.00
28.00	30.00	32.00	34.00	36.00	38.00	40.00	42.00
52.00	54.00	56.00	58.00	60.00	62.00	64.00	66.00
76.00	78.00	80.00	82.00	84.00	86.00	88.00	90.00

AMPLITUDES IN DB

-45.64	-45.42	-53.09	-45.65	-50.74	-47.99	-48.22	-55.78
-44.86	-46.32	-49.59	-50.97	-56.15	-46.76	-53.36	-48.54
-55.21	-49.79	-53.19	-51.44	-49.20	-46.41	-50.28	-48.97
-53.72	-47.85	-60.59	-50.88	-49.99	-47.13	-65.05	-53.92
-50.72	-50.16	-50.74	-53.53	-45.68	-47.93	-48.52	-49.61
-57.21	-45.27	-52.15	-51.64	-48.30	-62.24	-47.07	-51.39
-51.56	-53.80	-55.31	-43.09	-45.59	-45.24	-43.97	-47.46
-48.25	-45.98	-46.01	-47.74	-47.86	-56.28	-65.41	-49.61

PHASES IN DEGREES

339.95	159.13	153.88	195.34	170.16	180.86	163.34	180.00
198.01	213.63	242.87	225.62	244.09	252.77	252.10	314.40
239.74	154.16	161.64	112.98	196.81	212.31	256.19	19.56

172.16	127.02	148.93	174.81	163.93	273.26	66.18	47.41
205.93	93.84	223.43	255.16	219.89	194.69	229.44	237.40
212.97	283.97	276.29	131.11	127.02	16.62	312.67	310.13
326.12	350.80	208.94	249.02	272.95	225.69	217.02	209.22
328.79	280.46	323.04	268.64	237.74	220.63	192.55	256.26

AMP= 0.5363E-03 TO 0.7856E-02 VOLTS. (23.3 DB.)

PLOT AXES? N

PLOT AMPLITUDE? N

PLOT PHASE? N

MAXIMUM AMPLITUDE FOR THE AZIMUTH COMPONENT = 0.930

ELEVATION COMPONENT CENTRAL COLUMN

MAXIMUM AMPLITUDE = 0.932 AT POINT NO. 50

ANGLES OR INDICES

-92.00	-90.00	-88.00	-86.00	-84.00	-82.00	-80.00	-78.00
-68.00	-66.00	-64.00	-62.00	-60.00	-58.00	-56.00	-54.00
-44.00	-42.00	-40.00	-38.00	-36.00	-34.00	-32.00	-30.00
-20.00	-18.00	-16.00	-14.00	-12.00	-10.00	-8.00	-6.00
4.00	6.00	8.00	10.00	12.00	14.00	16.00	18.00
28.00	30.00	32.00	34.00	36.00	38.00	40.00	42.00
52.00	54.00	56.00	58.00	60.00	62.00	64.00	66.00
76.00	78.00	80.00	82.00	84.00	86.00	88.00	90.00

AMPLITUDES IN DB

-7.22	-6.97	-6.69	-6.35	-6.04	-5.82	-5.61	-5.46
-4.43	-4.22	-3.96	-3.77	-3.60	-3.47	-3.29	-3.09
-2.04	-1.85	-1.68	-1.52	-1.40	-1.28	-1.17	-1.06
-0.43	-0.37	-0.30	-0.23	-0.18	-0.12	-0.07	-0.04
-0.05	-0.07	-0.11	-0.15	-0.21	-0.27	-0.35	-0.44
-1.01	-1.13	-1.24	-1.39	-1.55	-1.71	-1.90	-2.06
-3.07	-3.25	-3.43	-3.62	-3.84	-4.06	-4.27	-4.46
-5.44	-5.62	-5.83	-6.13	-6.33	-6.60	-6.88	-7.12

PHASES IN DEGREES

18.90	16.65	195.46	194.36	193.36	193.11	192.61	191.95
188.36	187.86	187.56	187.20	187.30	186.50	186.15	185.35

```
   183.05    182.85    182.95    182.60    182.80    182.55    182.10    181.90
   180.95    180.65    180.35    180.45    180.15    180.15    180.20    180.15
   180.20    180.65    180.20    180.40    180.55    180.10    180.45    180.35
   181.45    181.30    181.80    181.45    181.65    182.15    181.90    182.25
   184.30    184.70    185.35    185.85    185.80    186.26    186.95    187.85
   190.79    190.95    192.00    192.40    193.79    194.55    196.23     17.53

AMP= 0.4356     TO    1.000     VOLTS.  (   7.2 DB.)

PLOT AXES?  N

PLOT AMPLITUDE? N

PLOT PHASE? N
        0.000    -180.000      -0.087       0.000        37          1         37

                                ELEVATION COMPONENT CENTRAL ROW

MAXIMUM AMPLITUDE =      0.932 AT POINT NO.     1


ANGLES OR INDICES
      0.00     -5.00    -10.00    -15.00    -20.00    -25.00    -30.00    -35.00
    -60.00    -65.00    -70.00    -75.00    -80.00    -85.00    -90.00    -95.00
   -120.00   -125.00   -130.00   -135.00   -140.00   -145.00   -150.00   -155.00
   -180.00


AMPLITUDES IN DB
     -0.02     -0.02     -0.02     -0.02     -0.02     -0.02     -0.02     -0.02
     -0.02     -0.02     -0.02     -0.02     -0.02     -0.02     -0.02     -0.02
     -0.02     -0.02     -0.02     -0.02     -0.02     -0.02     -0.02     -0.02
     -0.02


PHASES IN DEGREES
    180.00    180.00    180.00    180.00    180.00    180.00    180.00    180.00
    180.00    180.00    180.00    180.00    180.00    180.00    180.00    180.00
    180.00    180.00    180.00    180.00    180.00    180.00    180.00    180.00
    180.00

AMP= 0.9980     TO    0.9980     VOLTS.  (   0.0 DB.)

PLOT AXES?  N
```

PLOT AMPLITUDE? N

PLOT PHASE? N

AZIMUTH COMPONENT FILE HEADER
SOURCE ANTENNA POLARIZATION CORRECTED AZIMUTH DATA LPROBE.F3

AMPLITUDES FOR AZIMUTH COMPONENT PROBE ORIENTATION

ELEVATION COMPONENT FILE HEADER
SOURCE ANTENNA POLARIZATION CORRECTED ELEVATION DATA LPROBE.F3

AMPLITUDES FOR ELEVATION COMPONENT PROBE ORIENTATIO

CORRECTED THETA COMPONENT FILE HEADER
SOURCE ANTENNA POLARIZATION CORRECTED THETA DATA LPROBE.F3

CORRECTED PHI COMONENT FILE HEADER
SOURCE ANTENNA POLARIZATION CORRECTED PHI DATA LPROBE.F3

AMPLITUDES FOR THETA COMPONENT ORIENTATION 2

1	1	0.000	-1.745	0.000	1.000	1.000	-0.007	0.004	-0.357	-0.163
1	2	0.000	-1.710	0.000	1.000	1.000	-0.005	0.006	-0.352	-0.172
1	3	0.000	-1.676	0.000	1.000	1.000	-0.000	0.002	-0.365	-0.149
1	4	0.000	-1.641	0.000	1.000	1.000	-0.000	0.000	-0.373	-0.142
1	5	0.000	-1.606	0.000	1.000	1.000	0.001	0.001	-0.382	-0.131
1	6	0.000	-1.571	0.000	1.000	1.000	0.001	0.003	-0.391	-0.124
1	7	0.000	-1.536	0.000	1.000	1.000	0.000	0.000	-0.405	-0.118
1	8	0.000	-1.501	0.000	1.000	1.000	0.001	0.001	-0.422	-0.110
1	9	0.000	-1.466	0.000	1.000	1.000	0.002	0.003	-0.437	-0.107
1	10	0.000	-1.431	0.000	1.000	1.000	0.000	0.004	-0.449	-0.099
1	11	0.000	-1.396	0.000	1.000	1.000	-0.004	0.003	-0.466	-0.099
1	12	0.000	-1.361	0.000	1.000	1.000	-0.001	0.005	-0.479	-0.093
1	13	0.000	-1.326	0.000	1.000	1.000	-0.003	0.002	-0.489	-0.093
⋮										⋮
1	101	0.000	1.745	0.000	1.000	1.000	-0.001	-0.003	-0.345	-0.187
16	1	-1.309	-1.745	0.168	0.308	0.259	-0.009	0.062	-0.075	-0.016
⋮										⋮

16	81	-1.309	1.047	-0.483	0.548	0.259	-0.272	0.026	-0.114	0.022
16	82	-1.309	1.082	-0.453	0.522	0.259	-0.246	0.026	-0.110	0.020
16	83	-1.309	1.117	-0.423	0.496	0.259	-0.227	0.028	-0.106	0.022
16	84	-1.309	1.152	-0.393	0.470	0.259	-0.210	0.028	-0.101	0.021
16	85	-1.309	1.187	-0.362	0.445	0.259	-0.190	0.028	-0.095	0.020
16	86	-1.309	1.222	-0.330	0.420	0.259	-0.174	0.026	-0.090	0.016
16	87	-1.309	1.257	-0.298	0.395	0.259	-0.161	0.028	-0.089	0.014
16	88	-1.309	1.292	-0.266	0.371	0.259	-0.149	0.031	-0.089	0.011
16	89	-1.309	1.326	-0.234	0.349	0.259	-0.134	0.035	-0.089	0.011
16	90	-1.309	1.361	-0.201	0.328	0.259	-0.118	0.035	-0.087	0.012
16	91	-1.309	1.396	-0.168	0.308	0.259	-0.104	0.038	-0.084	0.013
16	92	-1.309	1.431	-0.134	0.292	0.259	-0.088	0.037	-0.084	0.010
16	93	-1.309	1.466	-0.101	0.278	0.259	-0.071	0.034	-0.084	0.009
16	94	-1.309	1.501	-0.067	0.267	0.259	-0.062	0.033	-0.081	0.009
16	95	-1.309	1.536	-0.034	0.261	0.259	-0.057	0.029	-0.077	0.009
16	96	-1.309	1.571	0.000	0.259	0.259	-0.056	0.029	-0.073	0.007
16	97	-1.309	1.606	0.034	0.261	0.259	-0.048	0.034	-0.071	0.002
16	98	-1.309	1.641	0.067	0.267	0.259	-0.041	0.044	-0.070	-0.002
16	99	-1.309	1.676	0.101	0.278	0.259	-0.033	0.050	-0.070	-0.005
16	100	-1.309	1.710	0.134	0.292	0.259	-0.022	0.059	-0.072	-0.009
16	101	-1.309	1.745	0.168	0.308	0.259	-0.012	0.062	-0.071	-0.019
		-90.000	90.000		0.035	-1.745		101	5	96

AZIMUTH COMPONENT CENTRAL COLUMN

MAXIMUM AMPLITUDE = 0.933 AT POINT NO. 52

ANGLES OR INDICES

-92.00	-90.00	-88.00	-86.00	-84.00	-82.00	-80.00	-78.00
-68.00	-66.00	-64.00	-62.00	-60.00	-58.00	-56.00	-54.00
-44.00	-42.00	-40.00	-38.00	-36.00	-34.00	-32.00	-30.00
-20.00	-18.00	-16.00	-14.00	-12.00	-10.00	-8.00	-6.00
4.00	6.00	8.00	10.00	12.00	14.00	16.00	18.00
28.00	30.00	32.00	34.00	36.00	38.00	40.00	42.00
52.00	54.00	56.00	58.00	60.00	62.00	64.00	66.00
76.00	78.00	80.00	82.00	84.00	86.00	88.00	90.00

AMPLITUDES IN DB

-24.46	-23.96	-23.70	-22.94	-21.64	-20.56	-19.31	-18.37
-14.05	-13.21	-12.56	-11.74	-10.90	-10.19	-9.53	-8.90
-6.11	-5.56	-5.04	-4.57	-4.13	-3.67	-3.26	-2.90
-1.30	-1.05	-0.81	-0.65	-0.47	-0.33	-0.22	-0.13
-0.06	-0.11	-0.22	-0.31	-0.47	-0.66	-0.86	-1.07
-2.50	-2.86	-3.23	-3.60	-4.02	-4.46	-4.93	-5.42
-8.26	-8.76	-9.32	-9.93	-10.67	-11.49	-12.34	-13.05
-16.83	-17.75	-18.70	-19.77	-20.99	-22.01	-22.81	-23.25

PHASES IN DEGREES

306.54	132.11	139.45	140.77	145.02	149.52	153.10	157.29
169.16	170.05	171.50	172.75	172.70	174.35	175.36	176.15
178.30	178.10	178.45	178.80	179.10	179.50	179.45	179.60
180.15	180.25	180.05	180.30	180.35	180.20	180.50	180.15
180.00	179.85	179.80	179.45	179.60	179.05	179.40	179.60
178.65	178.75	178.45	178.55	178.10	177.85	177.10	176.61
175.35	174.85	173.80	172.80	171.06	169.50	169.20	167.01
160.14	158.17	152.24	148.42	144.13	140.29	137.61	131.61

AMP= 0.5982E-01 TO 1.000 VOLTS. (24.5 DB.)

PLOT AXES? N

PLOT AMPLITUDE? N

PLOT PHASE? N

MAXIMUM AMPLITUDE FOR THE AZIMUTH COMPONENT = 0.933

ELEVATION COMPONENT CENTRAL COLUMN

MAXIMUM AMPLITUDE = 0.933 AT POINT NO. 1

ANGLES OR INDICES

-92.00	-90.00	-88.00	-86.00	-84.00	-82.00	-80.00	-78.00
-68.00	-66.00	-64.00	-62.00	-60.00	-58.00	-56.00	-54.00
-44.00	-42.00	-40.00	-38.00	-36.00	-34.00	-32.00	-30.00
-20.00	-18.00	-16.00	-14.00	-12.00	-10.00	-8.00	-6.00
4.00	6.00	8.00	10.00	12.00	14.00	16.00	18.00
28.00	30.00	32.00	34.00	36.00	38.00	40.00	42.00
52.00	54.00	56.00	58.00	60.00	62.00	64.00	66.00
76.00	78.00	80.00	82.00	84.00	86.00	88.00	90.00

AMPLITUDES IN DB

-64.68	-75.37	-55.72	-53.52	-58.90	-56.53	-58.57	-63.84
-56.92	-53.23	-57.70	-55.68	-55.54	-57.28	-56.16	-57.80
-56.92	-57.03	-62.60	-55.46	-59.01	-64.50	-51.58	-58.96
-59.51	-57.61	-59.75	-54.89	-53.42	-57.23	-57.64	-54.03
-59.64	-58.25	-59.62	-53.42	-59.10	-56.86	-57.45	-57.66
-53.44	-55.08	-58.87	-57.17	-62.11	-67.99	-76.98	-50.27
-55.36	-55.65	-57.89	-55.35	-57.75	-56.39	-54.13	-52.68
-65.85	-61.59	-67.83	-65.25	-62.12	-61.16	-54.73	-59.94

```
PHASES IN DEGREES
   190.56    44.81    11.44    14.60   106.32   123.90   233.85   320.04
   280.93   275.22   288.86   309.05   327.55   320.88   322.10    12.92
     5.06    26.50    37.84    83.46   309.22    43.16   314.20     0.23
   347.40    10.45    20.09   344.79   317.25   331.02   349.61     8.64
    25.75    38.64    33.91     9.58   351.33     1.13    28.39    18.05
    18.27    38.06    15.23   320.46   299.32    75.09    31.86   283.80
    90.50     7.23   346.69   289.02   321.70   326.83   321.12   291.15
    67.18   330.60   209.29   104.29   213.25   116.48    61.83   248.69

AMP= 0.1415E-03 TO  0.3065E-02 VOLTS.  (  26.7 DB.)

PLOT AXES? N

PLOT AMPLITUDE? N

PLOT PHASE? N
       0.000    -180.000      -0.087       0.000        37         1        37

                                ELEVATION COMPONENT CENTRAL ROW

MAXIMUM AMPLITUDE =      0.933 AT POINT NO.     1


ANGLES OR INDICES
     0.00    -5.00   -10.00   -15.00   -20.00   -25.00   -30.00   -35.00
   -60.00   -65.00   -70.00   -75.00   -80.00   -85.00   -90.00   -95.00
  -120.00  -125.00  -130.00  -135.00  -140.00  -145.00  -150.00  -155.00
  -180.00

AMPLITUDES IN DB
   -55.08   -55.08   -55.08   -55.08   -55.08   -55.08   -55.08   -55.08
   -55.08   -55.08   -55.08   -55.08   -55.08   -55.08   -55.08   -55.08
   -55.08   -55.08   -55.08   -55.08   -55.08   -55.08   -55.08   -55.08
   -55.08

PHASES IN DEGREES
     9.17     9.18     9.18     9.19     9.20     9.19     9.21     9.18
     9.18     9.19     9.19     9.17     9.19     9.18     9.17     9.17
     9.19     9.18     9.19     9.19     9.19     9.20     9.18     9.18
     9.17

AMP= 0.1761E-02 TO  0.1763E-02 VOLTS.  (   0.0 DB.)
```

```
PLOT AXES?  N

PLOT AMPLITUDE? N

PLOT PHASE? N

AZIMUTH COMPONENT FILE HEADER
SOURCE ANTENNA POLARIZATION CORRECTED AZIMUTH DATA          LPROBE.F3

                                AMPLITUDES FOR AZIMUTH COMPONENT PROBE ORIENTATION

ELEVATION COMPONENT FILE HEADER
SOURCE ANTENNA POLARIZATION CORRECTED ELEVATION DATA        LPROBE.F3

                                AMPLITUDES FOR ELEVATION COMPONENT PROBE ORIENTATIO

OK, COMO -E
```

NEWFIL

DESCRIPTION: Separates a complex data file into amplitude and phase files; the size of the data file can be optionally reduced.

NF PROCESSING APPLICATION: Required prior to contour plotting

INPUT: ASCII or Binary File - 512x512 maximum

OUTPUT: ASCII or Binary Files - Amplitude and phase

TIMING:
Connect (Min)	3.06
CPU (Sec)	112.87
I/O (Sec)	27.13

EXAMPLE RUN: The example run is for a 512x512 antenna pattern file.

```
OK, NEWFIL

THIS PROGRAM CREATES A NEW (SMALLER) FILE OF SCAN
SAMPLES FROM AN EXISTING FILE OF SCAN SAMPLES AND SEPERATES
THE DATA INTO SEPERATE AMPLITUDE AND PHASE FILES.


ENTER NAME OF EXISTING FILE
FFSCOBROADF10

ENTER NUMBER OF ROWS IN EXISTING FILE
512

ENTER NUMBER OF COLUMNS IN EXISTING FILE
512

ENTER NAME FOR NEW FILE
FFSCOBROADF10

ENTER THE BEGINNING ROW NUMBER FOR NEW FILE
1

CONTINUING FOR HOW MANY ROWS
512

ENTER THE BEGINNING COLUMN NUMBER FOR NEW FILE
1

CONTINUING FOR HOW MANY COLUMNS
512

IS FILE ASCII OR BINARY? (A/B)
B
OK, COMO -E
```

NFALTER

DESCRIPTION: NF data is synthetically smoothed in both amplitude and phase in the projected aperture region. NF phase error is reduced by division by a constant and NF amplitude error is reduced using a sliding window average. The program geometry accommodates NF data for the RCA SPY-1A phased array or the Westinghouse ULSA traveling wave array.

NF PROCESSING APPLICATION: Diagnostic Aid

INPUT: NF DATA FILE - BINARY

TIMING:
Connect (Min)	- 4.07
CPU (Sec)	- 3.73
I/O (Sec)	- 4.77

EXAMPLE RUN: The example run is a 101x275 NF raster obtained for the Westinghouse ULSA array.

```
OK, NFALTER

ENTER MEASURED NF DATA FILE NAME
NFDAY102B

ENTER ALTERED NF DATA FILE NAME
ALTERDAY102

ENTER PHASE SCALING FACTOR
5

ENTER AZIMUTHAL PHASE GRDAIENT IN DEGREES
-30.13

WANT RANDOM PHASE IN RECTANGULAR REGION? - Y/N
N

ENTER SLIDING WINDOW SIZE - 1,2,3,4,5, OR 6
4
OK, COMO -E
```

DESCRIPTION: Computes the complex average of multiple y-scans taken during x-translation of both the AUT and probe. The complex average is then subtracted from each of the y-scans to yield the random error in the NF due to room scattering.

NF PROCESSING APPLICATION: NF facility diagnostics

INPUT: Binary File - Multiple scan with AUT translation NF data

OUTPUT: ASCII File - NF average scan data

TIMING:
Connect (Min)	1.60
CPU (Sec)	50.59
I/O (Sec)	5.95

EXAMPLE RUN: The example run is for data taken at the NBS NF facility in Boulder, Colorado.

```
OK, NFAVG

ENTER INPUT DATA FILE NAME
SCATSUMF2


DATA FILE HEADER
04258502  TSC-ULSA F2 S H02 1-3 2900



NORMAL FORMAT OR SEPARATED FORMAT? - N/S
N
OK, COMO -E
```

NFVECTOR

DESCRIPTION: This is an adaptation of the NBS programs FARFLTR and FARPRBC. It performs FFT processing on an N-dimension ($N \leq 12$) set of near field amplitude and phase samples, scalar or vector probe compensation, spatial filtering, back transformation of data to the aperture or any other plane, has capability to zero pad back to original size followed by FFT for high resolution plane wave spectrum. The Cooley-Turey FFT algorithm is used.

NF PROCESSING APPLICATION: Primary NF data processing utility

INPUT: ASCII or binary file - measured NF amplitude and phase samples

OUTPUT: Binary file - Plane wave transmitting characteristic of AUT, coupling product, or NF data propagated to arbitrary distance z.

TIMING:

Connect (Min)	- 26.73
CPU (Sec)	- 684.13
I/O (Sec)	- 434.05

EXAMPLE RUN: The example run is 238x290 NF raster which was zero-padded to 512x512. The plane wave transmitting characteristic of the AUT is computed using scalar probe compensation.

```
OK, NFVECTOR

WHICH MODE- 0) FAR, 1)HRFLD, 2)Bo(P), 3)FFT:
0

ENTER #ROWS, #COLS OF DATA:
238,290

ENTER TIME CONVENTION +JWT OR -IWT +/-
+

PRINT 1ST FFT RESULTS AFTER RE-ARRANGE? - Y/N
N

ENTER DELX,DELY,DIST(CM), FREQ(GHZ)
2.2860,2.5146,28.412,*.**

ENTER PROBE GAIN(DB),PHSRAD(DEG),LOSS-Y(DB),LOSS-X(DB)
0,0,0,0

ELECTRICAL DISTANCES:
  DX=  0.2379     , DY=  0.2617     , DZ=   2.957

SCALAR OR VECTOR PROCESSING (S/V):
S

ENTER CO-POLARIZED DATA FILE NAME:
CO.S97128.F1


COMPLEX FORMAT? (X, Y): N


BINARY FORMAT?  Y

                    ***  FIELD DATA FILE HAS BEEN READ IN.  ***



HERE ARE THE FIRST 5 COPOL ELEMENTS:
      (  0.5082E-05,    61.97    )
      (  0.8877E-05,    140.6    )
      (  0.1005E-04,    175.1    )
      (  0.1782E-04,   -145.3    )
      (  0.5603E-05,   -87.52    )


IS IT POLAR (R, PHI) ?Y

      ZPAD:  NROW, NCOL=    238    290

ENTER #ROWS, #COLS TO ZERO:
274,222
```

```
CO-POL ANTENNA DATA IS CURRENTLY "POLAR"

CONVERT : TO POLAR=1, TO CARTESIAN=2, DISPLAY=3, RETURN=4
4


WRITE DATA TO FILE? N

FFT ELAPSED TIME =    339.523 SEC
FFT CPU TIME =    254.936 SEC
```

```
                    *** 1-ST FORWARD FFT PWS IS AVAILABLE ***


CO-POL ANTENNA DATA IS CURRENTLY "POLAR"

CONVERT : TO POLAR=1, TO CARTESIAN=2, DISPLAY=3, RETURN=4
4

WRITE DATA TO FILE? N

PERFORM PROBE COMPENSATION ?Y

ENTER MAXIMUM THETA (DEG) ALLOWED BY SCAN LIMITS
78

HORIZONTAL OR VERTICAL POLARIZATION? - H/V
V

ZERO INVISIBLE SPACE WAVE NUMBERS ONLY? - Y/N
N

ENTER PROBE CO-POLARIZED DATA FILE NAME:
COMP1.SPY1B.F1BMDJWT*

COMPLEX FORMAT? (X, Y): N

BINARY FORMAT?  Y

FILE READ IN ELAPSED TIME =    265.391 SEC
FILE READ IN CPU TIME =     78.506 SEC


HERE ARE THE FIRST 5 COPOL PATTERN POINTS:
     (  0.0000    ,   0.0000    )
     (  0.0000    ,   0.0000    )
     (  0.0000    ,   0.0000    )
     (  0.0000    ,   0.0000    )
     (  0.0000    ,   0.0000    )

IS IT POLAR (R, PHI) ?Y

PROBE CORRECTION ELAPSED TIME =    405.914 SEC
PROBE CORRECTION CPU TIME =    111.882 SEC
```

```
*** PROBE CORRECTED PWS IS AVAILABLE ***


DISPLAY ROW(AZIMUTH),COLUMN(EPSILON) OR NONE? - R/C/N
N

CO-POL ANTENNA DATA IS CURRENTLY "POLAR"

CONVERT : TO POLAR=1, TO CARTESIAN=2, DISPLAY=3, RETURN=4
3

# (ROWS, COLUMNS)=    512    512
** ANSWER K FOR ROW K, -M FOR COLUMN M

WHICH ROW(+) OR COLUMN(-)?
174

You need new PAPER to plot AXES !!


PRINT AMP AND PHASE?  N


GRAPH AMP OR PHASE? N


PLOT AMP OR PHASE?  N


WRITE AMP AND PHASE?  Y

ENTER FILE NAME
FFSCOS97128F1R174


VIEW ANOTHER ROW/COLUMN?  Y

# (ROWS, COLUMNS)=    512    512
** ANSWER K FOR ROW K, -M FOR COLUMN M

WHICH ROW(+) OR COLUMN(-)?
-241

You need new PAPER to plot AXES !!


PRINT AMP AND PHASE?  N


GRAPH AMP OR PHASE? N
```

```
PLOT AMP OR PHASE?  N

WRITE AMP AND PHASE?  Y

ENTER FILE NAME
FFSCOS97128F1C241

VIEW ANOTHER ROW/COLUMN?  N

CONVERT AGAIN?  N

WRITE DATA TO FILE? Y

ENTER OUTPUT DATA FILE NAME:
FFSCOS97128F1
 *** COLUMN     50 HAS BEEN WRITTEN WITH DATA( 50177... 51200)
 *** COLUMN    100 HAS BEEN WRITTEN WITH DATA(101377...102400)
 *** COLUMN    150 HAS BEEN WRITTEN WITH DATA(152577...153600)
 *** COLUMN    200 HAS BEEN WRITTEN WITH DATA(203777...204800)
 *** COLUMN    250 HAS BEEN WRITTEN WITH DATA(254977...256000)
 *** COLUMN    300 HAS BEEN WRITTEN WITH DATA(306177...307200)
 *** COLUMN    350 HAS BEEN WRITTEN WITH DATA(357377...358400)
 *** COLUMN    400 HAS BEEN WRITTEN WITH DATA(408577...409600)
 *** COLUMN    450 HAS BEEN WRITTEN WITH DATA(459777...460800)
 *** COLUMN    500 HAS BEEN WRITTEN WITH DATA(510977...512000)

   FIELD DATA FILE HAS BEEN WRITTEN OUT.


GET NEW FILE? N

GET NEW PARAMETERS? N

RESTART? N
OK, COMO -E
```

DESCRIPTION: Calculates the RMS sidelobe level for a two-dimensional antenna pattern. To achieve maximum accuracy the main beam periphery is modeled as an elliptical contour. The ellipse equation coefficients are provided as input. The option exists to exclude invisible space wavenumbers when computing the RMS SLL for an antenna pattern with known values at equal increments in k_x and k_y. Each far field voltage is weighted by $\cos^{-1}\theta$ to account for the nonlinearity in $\sin(k_x, k_y)$ space. Additional elliptical or rectangular regions can be excluded from the calculation. The RMS calculation can also be limited to a specified rectangular sector.

NF PROCESSING APPLICATION: Far field pattern figure of merit

INPUT: Binary file - Amplitude in dB with peak of main beam normalized to 0 dB

OUTPUT: RMS SLL in dB

TIMING:
Connect (Min)	2.47
CPU (Sec)	62.51
I/O (Sec)	25.41

EXAMPLE RUN: The example run is for 512x512 two-dimensional far field pattern. The main beam and $\theta \geq 78^0$ are excluded from the calculation. The latter limit is imposed by the ANFAST II scan plane geometry.

```
OK, RMS2D

ENTER # OF ROWS, # OF COLUMNS
512,512

ENTER ANTENNA PATTERN FILE NAME
AMP.FFSCOBROADF10C

DO YOU WANT TO EXCLUDE INVISIBLE SPACE? - Y/N
Y

ENTER SPATIAL FILTER ROW LENGTH, COLUMN LENGTH
512,512

ENTER SPATIAL FILTER CENTER - IFCC,IFRC
256,256

ENTER NF DATA SPACING IN CM. - DELX,DELY
2.2860,2.5146

ENTER NF MEASUREMENT FREQUENCY IN GHZ
*.**

ENTER MAX. THETA(DEG) ALLOWED BY SCAN LIMITS
78

ENTER MAIN BEAM ELLIPSE MAJOR AXIS - X/Y
X

ENTER MAIN BEAM ELLIPSE CENTER - XCOL,YROW
256,256

ENTER MB ELLIPSE MINOR AND MAJOR SEMI-AXIS LENGTHS - AXMIN,AXMAJ
8,8

EXCLUDE ANOTHER ELLIPTICAL REGION? - Y/N
N

EXCLUDE A RECTANGULAR REGION? - Y/N
N

TOTAL FOV RMS OR SPECIFIED SECTOR? - T/S
T

RMS SIDELOBE LEVEL =   -59.8399 DB
 % OF ARRAY USED =     1.00000
 SUM =    0.207814
 INDEX =         60840 ICOUNT =             0

REPEAT FOR ANOTHER FILE? - Y/N
N
OK, COMO -E
```

RMSRC

DESCRIPTION: Calculates the RMS SLL for a selected row or column of a two-dimensional antenna pattern voltage matrix.

NF PROCESSING APPLICATION: Far field figure of merit

INPUT: Binary file - complex far field amplitude and phase

OUTPUT: RMS SLL for a linear pattern cut

TIMING: Connect (Min) - 3.87
CPU (Sec) - 64.77
I/O (Sec) - 39.95

EXAMPLE RUN: The example run is for two selected rows from a 512x512 antenna pattern file.

```
OK, RMSRC

ENTER MATRIX SIZE - ROWS,COLUMNS
512,512

ENTER FILENAME
FFSCOSTEERF5

CALCULATE RMS FOR A ROW OR COLUMN - R/C
R

ENTER THE ROW NUMBER
247

RMS SIDELOBE LEVEL FOR ROW 493 =   -30.7312 DBI

REPEAT FOR ANOTHER ROW OR COLUMN - Y/N
Y

CALCULATE RMS FOR A ROW OR COLUMN - R/C
R

ENTER THE ROW NUMBER
265

RMS SIDELOBE LEVEL FOR ROW 529 =   -30.9235 DBI

REPEAT FOR ANOTHER ROW OR COLUMN - Y/N
N
OK, COMO -E
```

SKEWNF

DESCRIPTION: The measured NF amplitude is forced to be symmetric about the y-axis. The -x amplitudes are simply reflected into the +x region. The NF phase is left unchanged.

NF PROCESSING APPLICATION: NF diagnostics

INPUT: Binary file - measured NF data

OUTPUT: Binary file - modified NF data

TIMING: Connect (Min) - 0.93
CPU (Sec) - 7.36
I/O (Sec) - 2.21

EXAMPLE RUN: The example run is for a 101x275 NF scan raster.

```
OK, SKEWNF

ENTER THE NF AMPLITUDE FILE NAME
NFDAY102B

ENTER NEW FILE NAME
NFDAY102SYM
OK, COMO -E
```

STEER

DESCRIPTION: Applies a main beam steering phase gradient to illuminations for planar arrays with uniform element spacings. The time convention for the phase gradient is $e^{-i\omega t}$. The steering angles are for the azimuth/elevation spherical coordinate system.

NF PROCESSING APPLICATION: NF diagnostics

INPUT: Binary file - Amplitude and phase

OUTPUT: Binary file - Steered beam complex illumination data

TIMING:
Connect (Min)	- 1.13
CPU (Sec)	- 9.23
I/O (Sec)	- 5.87

EXAMPLE RUN: The example run is for a 79x141 illumination data file.

```
OK, STEER

THIS PROGRAM BEAM STEERING PHASE
GRADIENTS IN AZIMUTH/ELEVATION SPACE


ENTER NAME OF EXISTING ILLUMINATION FILE
TRANSMIT

ENTER NUMBER OF ROWS IN ILLUMINATION FILE
141

ENTER NUMBER OF COLUMNS IN ILLUMINATION FILE
79

IS FILE ASCII OR BINARY  (A/B)
B

ENTER THE STEERING ANGLES - AZDEG,ELDEG
0,-14.25

ENTER ELEMENT SPACINGS IN CM. -DELX,DELY
2.2860,2.5146

ENTER FREQUENCY IN GHZ
*.**

ENTER THE STEERED PHASE FILENAME
TRANSTEER

DO YOU DESIRE ANOTHER STEERED BEAM DIRECTION? - Y/N
N
OK, COMO -E
```

SUMSQAV

DESCRIPTION: Calculates the gain as a function of NF scan area starting at the center of the scan plane. The upper bound scan truncation errors (Eqs. 32 and 36 NBS Technical Note 667) are also calculated as a function of scan area. Gain vs scan area is determined for an arbitrary user-selectable azimuth and elevation angles.

NF PROCESSING APPLICATION: Estimate magnitude of far field error due to finite-scan plane

INPUT: ASCII or binary file - measured NF data

OUTPUT: Gain vs scan area and upper bounds vs scan area

TIMING:
Connect (Min) - 1.8
CPU (Sec) - 54.66
I/O (Sec) - 17.08

EXAMPLE RUN: The example run is for a sidelobe at 19.70^{0} in the azimuth plane. The NF data size is 101x275.

```
OK, SUMSQAV

ENTER THE # OF ROWS, # OF COLUMNS - NR,NC
101,275


# OF NF DATA ROWS =  101
# OF NF DATA COLUMNS =  275

ENTER FREQ,GP,PDIREC,ANSQ,DX,DY,D,AP
3.1,.80103,0.0,50.52,3.81,3.81,65,487.68


PROBE CORERECTION COEFFICIENT =     0.80 VOLTS
PROBE DIRECTIVITY =     0.00 DBI
INPUT TO OUTPUT RATIO =    50.52 DB
NF X-SPACING =     3.81 CM
NF Y-SPACING =     3.81 CM
NF Z-SPACING =    65.00 CM
MAXIMUM APERTURE DIMENSION =   487.68 CM

ENTER TAP,APAR,GR,AZ,EL
4.7,17837.38,556.2,19.70,0.0


ILLUMINATION TAPER FACTOR =     4.70
APERTURE AREA =   17837.38 SQ CM
FAR FIELD RATIO =   556.20
AZIMUTH ANGLE =    19.70 DEGREES
ELEVATION ANGLE =     0.00 DEGRRES

ENTER FAR FIELD IN VOLTS ABOVE ISOTROPIC
0.05058


FAR ELECTRIC FIELD = 0.5058E-01 VOLTS

ENTER THE NF DATA FILE NAME
NFDAY535B

IS THE FILE ASCII OR BINARY? - A/B
B

PLOT CENTRAL COLUMN OF NF DATA? - Y/N
N

PLOT CENTRAL ROW OF NF DATA? -Y/N
N

ITEST = 1
```

X(K)	TSUMSQ(DB)	AVSQ(DB)	RING SUM OF PRODUCT A,R,DPHI	EQ32(DB)	EQ36(DB)
243.8	15.34	0.1330E-01	-.3365E+02	-.3780E+01	0.1000E+38	0.1000E+38
247.6	16.69	0.2410E-01	-.1740E+01	-.3185E+01	0.7102E+02	0.4585E+02
251.5	20.34	0.1165E+00	0.6309E+01	-.1738E+02	0.6503E+02	0.5399E+02
255.3	20.64	0.1422E-01	0.1254E+02	-.2316E+01	0.6177E+02	0.4733E+02
259.1	20.63	0.1707E-03	0.6437E+01	0.8726E+00	0.5951E+02	0.3914E+02
262.9	19.87	0.3370E-01	-.3970E+01	0.2407E+01	0.5775E+02	0.3448E+02
266.7	18.32	0.5217E-01	-.1455E+02	0.7061E+01	0.5634E+02	0.4377E+02
270.5	18.14	0.4846E-02	0.5963E+01	-.1047E+00	0.5540E+02	0.3405E+02
274.3	20.37	0.7602E-01	0.9303E+00	-.8923E+01	0.5437E+02	0.3658E+02
278.1	21.44	0.5224E-01	-.1290E+01	-.5477E+01	0.5367E+02	0.3181E+02
281.9	20.46	0.4770E-01	0.3439E+01	0.4419E+01	0.5292E+02	0.3109E+02
285.8	18.99	0.5345E-01	0.2164E+01	0.6164E+01	0.5236E+02	0.3181E+02
289.6	18.40	0.1634E-01	0.1605E+01	0.2496E+01	0.5190E+02	0.2472E+02
293.4	18.33	0.1976E-02	-.3920E+01	0.2320E+00	0.5148E+02	0.2660E+02
297.2	21.09	0.9676E-01	-.6107E+01	-.1117E+02	0.5090E+02	0.3614E+02
301.0	21.83	0.3819E-01	0.2040E+01	-.4276E+01	0.5063E+02	0.2745E+02
304.8	21.02	0.4069E-01	0.3478E+01	0.3673E+01	0.5030E+02	0.2770E+02
308.6	19.57	0.5550E-01	-.8175E+01	0.7214E+01	0.4997E+02	0.3391E+02
312.4	19.62	0.1728E-02	-.7792E+01	0.2444E+01	0.4971E+02	0.3122E+02
316.2	20.91	0.4787E-01	-.1126E+02	0.7631E+00	0.4937E+02	0.3376E+02
320.0	22.94	0.1089E+00	-.8367E+01	-.7364E+01	0.4922E+02	0.3346E+02
323.8	23.18	0.1675E-01	-.2688E+01	-.1095E+00	0.4892E+02	0.2151E+02
327.7	24.26	0.8550E-01	-.5618E+01	-.5073E+01	0.4884E+02	0.2987E+02
331.5	24.81	0.5103E-01	0.2175E+00	-.5667E+01	0.4847E+02	0.2732E+02
335.3	24.89	0.8009E-02	0.1538E+01	-.1670E+01	0.4834E+02	0.1979E+02
339.1	24.76	0.1276E-01	0.3341E+01	-.1040E+01	0.4815E+02	0.2313E+02
342.9	24.09	0.5925E-01	0.2810E+01	0.4113E+01	0.4799E+02	0.2591E+02
346.7	24.63	0.4701E-01	-.3298E+01	-.2528E+01	0.4782E+02	0.2433E+02
350.5	24.29	0.3012E-01	0.3918E+01	0.4285E-01	0.4782E+02	0.2377E+02
354.3	24.34	0.4668E-02	-.2242E+01	0.9072E+00	0.4759E+02	0.1985E+02
358.1	23.92	0.3330E-01	0.6733E+00	0.3238E+01	0.4749E+02	0.2226E+02
362.0	24.71	0.6461E-01	-.6787E+01	-.1380E+01	0.4730E+02	0.2826E+02
365.8	24.77	0.5329E-02	0.4110E+01	-.3995E+01	0.4719E+02	0.2662E+02
369.6	24.58	0.1624E-01	0.3100E+01	-.5395E+00	0.4722E+02	0.2169E+02
373.4	23.73	0.6516E-01	0.5230E+01	0.3578E+01	0.4701E+02	0.2735E+02
377.2	23.54	0.1298E-01	-.4160E+01	0.4260E+01	0.4674E+02	0.2679E+02
381.0	23.77	0.1544E-01	-.1297E+01	-.1137E+01	0.4647E+02	0.1691E+02
384.8	24.09	0.2222E-01	-.6056E+00	-.2071E+01	0.4629E+02	0.1857E+02
388.6	23.72	0.2550E-01	0.2835E+01	0.1089E+01	0.4577E+02	0.2119E+02
392.4	23.65	0.4552E-02	-.2229E+01	0.2373E+01	0.4521E+02	0.2171E+02
396.2	24.04	0.2643E-01	-.1200E+01	-.2592E+01	0.4457E+02	0.2064E+02
400.0	23.97	0.4885E-02	0.2405E+01	-.1374E+01	0.4405E+02	0.2038E+02
403.9	23.45	0.3320E-01	0.2887E+01	0.2165E+01	0.4373E+02	0.2245E+02
407.7	23.05	0.2292E-01	-.1641E+01	0.4493E+01	0.4307E+02	0.2471E+02
411.5	23.73	0.3961E-01	-.4509E+01	-.1802E+01	0.4252E+02	0.2480E+02
415.3	24.21	0.3143E-01	-.1049E+00	-.4173E+01	0.4226E+02	0.2355E+02
419.1	23.97	0.1619E-01	0.4922E+01	-.1591E+01	0.4174E+02	0.2528E+02
422.9	23.11	0.5035E-01	0.2238E+01	0.5202E+01	0.4139E+02	0.2600E+02
426.7	23.12	0.8921E-03	-.3298E+01	0.2309E+01	0.4075E+02	0.2319E+02
430.5	23.64	0.2859E-01	-.3225E+01	-.1617E+01	0.3998E+02	0.2229E+02
434.3	23.99	0.2146E-01	0.1025E+01	-.3837E+01	0.3946E+02	0.2305E+02
438.1	23.54	0.2703E-01	0.2569E+01	0.1935E+01	0.3817E+02	0.2134E+02
442.0	23.39	0.8209E-02	-.5956E+00	0.1685E+01	0.3767E+02	0.1680E+02

445.8	23.56	0.9185E-02	-.2161E+01	0.2979E+00	0.3620E+02	0.1829E+02
449.6	23.72	0.9465E-02	0.1177E+01	-.2438E+01	0.3533E+02	0.1994E+02
453.4	23.39	0.1819E-01	0.1655E+01	0.1480E+01	0.3482E+02	0.1840E+02
457.2	23.19	0.1016E-01	-.1250E+00	0.1751E+01	0.3335E+02	0.1662E+02
461.0	23.42	0.1162E-01	-.2275E+01	0.1399E-01	0.3283E+02	0.1856E+02
464.8	23.58	0.8495E-02	0.9143E+00	-.2128E+01	0.3195E+02	0.1869E+02
468.6	23.44	0.7681E-02	0.1018E+01	0.3690E+00	0.3167E+02	0.1316E+02
472.4	23.16	0.1386E-01	0.6074E+00	0.1842E+01	0.3063E+02	0.1732E+02
476.3	23.33	0.8528E-02	-.1691E+01	-.4585E-01	0.2942E+02	0.1629E+02
480.1	23.28	0.2459E-02	0.8659E+00	-.3568E+00	0.3034E+02	0.1216E+02
483.9	23.41	0.6080E-02	-.1093E+01	-.1129E+00	0.3060E+02	0.1322E+02
487.7	23.25	0.7448E-02	0.2555E+01	-.6975E+00	0.2888E+02	0.1967E+02
491.5	23.13	0.5637E-02	0.2339E+00	0.7113E+00	0.2948E+02	0.1072E+02
495.3	23.04	0.4321E-02	-.6676E+00	0.1213E+01	0.2900E+02	0.1481E+02
499.1	23.47	0.2035E-01	-.1716E+01	-.2106E+01	0.2868E+02	0.1984E+02
502.9	23.04	0.2022E-01	0.3786E+01	0.6216E+00	0.2911E+02	0.2257E+02
506.7	22.81	0.9597E-02	-.1150E+01	0.2525E+01	0.2980E+02	0.2000E+02
510.5	23.09	0.1197E-01	-.1321E+01	-.1113E+01	0.3036E+02	0.1638E+02
514.3	23.32	0.1036E-01	0.1108E+01	-.2684E+01	0.3008E+02	0.2034E+02
518.2	22.79	0.2305E-01	0.2746E+01	0.2110E+01	0.2988E+02	0.2173E+02
522.0	22.90	0.4797E-02	-.2642E+01	0.1022E+01	0.2901E+02	0.2013E+02

X(K) = 243.8400 GH = -35.2249
X(K) = 247.6500 GH = -33.8680
X(K) = 251.4600 GH = -30.2177
X(K) = 255.2700 GH = -29.9222
X(K) = 259.0800 GH = -29.9257
X(K) = 262.8900 GH = -30.6865
X(K) = 266.7000 GH = -32.2400
X(K) = 270.5100 GH = -32.4197
X(K) = 274.3200 GH = -30.1877
X(K) = 278.1300 GH = -29.1156
X(K) = 281.9400 GH = -30.0982
X(K) = 285.7500 GH = -31.5753
X(K) = 289.5600 GH = -32.1576
X(K) = 293.3700 GH = -32.2346
X(K) = 297.1800 GH = -29.4751
X(K) = 300.9900 GH = -28.7270
X(K) = 304.8000 GH = -29.5401
X(K) = 308.6100 GH = -30.9930
X(K) = 312.4200 GH = -30.9389
X(K) = 316.2300 GH = -29.6458
X(K) = 320.0400 GH = -27.6239
X(K) = 323.8500 GH = -27.3794
X(K) = 327.6600 GH = -26.2979
X(K) = 331.4700 GH = -25.7552
X(K) = 335.2800 GH = -25.6750
X(K) = 339.0900 GH = -25.8051
X(K) = 342.9000 GH = -26.4739
X(K) = 346.7100 GH = -25.9294
X(K) = 350.5200 GH = -26.2742
X(K) = 354.3300 GH = -26.2183
X(K) = 358.1400 GH = -26.6381
X(K) = 361.9500 GH = -25.8500
X(K) = 365.7600 GH = -25.7903
X(K) = 369.5700 GH = -25.9768
X(K) = 373.3800 GH = -26.8270

```
X(K) =   377.1900 GH =   -27.0202
X(K) =   381.0000 GH =   -26.7891
X(K) =   384.8100 GH =   -26.4737
X(K) =   388.6200 GH =   -26.8414
X(K) =   392.4300 GH =   -26.9111
X(K) =   396.2400 GH =   -26.5174
X(K) =   400.0500 GH =   -26.5882
X(K) =   403.8600 GH =   -27.1080
X(K) =   407.6700 GH =   -27.5109
X(K) =   411.4800 GH =   -26.8307
X(K) =   415.2900 GH =   -26.3537
X(K) =   419.1000 GH =   -26.5951
X(K) =   422.9100 GH =   -27.4539
X(K) =   426.7200 GH =   -27.4369
X(K) =   430.5300 GH =   -26.9219
X(K) =   434.3400 GH =   -26.5688
X(K) =   438.1500 GH =   -27.0224
X(K) =   441.9600 GH =   -27.1714
X(K) =   445.7700 GH =   -27.0036
X(K) =   449.5800 GH =   -26.8358
X(K) =   453.3900 GH =   -27.1672
X(K) =   457.2000 GH =   -27.3655
X(K) =   461.0100 GH =   -27.1376
X(K) =   464.8200 GH =   -26.9769
X(K) =   468.6300 GH =   -27.1232
X(K) =   472.4400 GH =   -27.4026
X(K) =   476.2500 GH =   -27.2272
X(K) =   480.0600 GH =   -27.2774
X(K) =   483.8700 GH =   -27.1532
X(K) =   487.6800 GH =   -27.3071
X(K) =   491.4900 GH =   -27.4282
X(K) =   495.3000 GH =   -27.5241
X(K) =   499.1100 GH =   -27.0865
X(K) =   502.9200 GH =   -27.5246
X(K) =   506.7300 GH =   -27.7508
X(K) =   510.5400 GH =   -27.4685
X(K) =   514.3500 GH =   -27.2363
X(K) =   518.1600 GH =   -27.7749
X(K) =   521.9700 GH =   -27.6563

SMOOTH EQ36? - Y/N
N

ENTER DISK FILE SUFFIX
NODISK

PLOT GH VS. SCAN LENGTH? - Y/N
N

SMOOTH AGAIN? - Y/N
N

PLOT AVSQ VS. SCAN LENGTH? - Y/N
N
OK, COMO -E
```

YTILT

DESCRIPTION: Calculates two-dimensional antenna patterns in the AZ/EL earth spherical coordinates from a two-dimensional antenna pattern which is known in k_x, k_y array coordinates for an antenna which has been rotated about the x-axis. A four point bivariate interpolation is used to obtain equally-spaced far field amplitude data in a user selectable AZ/EL sector of earth spherical coordinates.

NF PROCESSING APPLICATION: Coordinate transformation of resultant two-dimensional far field patterns

INPUT: Binary file - Two-dimensional antenna pattern-amplitude and phase

OUTPUT: Binary file - Interpolated two-dimensional antenna pattern (amplitude) sector in earth spherical coordinates

TIMING:
Connect (Min)	- 2.67
CPU (Sec)	- 27.40
I/O (Sec)	- 19.36

EXAMPLE RUN: The example run computes the earth coordinate pattern in a $\pm 75^0$ azimuth sector and a $\pm 10^0$ elevation sector in $.5^0$ increments for an antenna which has been tilted back 15^0. The input far field data file size is 256x256.

```
OK, YTILT

ENTER ANTENNA PATTERN FILE NAME
FFTRANSOOM1425F5

ENTER # ROWS, # COLUMNS
256,256

ENTER NF/ELEMENT SPACINGS IN CM. - DELX,DELY
2.2860,2.5146

ENTER FREQUENCY IN GHZ
*.**

ENTER TILT ANGLE IN DEGREES
15

ENTER EARTH COORD. AZ ANGLES IN DEG - START,STOP,INC
-75,75,.5

ENTER EARTH COORD. EL ANGLES IN DEG - START,STOP,INC
-10,10,.5

ENTER EARTH COORD. ANTENNA PATTERN FILE NAME
SECHORIZONF5
OK, COMO -E
```

Appendix A.3

PUBLICATIONS AND REPORTS AVAILABLE

The following bibliography is a partial compilation of internal reports and open literature publications which have been produced during the DESAT II low sidelobe near field testing demonstration. They are available upon request.

Memos and Reports

1. "Mechanical Delta Probe Pattern Anomalies at f_2 and f_3", TSC-W75-26, November 12, 1985. This TSC memo describes measured Δ-probe patterns in contour space and their effect on probe correction processing for both DESAT test arrays (unclassified).

2. "Possible Use of the TSC Δ-Probe for Compact Range Reflectivity Probing", TSC-W41-304, 8 July 1985 (unclassified). This TSC memo proposes scanning a TSC Δ-probe in front of large reflector antennas in order to extend the dynamic range when certifying the columnating properties of compact ranges.

3. "Memo for Record--DESAT Transition Experiment", TSC-W41-310, July 25, 1985, (unclassified); "Proposed DESAT II Transition Experiment", TSC-W41-272, January 10, 1985 (unclassified); "Memo for Record", TSC-W41-303, July 5, 1985 (unclassified). These TSC memos describe a proposed (and subsequently funded) extension to the DESAT II demonstration program, in order to show feasibility of low RCS testing by scanning the Δ-probe in the presence of an RCS target.

4. "Test Plan for Ultralow Sidelobe Near Field Measurement Demonstration--DESAT II", TSC-W41-273, January 1985 (unclassified). This TSC report describes the details, procedures, and goals of the testing demonstration with ultralow sidelobe arrays at the NBS planar near field facility.

5. TSC letter dated April 13, 1984 (Reference TSC-W75-02 unclassified), documenting the shipment of three DESAT probes from TSC, Silver Spring, to NBS labs, Boulder, Colorado. The three DESAT probes were manufactured by Westinghosue Defense Electronics System Center, Baltimore under subcontract to TSC.

6. S-band Near Field Probe Fabrication Specification", TSC-W41-194/Revision 2 (issue #3), November 2, 1983; TSC-W41-194/Revision 1 (issue #2), October 5, 1983; TSC-W41-194 (issue #1), September 9, 1983 (unclassified). This TSC specification sets forth the fabrication instructions for Westinghouse to build the DESAT II probes under TSC subcontract LAD-53092AA, July 7, 1983.

7. "Optimum Near Field Probe Pattern Effectiveness Simulation", TSC-W35-46, September 13, 1983 (unclassified). This TSC memo describes the requirements for a computer simulation to show the feasibility of near field scanning with a new mainbeam nulling probe.

8. "Optimum Probe Design", TSC-W41-193, September 1, 1983 (unclassified). This TSC memo first describes the approach to design for a new class of near field probes capable of improved low sidelobe measurement accuracy for large test antennas.

9. "Supplemental Progress Report (January 1 - April 19, 1985)"--Planar Near-Field Measurements of Low Sidelobe Arrays", NBS Report No. SR-723-34-85, September 1985 (unclassified). This technical report gives contract progress at NBS for the indicated period.

10. "Progress Reports--DESAT II Testing Demonstration"
#6--TSC-W41-312, August 1, 1985 (unclassified)
#5--TSC-W41-280, March 7, 1985 (unclassified)
#4--TSC-W41-248, October 5, 1984 (unclassified)
#3--TSC-W41-204, December 21, 1983 (unclassified)
#2--TSC-W41-201, October 14, 1983 (unclassified)
#1--TSC-W41-189, August 17, 1983 (unclassified)
These TSC technical progress reports provide contractually required updates to the sponsor for the work periods indicated. They are contract deliverables.

11. "Progress Report (January 1 - April 19, 1985)"--Planar Near Field Measurements of Low Sidelobe Arrays", NBS Report No. SR-723-11-85, May 1985 (unclassified). This technical report was produced by NBS and contains the initial test results from Block 1,2 testing with the ULSA array at NBS. RF scanning data for tests TSTMULT, TSTSPAC, and TSTSCAN are included.

12. "Low Sidelobe Array Near Field Measurements Study--Final Engineering Report", submitted by Westinghouse Defense Electronics Systems Center to TSC, November 27, 1984. This Westinghouse final technical report documents subcontract efforts for TSC which included refurbishment and far field range testing of the ULSA and AWACS face arrays, and fabrication of the three DESAT probes.

13. "Preliminary RCS Results for DESAT II Transition Experiment", TSC-W41-331, December 18, 1985 (confidential). This TSC technical memo gives test results for block 3 tests at NBS to measure the bistatic RCS of a small laboratory cylinder target, when illuminated by the AWACS array in its near field.

14. "Errors in Target RCS Measurement using Planar Near Field Scanning", TSC-CTM-14, September 10, 1984 (unclassified). This TSC memo describes analytic study results to apply near field scanning to the general problem of radar target RCS measurement.

15. "Optimum Near Field Probe Pattern Effectiveness Simulation Part 2: Software Implementation and Preliminary Results", TSC-W55-39/rev, May 10, 1984 (unclassified). This extensive TSC memo is a final description

of a computer simulation to predict the performance of the new near field Δ-probe.

Open Literature Publications

16. "Ultralow Sidelobe Planar Near Field Measurement Study", by Kenneth Grimm (TSC), prepared for the 1982 Antenna Applications Symposium, University of Illinois, September 1982.

17. "Optimum Probe Design for Near Field Scanning of Ultralow Sidelobe Antennas", by Kenneth Grimm (TSC), prepared for the 1984 Antenna Applications Symposium, University of Illinois, September 1984.

18. "Results of Planar Near Field Testing with Ultralow Sidelobe Antennas", K. Grimm, J. Hoffman (TSC), A. Newell, M. Francis (NBS), 1985 IEEE AP-S/URSI Symposium Proceedings, Vancouver, B.C. Canada, June 1985.

19. "Near Field Probing for Improved Accuracy Low Sidelobe Measurement", K. Grimm, J. Hoffman (TSC), A. Newell, M. Francis (NBS), 1985 Proceedings of the Antenna Measurement Techniques Association, Melbourne, Florida, October 29, 1985.

20. "The Results and Estimates of Uncertainities from Planar Near Field Measurements on Very Low Sidelobe Antennas", A. Newell, M. Francis (NBS), K. Grimm, J. Hoffman (TSC), IEEE AP-S/URSI Proceedings of the 1986 Symposium, Philadelphia, June 1986.

21. "Measurement of Small Radar Target Forward Scattering by Planar Near Field Scanning", K. Grimm, J. Hoffman (TSC), Proceeding of the 1986 Conference on Precision Electromagnetic Measurements, NBS, Gaithersburg, Maryland, June 23, 1986.